

DESIGN AND ANALYSIS OF VEHICLE AND GUIDANCE CONCEPT FOR INTERPLANETARY RETURN MISSION

A Thesis accepted by the Faculty of Aerospace Engineering and Geodesy of the
Universität Stuttgart in partial fulfilment of the requirements for the degree of
Doctor of Engineering Sciences (Dr.-Ing.)

by

Muhammad Imran Afzal

Born in: Karachi / Pakistan

Chairman: Prof. Rudolf Voit-Nitschmann
Main Referee: Prof. Dr. rer. nat. Hans-Peter Röser
Co-referee: Prof. Dr.-Ing. Peter Vörsmann

Date of Defence: 4th October 2010

Institute of Space Systems
Universität Stuttgart
2010

Table of Contents

Table of Contents	iii
Abstract	vii
Zusammenfassung	ix
Acknowledgements	xi
Nomenclature	xiii
1 Introduction	1
1.1 BACKGROUND, OBJECTIVE AND SCOPE	2
1.2 THEORETICAL BACKGROUND	3
1.2.1 <i>Hyperbolic Re-entry</i>	3
1.2.2 <i>Guidance of Re-entry Vehicles</i>	7
1.3 THESIS OVERVIEW	9
2 Methodology	11
2.1 SIMULATION MODELS	11
2.1.1 <i>Equations of Motion</i>	12
2.1.2 <i>Earth's Form and Gravity Field</i>	13
2.1.3 <i>Earth Atmosphere</i>	14
2.1.4 <i>Re-entry Heating</i>	15
2.2 VEHICLE MODEL	17
2.3 OPTIMIZATION MODELS	18
2.3.1 <i>NLPQL Subroutine</i>	20
2.3.2 <i>Gradient Projection Algorithm</i>	20
2.4 TDS SIMULATION TOOL	21
2.5 PERFORMANCE OF SIMULATION TOOL	21
2.5.1 <i>Comparison with Stardust Data</i>	22
2.5.2 <i>Qualitative Performance</i>	24
2.6 SUMMARY	27

3	Mission and Vehicle Analyses.....	29
3.1	REFERENCE MISSION	29
3.2	RE-ENTRY STRATEGY	30
3.2.1	<i>Direct Re-entry.....</i>	<i>31</i>
3.2.2	<i>Re-entry with Constant Altitude Phase.....</i>	<i>31</i>
3.3	VEHICLE CONFIGURATIONS	32
3.3.1	<i>Apollo Re-entry Vehicle.....</i>	<i>32</i>
3.3.2	<i>Lifting Re-entry Vehicle.....</i>	<i>34</i>
3.3.3	<i>Flattened Bi-conic Re-entry Vehicle.....</i>	<i>35</i>
3.4	TRAJECTORY SIMULATIONS	36
3.4.1	<i>Apollo Vehicle Re-entry Simulation.....</i>	<i>36</i>
3.4.2	<i>Lifting Vehicle Re-entry Simulation.....</i>	<i>37</i>
3.4.3	<i>Flattened Bi-conic Vehicle Re-entry Simulation.....</i>	<i>38</i>
3.5	ASSESSMENT OF PERFORMANCE PARAMETERS	39
3.5.1	<i>Volumetric Efficiency.....</i>	<i>40</i>
3.5.2	<i>Controllability.....</i>	<i>40</i>
3.5.3	<i>Deceleration.....</i>	<i>41</i>
3.5.4	<i>Maximum Heat Rate.....</i>	<i>42</i>
3.5.5	<i>Integral Heat Load.....</i>	<i>44</i>
3.5.6	<i>Result of Performance Analysis.....</i>	<i>44</i>
3.6	SUMMARY.....	45
4	Guidance Algorithm	47
4.1	IRS GUIDANCE CONCEPT.....	48
4.2	RE-ENTRY GUIDANCE STRATEGY OF FLATTENED BI-CONIC VEHICLE	50
4.3	IMPLEMENTATION OF GUIDANCE ALGORITHM.....	52
4.3.1	<i>Hyperbolic Approach Phase with Predicted Guidance.....</i>	<i>52</i>
4.3.2	<i>Constant Altitude Flight Phase with Control Law.....</i>	<i>58</i>
4.3.3	<i>Descend Phase with Predicted Guidance.....</i>	<i>61</i>
5	Evaluation of Guidance Scheme	65
5.1	GUIDANCE EVALUATION OF EACH FLIGHT PHASE	66
5.1.1	<i>Hyperbolic Approach Phase.....</i>	<i>66</i>
5.1.2	<i>Constant Altitude Flight Phase.....</i>	<i>69</i>
5.1.3	<i>Descend Phase with Predicted Guidance.....</i>	<i>72</i>
5.2	SENSITIVITY ANALYSIS.....	73
5.2.1	<i>Influence of variations on Heat Flux.....</i>	<i>74</i>
5.2.2	<i>Influence of variations on Deceleration Load.....</i>	<i>74</i>
5.3	ROBUST ANALYSIS OF ENTIRE RE-ENTRY FLIGHT	75
5.3.1	<i>Altitude vs. Range.....</i>	<i>75</i>
5.3.2	<i>Dispersion of Landing Point.....</i>	<i>76</i>
5.3.3	<i>Heat Flux.....</i>	<i>77</i>
5.3.4	<i>Deceleration Load.....</i>	<i>78</i>
5.3.5	<i>End Velocity and Mach number.....</i>	<i>78</i>
5.4	STABILITY OF GUIDANCE ALGORITHM.....	79

5.5	COMPARISON WITH OTHER GUIDANCE SCHEMES.....	80
5.6	SUMMARY	84
6	Conclusion	87
6.1	SUMMARY OF THE RESEARCH.....	87
6.2	FUTURE IMPROVEMENTS	90
	References	91
	Appendix.....	97
A.1	REFERENCE COORDINATE SYSTEMS AND TRANSFORMATIONS	97
A.2	FORCES ACTING ON RE-ENTRY VEHICLE.....	103
A.3	PROPERTIES OF EARTH FORM, GRAVITY AND ATMOSPHERE.....	105
A.4	RANGE AND AZIMUTH BETWEEN TWO POINTS ON SURFACE OF SPHERICAL EARTH	106
A.5	RADIATIVE HEATING VELOCITY FUNCTION	107
A.6	ORIGINAL APOLLO RE-ENTRY GUIDANCE STRATEGY	108

Abstract

Future space transportation scenarios will include Earth orbit transportation, orbit and interplanetary transfer as well as entry and re-entry. Sample return from interplanetary missions to Moon, Mars and beyond as well as ISS sample return and manned crew return vehicles from Earth orbit but also beyond, has to be established for research programs planned for the near future. Such long-term plans for the robotic or human space exploration of solar system bodies demand new and innovative concepts for the design of vehicles which can enter a planetary atmosphere and land on its surface safely.

This thesis presents different vehicle concepts and new method for trajectory design, optimization and guidance of Earth capture and re-entry phase of human interplanetary return mission. The reference mission for this investigation is the Earth capture and re-entry phase of lunar return mission with crew inside. The early lunar return missions were accomplished with a so-called 'capsule' shaped vehicle. There are however significant disadvantages of capsule design, especially the load factor of more than 7 times of Earth gravitation, which exceeds 4.0 g's limit of NASA's safety standards for astronauts [40].

The report assesses the performance of 3 different configurations of re-entry vehicles. Apollo like capsule [5, 6, 7] with an L/D ratio of about 0.3, flattened bi-conic [68] with an L/D ratio of about 0.7 and winged vehicle [58] with an L/D ratio of about 2.2 are categorised as low, medium and high lifting vehicles. Flattened bi-conic and winged vehicles use aerodynamic lift to remain at certain constant altitude to get rid of excessive kinetic energy before descending to the earth surface, whereas Apollo like capsule, due to its low lift to drag ratio, can stay at constant altitude for only a short period of time and descends faster through the earth atmosphere. A comparative re-entry performance analysis is performed among three configurations for parameters like stagnation point heat flux, integral heat load, peak deceleration (g-load).

A three degree of freedom trajectory simulation tool is used to simulate re-entry trajectories in a three dimensional space while treating the vehicle as a point mass. The simulation tool uses a non-linear programming (NLP) approach to find optimum trajectories as a function of a finite number of control parameters with

upper and lower bounds and subjected to equality and inequality constraints. Stagnation point convective and radiative heat fluxes and integrated heat load are calculated during trajectory simulation to study the influence of vehicle and atmospheric properties on these important parameters.

A predictive guidance scheme is developed and implemented for flattened bi-conic vehicle re-entering the Earth atmosphere after returning from an arbitrary lunar mission. The guidance scheme is implemented in three phases, namely *hyperbolic approach phase (or the capture phase)* with predicted guidance, *constant altitude phase* with control law, and *final descend phase* with predicted guidance.

The core guidance algorithm is an evolution of the predictive guidance (explicit guidance) methods developed at the *Institute of Space Systems (IRS), University of Stuttgart* [15,16,27,28,29,32,36,37,46-50,62,65], which is a combination of onboard flight path prediction and trajectory optimization utilizing non-linear programming techniques with steering command parameterisation. The optimization program makes use of a complex optimization routine to find an optimized set of control parameters for a prescribed cost function and restrictions only once at the beginning of a mission phase, whereas the guidance program makes use of a simplified and fast routine of a Gradient Projection Algorithm (GPA) [31] in order to have less computation load onboard during the entry flight.

The performance of guidance scheme is evaluated against a variety of off-nominal conditions. These off-nominal conditions include variations of atmospheric density, variations of aerodynamic and mass properties of the vehicle, and errors in initial conditions at entry interface. An extensive performance analysis of the proposed guidance scheme with the help of Monte Carlo simulations has proved its functionality and reliability.

Keywords:

- Hyperbolic re-entry
- 3DOF Trajectory Simulation
- Numerical Trajectory Optimization
- Predictive (explicit) guidance
- Sensitivity Analysis

Zusammenfassung

Zukünftige Raumtransportscenarios werden den Transport in den Erdorbit, Umlauf- und interplanetare Bahntransfers sowie den Eintritt und Wiedereintritt in Atmosphären einschließen. Die Probenrückführung von interplanetaren Missionen zu Mond, Mars und darüber hinaus sowie eine Probenrückführung von der ISS und bemannte Rückkehrfahrzeuge vom Erdorbit aber auch außerhalb davon, müssen für Forschungsprogramme, die für die nahe Zukunft geplant sind, eingerichtet werden. Solche langfristigen Pläne für die robotische oder bemannte Erforschung von Himmelskörpern in unserem Sonnensystem verlangen neue und innovative Konzepte für den Entwurf von Fahrzeugen, die sicher in eine planetare Atmosphäre eintreten und auf der Oberfläche landen können.

Diese Doktorarbeit zeigt verschiedene Fahrzeugkonzepte und neue Methoden für Flugbahnentwurf, Optimierung und Steuerung der Einfangmanöver an der Erde und der Wiedereintrittsphase von bemannten, interplanetaren Rückkehrmissionen auf. Die Referenzmission für diese Untersuchung ist ein Einfangmanöver an der Erde und die Wiedereintrittsphase einer lunaren, bemannten Rückkehrmission. Die frühen lunaren Rückkehrmissionen wurden mit einem kapselförmigen Fahrzeug durchgeführt. Eine Kapselform hat jedoch bedeutsame Nachteile. Insbesondere der Lastfaktor liegt bei mehr als dem Siebenfachen der Erdgravitation, was die Grenze von 4,0 g aus den Sicherheitsstandards der NASA für Astronauten überschreitet [40].

Der Bericht bewertet die Leistung von drei verschiedenen Konfigurationen von Wiedereintrittsfahrzeugen. Apollo-ähnliche Kapseln [5,6,7] mit einem L/D Verhältnis von ungefähr 0,3, Fahrzeuge mit abgeplatteter bi-konischer Form [68] mit einem L/D Verhältnis von ungefähr 0,7 und geflügelte Fahrzeuge [58] mit einem L/D Verhältnis von ungefähr 2,2 werden kategorisiert als Fahrzeuge mit kleinem, mittlerem und großem Auftrieb. Fahrzeuge mit abgeplatteter bi-konischer Form und geflügelte Fahrzeuge benutzen aerodynamischen Auftrieb, um in einer bestimmten konstanten Flughöhe zu bleiben und damit übermäßige kinetische Energie vor dem Abstieg zur Erdoberfläche abzubauen. Kapseln wie Apollo hingegen können auf Grund ihres niedrigen Auftrieb zu Widerstand Verhältnisses nur für kurze Zeit in konstanter Flughöhe bleiben und steigen schneller durch die Erdatmosphäre ab. Eine vergleichende Wiedereintrittsleistungsanalyse wird mit drei Konfigurationen für Parameter wie Staupunktswärmefluss, integrale Wärmelast und maximale Verzögerung. (g-load) durchgeführt.

Ein Flugbahnsimulationswerkzeug mit drei Freiheitsgraden wird benutzt, um die Wiedereintrittsflugbahnen in einem dreidimensionalen Raum zu simulieren, bei dem das Fahrzeug als Punktmasse behandelt wird. Das Simulationswerkzeug benutzt einen nichtlinearen Programmierungsansatz (NLP), um die optimalen Flugbahnen als Funktion einer begrenzten Zahl von Steuerparametern mit oberer und unterer Grenze zu finden. Konvektive und Strahlungswärme flüsse und integrale Wärmelast im Staupunkt werden während der Flugbahnsimulation berechnet, um den Einfluss von Fahrzeug- und atmosphärischen Eigenschaften auf diese wichtigen Größen zu untersuchen.

Ein prädiktives Lenkkonzept wird für ein nach der Rückkehr von einer beliebigen lunaren Mission in die Erdatmosphäre eintretendes Fahrzeug mit abgeplatteter bikonischer Form entwickelt und ausgeführt. Das Lenkkonzept ist in drei Phasen aufgeteilt, nämlich die *hyperbolische Annäherungsphase (oder das Einfangmanöver an der Erde)* mit prädiktiver Lenkung, die *Flugphase mit konstanter Flughöhe* mit Steuergesetz und die *Abstiegsschlussphase* mit prädiktiver Lenkung.

Der Kern des Lenkalgorithmus ist eine Weiterentwicklung einer prädiktiven Lenkmethode (expliziter Lenkung), die am Institut für Raumfahrtssysteme (IRS), Universität Stuttgart [15,16,27,28,29,32,36,37,46-50,62,65] entwickelt wurde und eine Kombination aus einer bordeigenen Flugbahnvoraussage und Flugbahnoptimierung ist und eine nichtlineare Programmierungstechnik mit Steuerkommandoparametrisierung verwendet. Das Optimierungsprogramm benutzt eine komplizierte Optimierungsroutine, um nur einmal - am Anfang einer Missionsphase - einen optimierten Satz von Steuerparametern für eine vorgeschriebene Kostenfunktion und Einschränkungen zu finden, wohingegen das Lenkprogramm eine vereinfachte und schnelle Routine eines Gradientenprojektionsalgorithmus (GPA) [31] benutzt, um während des Eintrittsflugs weniger Rechenlast an Bord zu haben.

Die Leistung des Lenkverfahrens wird für verschiedene nicht nominale Bedingungen bewertet. Diese nicht nominalen Bedingungen schließen Veränderungen der atmosphärischen Dichte, sowie der aerodynamischen und Masseneigenschaften des Fahrzeugs und Fehler in den anfänglichen Bedingungen am Eintrittspunkt mit ein. Eine umfangreiche Leistungsanalyse des vorgeschlagenen Lenkverfahrens mit Hilfe von Monte Carlo Simulationen hat seine Funktionalität und Zuverlässigkeit bewiesen.

Keywords:

- Hyperbolisches Wiedereintritt
- 3DOF Trajectory Simulation
- Numerical Trajectory Optimization
- Prädiktive (explizit) Lenkung
- Leistungsanalyse

Acknowledgements

At first I would like to thank to the Almighty, whose mercy and help is always there whenever the difficulties and problems surround me. He gave me strength and knowledge to handle and complete this useful research work.

I would like to thank to my supervisor *Professor Dr. rer. nat. Hans-Peter Roeser* for giving an opportunity to work on such an interesting topic in the top quality research environment of *Institute of Space Systems, Stuttgart*. His generosity and positive steps in favour of me during my stay at the institute helped me to come out of difficulties and problems and to continue my studies and research.

I am extremely thankful to the technical advisor of my work *Dr.-Ing. Michael Graesslin* for his valuable guidance and help throughout the execution of this research work and his support in the development and assessment of computer programs and soft-wares. His technical comments on simulation results made it possible for me to quickly move to the next steps, which resulted in an accelerated progress on this research.

I am also thankful to *Professor Dr.-Ing. Peter Voersmann* for sparing time out of his busy schedule to review my research work, my publications and finally my thesis report. A short discussion with his students and his colleagues at the *Institute of Aerospace Systems in Braunschweig* was very fruitful.

I am grateful to all those at *Institute of Space Systems* who assisted me in my research, as well as all my friends in *Germany* for making my time more enjoyable.

I would like to mention here the names of *Higher Education Commission of Pakistan* (HEC) and *Pakistan Space and Upper Atmospheric Research Commission* (SUPARCO) for providing me financial support to carry out this research work during my stay in *Germany*, as well as providing financial support for presenting research papers in international conferences and seminars. The efforts of both HEC and SUPARCO for providing opportunities to engineers and scientists of *Pakistan* and supporting them financially, despite poor economical and miserable political conditions of the country, are highly appreciable.

I am also thankful to *Deutscher Akademischer Austausch Dienst* (DAAD) and *Office of International Affairs* (IA) of *Universität Stuttgart*. The German language courses organized by DAAD in *Pakistan* and in *Germany* were very helpful to integrate and communicate in the German society. I am especially thankful to Miss Ursula Habel

of IA for her help and support while dealing with public offices for foreigners, as well as her efforts for exploring various financial sources for my medical treatments which were outside the limits of my insurance cover. I also enjoyed a number of interesting events and excursions organised by IA for PhD students.

I am especially thankful to my parents for their great love and prayers and their encouragement throughout my life.

Finally, I wish to express my deep appreciation and gratitude to my family to accompany me in Germany during my studies. The sweet smiles and hugs of my sons *Sufyan* and *Sarmad* always refreshed and cheered me when I was tired at the end of hard working days at the institute. I also appreciate the patience of my wife, during her stay of one and a half year in *Pakistan*, because of lengthy formal procedure of visa application for *Germany*.

Nomenclature

Latin Letters

A	<i>Aerodynamic side force</i>
a	<i>Acceleration</i>
a_{grav}	<i>Acceleration due to gravity</i>
a_{aer}	<i>Acceleration due to aerodynamic forces</i>
a_{rel}	<i>Acceleration due to rotation of horizontal coordinate system</i>
C	<i>Reference coordinate system</i>
C_A	<i>Aerodynamic side force coefficient</i>
C_D	<i>Drag coefficient</i>
$C_{D,0}$	<i>Zero lift drag coefficient</i>
C_L	<i>Lift coefficient</i>
D	<i>Aerodynamic drag force</i>
F	<i>Objective function</i>
f	<i>Flatness of Earth</i>
G	<i>Universal gravitational constant</i>
\bar{G}	<i>Jacobian matrix containing gradient of constraint violation</i>
g	<i>Gravitational acceleration</i>
g_e	<i>Gravitational acceleration at equator</i>
\bar{g}_i	<i>Equality constraints vector</i>
\bar{g}_j	<i>Inequality constraints vector</i>
g_r, g_λ, g_δ	<i>Components of gravity vector in Geocentric Earth-fixed frame</i>
\bar{H}	<i>Quasi-Newtonian matrix</i>
h	<i>Local height</i>
h_{ref}	<i>Reference constant altitude</i>
J_2, J_3, J_4	<i>2nd, 3rd and 4th order Jaffery's constants</i>
K_h, K_i	<i>Feedback coefficients</i>
k	<i>Specific heat ratio</i>
L	<i>Aerodynamic lift force</i>

lb	<i>Lower bound</i>
M_E	<i>Mass of Earth</i>
m	<i>Instantaneous mass of spacecraft</i>
P	<i>Atmospheric pressure</i>
\bar{p}	<i>Parameterized control vector</i>
Q	<i>Dynamic pressure</i>
q_c	<i>Stagnation point convective heat flux</i>
q_r	<i>Radiation heat flux</i>
R	<i>Gas constant (Air)</i>
R^*	<i>Universal gas constant</i>
R_N	<i>Nose radius</i>
R_e	<i>Equatorial radius of Earth</i>
R_l	<i>Local radius of Earth</i>
R_p	<i>Polar radius of Earth</i>
R_x, R_y, R_z	<i>Elementary matrices of rotations of Euler angles</i>
r	<i>Distance from centre of Earth</i>
S_{ref}	<i>Reference area</i>
s	<i>Point in space</i>
s'	<i>Sub-point of a point "s" on Earth surface</i>
T	<i>Atmospheric temperature</i>
t	<i>Time</i>
T_a^b	<i>Transformation matrix from frame "a" to frame "b"</i>
U	<i>Gravitational potential of Earth</i>
ub	<i>Upper bound</i>
$\bar{u}(t)$	<i>Continuous control vector</i>
V	<i>Velocity</i>
V_{rel}	<i>Relative ground velocity</i>
\vec{X}	<i>State vector</i>
x, y, z	<i>Rectangular components of position vector</i>

Greek Letters

α	<i>Angle of attack</i>
α_G	<i>Right ascension of Greenwich</i>
β	<i>Side slip angle</i>
	<i>Ballistic coefficient</i>
χ	<i>Flight azimuth angle</i>
δ	<i>Geocentric latitude</i>
ϕ	<i>Geodetic latitude</i>
ϕ'	<i>Declination of a point in space</i>
γ	<i>Flight path angle w.r.t. local horizontal</i>

λ	<i>Longitude</i>
μ	<i>Earth gravitation parameter = GM_E</i>
θ	<i>Half cone angle</i>
ρ	<i>Density of air</i>
σ	<i>Standard deviation</i>
ω_E	<i>Angular velocity of Earth</i>
ψ	<i>Bank angle</i>
Ψ	<i>Range Angle</i>

Mathematical Operators

∇	<i>Gradient</i>
\int	<i>Integral</i>
Σ	<i>Summation</i>

Acronyms

AOA	<i><u>A</u>ngle of <u>A</u>ttack</i>
ASTRA	<i><u>A</u>usgewählte <u>S</u>ysteme und <u>T</u>echnologien für zukünftige <u>R</u>aumtrasportsystem-<u>A</u>nwendungen</i>
CEV	<i><u>C</u>rew <u>E</u>ntry <u>V</u>ehicle</i>
CG	<i><u>C</u>entre of <u>G</u>ravity</i>
COLIBRI	<i><u>C</u>oncept of a <u>L</u>ifting <u>B</u>ody for <u>R</u>e-entry <u>I</u>nvestigations</i>
DOF	<i><u>D</u>egrees of <u>F</u>reedom</i>
ESA	<i><u>E</u>uropean <u>S</u>pace <u>A</u>gency</i>
GPA	<i><u>G</u>radient <u>P</u>rojection <u>A</u>lgorithm</i>
GNC	<i><u>G</u>uidance <u>N</u>avigation and <u>C</u>ontrol</i>
IMSL	<i><u>I</u>nternational <u>M</u>athematics <u>S</u>tandard <u>L</u>ibrary</i>
IRS	<i><u>I</u>nstitut für <u>R</u>aumfahrtsysteme</i>
ISS	<i><u>I</u>nternational <u>S</u>pace <u>S</u>tation</i>
L/D	<i><u>L</u>ift to <u>D</u>rag ratio</i>
LEO	<i><u>L</u>ow <u>E</u>arth <u>O</u>rbital</i>
MSIS	<i><u>M</u>ass <u>S</u>pectrometer <u>I</u>ncoherent <u>S</u>catter</i>
NASA	<i><u>N</u>ational <u>A</u>eronautics and <u>S</u>pace <u>A</u>dmistration</i>
NLP	<i><u>N</u>on <u>L</u>inear <u>P</u>rogramming</i>
NLPQL	<i>A FORTRAN Subroutine in IMSL for solving NLP problems: <u>N</u>on <u>L</u>inear <u>P</u>rogramming - <u>Q</u>uadratic <u>L</u>inearization</i>
SQP	<i><u>S</u>equential <u>Q</u>uadratic <u>P</u>rogramming</i>
TAEM	<i><u>T</u>erminal <u>A</u>rea <u>E</u>nergy <u>M</u>anagement</i>
TETRA	<i><u>T</u>echnologien für zukünftige <u>R</u>aumtrasportsysteme</i>
TDS	<i><u>T</u>rajectory <u>D</u>ynamic <u>S</u>imulation</i>
WGS	<i><u>W</u>orld <u>G</u>eodetic <u>S</u>ociety</i>

1 Introduction

Space exploration is the use of astronomy and space technology to explore outer space. Physical exploration of space is conducted both by human spaceflights and by robotic spacecraft. With NASA's Constellation program, the United States has committed to return to the Moon by 2018 and later Mars [33,59,71]. China [41], Russia [72], Japan [39], and India [25] have plans of manned missions to the Moon during the 21st century, while the European Union has also plans of manned missions to both the Moon and Mars during the 21st century [10]. Space transportation scenarios of these future missions include Earth orbit transportation, orbit and interplanetary transfer as well as entry and re-entry. Sample return from interplanetary missions to Moon, Mars and beyond as well as ISS sample return and manned crew return vehicles from Earth orbit but also beyond. Such long-term plans for the robotic or human exploration of solar system bodies demand new and innovative concepts for the design of vehicles which can enter a planetary atmosphere and land on its surface safely. There has been and continues to be, considerable interest and research into the development of new trajectory generators and guidance systems for aerospace vehicles re-entering a planetary atmosphere. Vehicle and mission design process requires a thorough investigation of this flight phase and its sensitivity to environmental influences and uncertainties as well as vehicle properties.

The research presented in this thesis report focuses on the mission and vehicle analysis as well as the development and evaluation of trajectory design and guidance of re-entry vehicles returning to the Earth after interplanetary exploration missions. The research consists of three areas of interest of a re-entry mission.

1. Mission and vehicle analysis of different types of vehicles suitable for such missions.
2. The development and implementation of guidance logics during different flight segments of the re-entry flight till parachute deployment.
3. The evaluation of re-entry flight and the guidance scheme with the help of sensitivity analysis to determine the influence of off-nominal conditions.

1.1 Background, Objective and Scope

Re-entry mission trajectory design has been under investigation at IRS for more than a decade [15,16,27,28,29,32,36,37,46-50,62,65]. Trajectory simulation tools and guidance algorithms has been developed and implemented to vehicles re-entering the earth atmosphere from *sub-orbital* and *orbital* missions. Within the Stuttgart small satellite program, an autonomous re-entry vehicle has been considered as a step towards technology demonstration and technology research facility. The development of guidance algorithms at the Institute of Space Systems (IRS) focused on an algorithm that offers a high degree of autonomy and generality. Originally intended for the COLIBRI capsule [65] the core of the guidance algorithm was further developed and remained under investigation in the last years within the German technology programs of TETRA (Technology for future space transportation systems [69]) and ASTRA (Advanced systems and technologies for future space transportation applications [66]). The reference missions have been the X-38 [15,16,32] demonstrator and the Hopper vehicle [29,36,48]. For X-38 the guidance algorithm was not only applied to the hypersonic [47,49] but also to the terminal area flight phase (known as terminal area energy management; TAEM) [27,28,29]. The guidance methods, till the start of this research work, were developed for various sub-orbital and orbital missions, and applied to complete flight scenarios (including launch, coasting and re-entry phases) as well as to individual flight phases e.g. only re-entry, TAEM, etc.

With an increasing interest in the space exploration missions, either manned or unmanned, it was also needed at IRS to do mission and system analysis of re-entry vehicles returning from inter-planetary missions, and to set up guidance logics and implement them with the help of computer programs. Vehicles returning from interplanetary exploration missions approach a planetary atmosphere at *super-orbital* speed. Because of very high speed at entry interface, the type of orbit which a vehicle makes about the approaching planet is hyperbolic. Therefore such a re-entry is also known as *hyperbolic re-entry* and the speed as *hyperbolic speed*. Apollo missions took human beings to the moon in the decades of 60's and 70's, and successfully re-entered the Earth atmosphere to bring back the crew as well the samples form moon surface. The classical capsule like design of Apollo re-entry vehicle, re-entered the Earth atmosphere, with deceleration loads of more than 7 times of Earth gravitation, which exceeded 4.0 g's limit of NASA's safety standards for astronauts [40]. Analysis of alternate re-entry configuration, in order to re-enter not only at lower g-loads, but also to find vehicle configurations and mission strategies with lower heat loads, is always an interesting topic.

The primary objective of this work is to extend the vehicle and mission analysis process of IRS from sub-orbital and orbital missions to interplanetary return missions i.e. for hyperbolic re-entries. The reference mission for this investigation is the Earth capture and re-entry phase of lunar return mission with crew inside. An in-house trajectory simulation tool is used and modified (wherever required) to simulate re-entry trajectories for several vehicle types and re-entry strategies. Flight simulation process helped in the selection of vehicle configuration and re-entry

strategy. Finally the goal was to set up a guidance method for the selected re-entry vehicle with suitable re-entry strategy, which was analysed in the vehicle and mission design process. The methodology was translated into a computer program with which the guided flights of the re-entry vehicle were analysed for nominal as well as for several off-nominal conditions. The entire work was presented and published in various conferences [51,52] to exchange knowledge and gain feedback from other people.

1.2 Theoretical Background

1.2.1 Hyperbolic Re-entry

A spacecraft approaching a planetary atmosphere from an interplanetary exploration mission possesses a large amount of kinetic energy. While the vehicle passes through planetary atmosphere this energy is converted into heat and at the same time the velocity of the vehicle is reduced greatly due to atmospheric drag, therefore the vehicle faces very high thermal and mechanical loads during re-entry. Trajectory analysis of such missions involves both dynamic and thermal requirements, and due to complex interacting phenomena, usually requires a numerical analysis.

Analysis of re-entry trajectories allows an attempt of systematic classification of spacecraft types and re-entry methods. As far as spacecraft is concerned, the aspect of lift to drag ratio leads to the difference between ballistic, semi-ballistic and lifting trajectories.

Ballistic re-entry: Vast majority of unmanned spacecrafts returning to Earth follow a ballistic entry trajectory, where the vehicle does not generate aerodynamic lift [55,56,62]. The spacecraft enters into the atmosphere and falls through it under the influence of gravity and drag. The drag force slows the vehicle till parachutes can be deployed for a soft touchdown. The landing point is predetermined by conditions when the vehicle first enters the atmosphere, and no control over the spacecraft is available once it begins the ballistic entry. Furthermore the variation of atmospheric conditions influences the heat and deceleration loads as well the landing accuracy. Since the spacecraft enters at steep entry angle into the atmosphere, its downrange distance, or ground track, from the point where it first entered the atmosphere to landing is small as compared to a vehicle following semi-ballistic or lifting re-entry.

Semi-ballistic re-entry: An alternate re-entry approach is the semi-ballistic trajectory. In this case, the vehicle descends through the atmosphere till vehicle achieves the aerodynamic control capability. Appropriate control method is then used to generate lift in order to keep the vehicle within the specified limits mechanical and heat loads. The spacecraft slows down gradually with controlled lift profile until it is safe to descend it to the planetary surface. Manned space capsules like Apollo [5,6,7] followed semi-ballistic entry trajectories to a splashdown at sea. Russian Soyuz [13] and Chinese Shenzhou [41] capsules

continue to use semi-ballistic entry paths and usually touchdown on land. Orion crew entry vehicle (CEV) [11,30] which will be used in constellation program will also use the semi-ballistic re-entry.

Lifting re-entry: Another re-entry approach is the lifting trajectory in which the spacecraft flies through the atmosphere similarly to an aircraft. The spacecraft enters the atmosphere at a high angle of attack and generates aerodynamic lift that allows it to travel further downrange than semi-ballistic vehicle. The main advantage of this technique is that the vehicle has more control over the trajectory and can perform precise landing. A further advantage is that the vehicle would typically be landed intact on a runway and can possibly be reused again. This technique is true in case of Space Shuttle [34], the only vehicle that currently uses a lifting entry trajectory returning from orbital mission. Monti et al. [58] and Wingrove [61] have analyzed the re-entry scenarios using lift forces for interplanetary re-entry missions.

An important problem associated with entries at super-orbital speed or hyperbolic speed, is that of entry corridor required in order to accomplish a desired entry maneuver, such as entering without encountering excessive deceleration or heating loads. The upper and lower limits on this re-entry corridor are determined by a combination of two factors: its rate of deceleration, and aerodynamic heating. In contradiction to sub-orbital flights, the tolerances at entry condition for super-orbital flights are narrow, since an undershoot or a steep entrance may cause destruction of vehicle during entry, and an overshoot may result in a skip-out or a homeless exit into space. The narrow region dictated by these parameters is known as the entry corridor illustrated below in Figure 1-1.

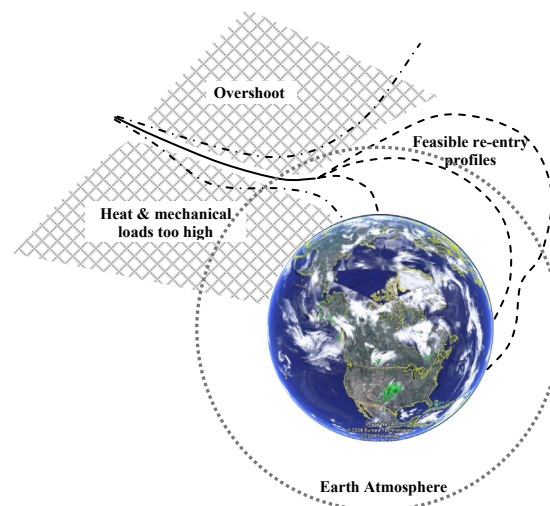


Figure 1-1: Boundaries defining typical spacecraft re-entry corridor

The trajectory of a vehicle returning to Earth depends in part on the type of orbit the object travelled in order to reach the planet. The orbital path is significant because it determines how fast the vehicle is travelling when it first encounters the

atmosphere. One special type of orbit is the circular orbit that approximates the path most spacecraft like satellites and the Space Shuttle follow while orbiting the Earth. These vehicles typically circle the Earth at speed between 7,200 and 8,000 km/sec and will re-enter the outer layers of the atmosphere at these velocities.

Vehicles travelling beyond Earth orbit, like the Apollo missions to the Moon, follow parabolic or hyperbolic orbits that result in much higher speed upon returning to Earth. Apollo capsules, for example, re-entered the atmosphere at speed of nearly 11 km/s [5]. Although out of the scope of this thesis but mentioned for comparison, that the energy in case of Mars return mission will be much more higher since the vehicle speed upon arrival at Earth returning from a Mars mission, depending on launch time and type of trajectory, will range roughly from 15 to 21 km/sec [24].

For a minimum energy lunar return transfer orbit, the semi-major axis of the transfer orbit is approximately 383,200 km. The difference in energy between the transfer orbit and a 150 km LEO orbit for a 10000 kg spacecraft is 3.0×10^8 kJ [68] and the energy that must be dissipated by the same spacecraft to return from the LEO orbit to landing is approximately 3.2×10^8 kJ [68]. Excess lunar return energy when compared to LEO (i.e. difference in energy between the transfer orbit and a 150 km LEO orbit) is approximately 94% of the energy that must be dissipated to return from the LEO orbit to landing. Thus, a lunar return trajectory presents roughly twice the amount of energy that must be dissipated when compared to a typical Space Shuttle re-entry. This incredible amount of energy is converted into thermal energy through shock wave compression (stagnation) heating. The challenge is to design a vehicle that performs this energy conversion as safely as possible so that the internal environment of the spacecraft remains survivable for a human crew.

There are three primary approaches that may be taken to dissipate energy of interplanetary return vehicle before final atmospheric re-entry (Figure 1-2). These are:

1. Direct Re-entry
2. Aero-braking
3. Aero-capture

Direct re-entry: Direct re-entry is the method chosen by the early Apollo [5,6,7] and Soyuz [13] missions. In this approach the lunar return trajectory is so designed that the orbital track directly intercepts the Earth's surface. Direct re-entry angles are typically fairly steep. The result is a very high level of deceleration and extreme heating as the energy is dissipated at very high dynamic pressures. Since the spacecraft enters at steep entry angle into the atmosphere, its downrange distance, or ground track, from the point where it first entered the atmosphere to landing is comparatively small.

Aero-braking: Mars Global Surveyor [8] spacecraft launched for exploration of Mars by NASA was placed in to Mars orbit in September 1997, and by May 1999 it was slowly circularized through *aero-braking* to a Sun synchronous orbit. In *aero-*

braking method, the perigee of the entry/re-entry orbit is set to only pass through the outer layers of atmosphere, achieving very small deceleration levels - less than 1/100 g - but at substantially lower dynamic pressures and heating levels. Typically multiple aero-braking passes must be performed in order to gradually reduce the orbit apogee to the point where capture in low Earth orbit is possible. This approach often involves a time period of many days for LEO capture and multiple passes through the Van-Allen radiation belts in case of Earth re-entry. Neither of these options is acceptable for a human crewed vehicle.

Aero-capture: Aero-capture [1,60,70] is a flight manoeuvre that inserts a spacecraft into its proper orbit once it arrives at a planet. In Aero-capture method, the orbit is so designed that the spacecraft trajectory does not intercept the planetary surface; instead the spacecraft intercepts the outer atmosphere and then uses substantial aerodynamic forces to dissipate enough energy to allow the spacecraft to be captured into a low altitude orbit. Once the spacecraft is captured, bank angle modulation is used to safely remain within the flight corridor, preventing skip-out or planetary impact.

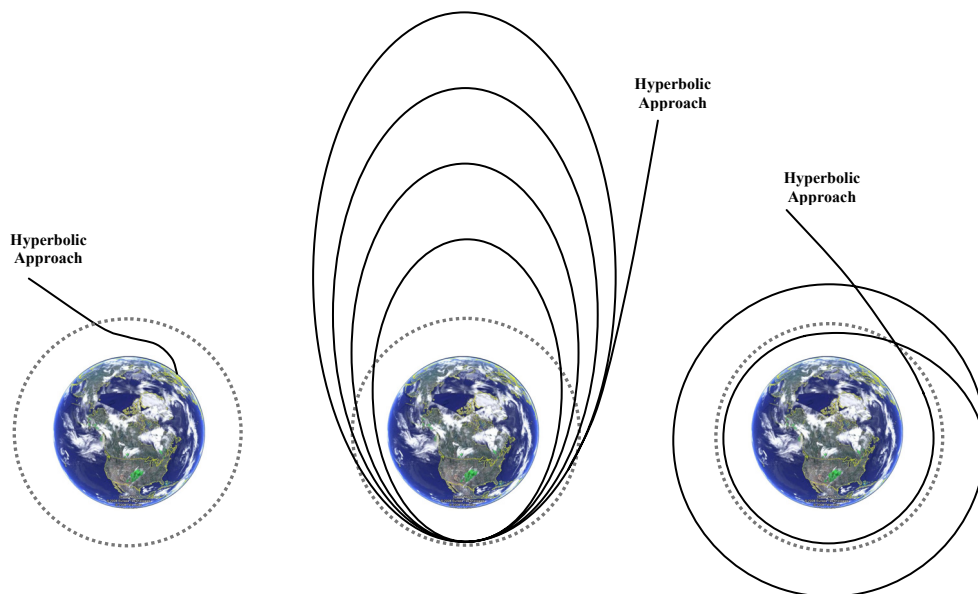


Figure 1-2: Direct entry, aero-braking and aero-capture

Direct Entry + Aero-capture: When re-entering from planetary missions one can show that a combination of direct entry and aero-capture of the vehicle till touch down is possible by properly modulating the lift force [58] (Figure 1-3). In particular for bodies re-entering from exploration missions at super-orbital velocities, a negative lift (i.e. a lift force pointing toward the centre of the Earth) allows to fly at constant high altitudes and to reduce smoothly the speed to orbital speed; below the orbital velocity a positive modulated lift force (pointing outward of the centre of the Earth) can be used to properly keep the vehicle at high altitudes, avoiding large decelerations and high heat fluxes.

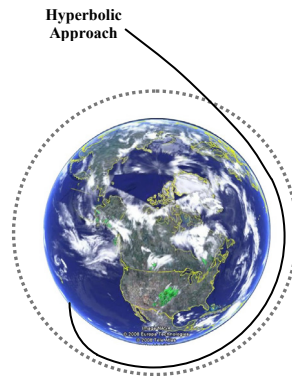


Figure 1-3: A combination of direct entry and aero-capture till touch down

1.2.2 Guidance of Re-entry Vehicles

The guidance system for vehicles entering the planetary atmosphere must provide steering commands which guide the vehicle to reach the desired landing point with specified accuracy. Inadequate guidance during entry can cause large deviations from the desired target point, excessive aerodynamic heating of the vehicle, deceleration in excess of crew tolerance limits, or, in the extreme, the loss of the vehicle and its crew.

Uncertainties in vehicle characteristics, e.g. in the lift-drag (L/D) ratio and vehicle mass properties, uncertainties in atmospheric variations as well as errors in vehicle states at entry interface affect guidance performance. Therefore a guidance system should be as insensitive as possible to uncertainties in those parameters over which the guidance designer has no control, in particular, vehicle.

A useful discussion on several publications related to the entry of guidance problem is done by *Wingrove* [73]. The guidance methods are presented there under two general classifications: guidance using a nominal trajectory (trajectory following guidance) and guidance using prediction (predictive guidance) by either fast-time solution or approximate closed-form solution of the equations of motion (Figure 1-4). The reference concludes that the choice of which type to use depends on considerations such as the size and speed of the onboard computer, the range of entry conditions which the guidance system must be capable of handling, the flexibility to maintain trajectories with desired heating or acceleration profiles. It is possible that entry guidance logic will use elements of both techniques.

Trajectory following guidance: Guidance about nominal trajectories provides a simple guidance method that can be designed to handle many off design conditions. In this method the state variables along the nominal path are precomputed and stored onboard the spacecraft. The variations in the measured variables from the stored values are used in the guidance logic either to control the spacecraft back to the nominal trajectory (path controller) or to establish a new trajectory to reach the destination (terminal controller). For this guidance logic, a desirable nominal trajectory must be selected prior to entry. The selection of the

nominal may be influenced by operational considerations and/or by optimization procedures. Constant feedback gains for guidance or time-varying feedback gains may be used.

The advantage of trajectory following guidance is that a minimal on-board computational effort is required, as the profiles are calculated prior to launch. Since the profiles are not generated by an on-board guidance computer there are no issues with solution convergence or stability. Many re-entry missions were performed using trajectory following guidance in the past and still in use e.g. *Gemini* [22], *Soyuz* [13], and *Space Shuttle* [34]. Apollo missions also used trajectory following guidance during the final phase of re-entry flight [22].

The disadvantage of trajectory following guidance is a need of considerable pre-mission planning to account for all the expected conditions at the time of launch. The use of many stored trajectories and stored feedback gains also implies a large onboard storage requirement. The pre-computed guidance commands are only suited to the mission profiles considered and can not be adapted if the profiles differ. Consequently if the flight conditions or mission profile differs from the reference trajectory it can result in large deviations from the required final conditions or even mission failure.

Predictive guidance: In most cases the method of guidance using fast-time prediction is capable of handling a wider variety of entry conditions than the guidance about a nominal trajectory. This guidance technique predicts the path by which the vehicle will reach the desired destination without violating the heating and acceleration limits. Trajectory prediction may be accomplished by a rapid forward integration of the equations of motion for the remainder of the flight, or by using an approximate empirical equation derived from many numerical solutions to the equations of motion.

Apollo missions used predictive guidance during the initial flight phase of re-entry into the Earth Atmosphere till a capture is ensured [22]. A number of studies have been done on the application of predictive guidance methods for future re-entry and space transportation vehicle e.g. X-38 demonstrator [15,16,32] and the Hopper vehicle [29,36,48].

The main advantages of the predictive guidance methods are that they are able to handle any possible flight condition and they can adapt to current flight conditions, i.e. if unexpected flight conditions arise the trajectory can be adapted to take them into account and theoretically reduce the requirements for launch delays. The real time trajectory generation methods reduce the amount of pre-mission planning that must be performed.

The principal disadvantages of these methods are the requirement for speed in the computer, since they require large amount of computational effort in comparison to trajectory following guidance. However the use of empirical equations reduces the required computational speed of the guidance system. Convergence and instability

issues may arise in finding new guidance commands based on future trajectory predictions.

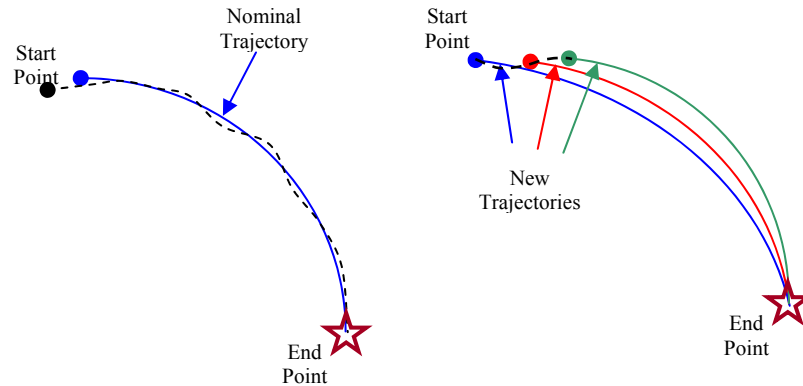


Figure 1-4: Trajectory following guidance and predictive guidance methods

1.3 Thesis Overview

The research presented in this thesis report focuses on the mission and vehicle analysis as well as the development and evaluation of trajectory design and guidance of re-entry vehicles returning to the Earth after interplanetary exploration missions. The research consists of three areas of interest of a re-entry mission.

1. Mission and vehicle analysis of different types of vehicles suitable for such missions.
2. The development and implementation of guidance logics during different flight segments of the entire re-entry flight.
3. The evaluation of re-entry flight and guidance scheme with the help of sensitivity analysis to determine the influence of off-nominal conditions.

This research incorporates in principle three fields of study i.e. flight mechanics, numerical optimization, and guidance of aerospace vehicles. The theoretical background of these fields of study, which is supposed to be necessary for a reader, is given in this report wherever it was required. However the reader is referred to the references for more detail.

Chapter 1 presents the objective and scope of the work followed by a short introduction to the problem of re-entry at hyperbolic speed, re-entry methods, and optimization and guidance methods of re-entry vehicles.

Chapter 2 presents the methodology used for this thesis to simulate, and optimize the re-entry trajectories including description of three degree of simulation model, Earth shape, gravity and environment models as well as the optimization models. The performance of the simulation tool both in qualitative and quantitative terms is also evaluated. Trajectories were simulated for a mission of an existing space vehicle, STARDUST and the results were compared with the actual flight data.

Chapter 3 presents the mission and system analysis of three different kinds of vehicles; an Apollo like capsule [5,6,7], a flattened bi-conic [68] and a winged vehicle [58]. The reference mission for the investigation is Earth capture and re-entry phase of lunar return mission with crew inside. Two kinds of re-entry approaches are considered for investigations; direct re-entry with steep entry angle for low lift to drag vehicles and re-entry with constant altitude phase for lifting vehicles, which utilize their lift to maintain a constant altitude.

Chapter 4 includes the description and evaluation of the proposed guidance scheme for above mentioned reference mission. The guidance scheme is an evolution of the predictive guidance (explicit guidance) methods developed at the *Institute of Space Systems (IRS), University of Stuttgart*. The optimization and guidance programs utilise non linear programming techniques combined with steering command parameterisation to generate and evaluate trajectories. The optimization program makes use of a complex optimization routine to find an optimized set of control parameters for a prescribed cost function and restrictions only once at the beginning of a mission phase, whereas the guidance program makes use of a simplified and fast routine of a Gradient Projection Algorithm (GPA) [31] in order to have less computation load onboard during the entry flight.

Chapter 5 evaluates the performance of guidance scheme against a variety of off-nominal conditions. These off-nominal conditions include variations of atmospheric density, variations of aerodynamic and mass properties of the vehicle, and errors in initial conditions at entry interface. An extensive performance analysis of the proposed guidance scheme with the help of Monte Carlo simulations has proved its functionality and reliability.

Chapter 6 provides an over all conclusion of the research drawn from the results from the trajectory simulations of different kinds of re-entry vehicles as well as from the results of guided simulations. Possible improvements to the simulation and guidance tools are suggested in the end.

2 Methodology

This chapter describes the simulation environment and different kinds of simulation models used to perform analysis presented in this thesis. The simulation program used is Trajectory Dynamics Simulation (TDS) which is an IRS in-house simulation tool to optimize and simulate trajectories of space flight vehicles entering into planetary atmosphere. The results of the simulator are dependent on specific models used and these models are described in following sections of this chapter.

2.1 Simulation Models

In general, a vehicle flying through atmosphere in a three dimensional space under the influence of external forces may be considered as an elastic, mass-varying body. The three dimensional motion of vehicle can be distinguished by the motion of centre of mass of the vehicle and the motion of the vehicle around its centre of mass. For a rigid vehicle, there exist three components of translation of centre of mass and three components of rotation of vehicle around centre of mass. Analysis of re-entry trajectories can be done on one hand by considering only translational motion of centre of mass, so called three degrees of freedom 3-DOF and on the other hand by considering both translational and rotational mission, so called six degree of freedom 6-DOF.

Many aspects of re-entry flight (either considering the vehicle as an elastic or rigid body) in relation with guidance and control, necessitate a detailed analysis of flight dynamics at early stages of the design process. However, within the framework of this thesis it is just not possible to study many of these aspects. For instance, the inclusion of elastic-body dynamics and the influence of mass variations due to ablation are considered to be out of the scope of this study. Moreover, in the framework of this thesis only 3-DOF simulations are meaningful, because when the guidance of a vehicle is designed and investigated it is assumed that the control system can generate the required moments to change the attitude of the vehicle. It is also assumed that the attitude changes take place instantaneously or the attitude changes with predefined attitude rate.

2.1.1 Equations of Motion

Various coordinate systems are required, to express the equations of motion of an aerospace vehicle as well as to describe its position and orientation. The choice of some of these coordinate systems depends on the type of mission. The coordinate systems which are Earth-bound in some way, has been used for simulations and some of them has been presented in section A.1 of this report.

Theory upon which the simulation is based is presented in [19] and [20]. The references may be consulted for derivation of the equations and coordinate transformations, however, principle equations of motions are presented below for completeness.

Non propulsive and non varying mass system is considered for re-entry vehicles to simulate re-entry trajectories in 3-DOF. The state vector of the motion of vehicle includes three components of position vector in geocentric Earth-fixed coordinate system (i.e. radial distance of vehicle from the centre of Earth r , and latitude δ and longitude λ of vehicle) and three components of velocity vector in local horizontal coordinate system (i.e. vehicle's velocity w.r.t. ground V_{rel} , its flight path angle γ and azimuth angle χ).

The velocity of the vehicle is ground related and solving the equations of motion directly gives us the trajectory with respect to the Earth. The state vector of six components mentioned above can be written as

$$\vec{X} = [r \quad \lambda \quad \delta \quad V_{rel} \quad \gamma \quad \chi]^T \quad 2-1$$

The dynamical equations are expressed with the help of vehicle's relative velocity V_{rel} w.r.t ground and orientation of velocity vector w.r.t local horizontal frame as

$$\begin{bmatrix} \dot{V}_{rel} \\ V_{rel} \cdot \dot{\gamma} \\ V_{rel} \cdot \cos \gamma \cdot \dot{\chi} \end{bmatrix} = \begin{bmatrix} \cos \gamma \cos \chi & \sin \gamma & \cos \gamma \sin \chi \\ -\sin \gamma \cos \chi & \cos \gamma & -\sin \gamma \sin \chi \\ -\sin \chi & 0 & \cos \chi \end{bmatrix} \cdot \vec{a} \quad 2-2$$

\vec{a} in Equation 2-2, is the sum of accelerations due to gravitation \vec{a}_{grav} , aerodynamic forces \vec{a}_{aer} and rotation and angular rate of the horizontal coordinate system \vec{a}_{rel} are computed according to the equations presented in section A.2.

The kinematical equations are expressed with the help of polar coordinates in geocentric Earth-fixed coordinate system:

$$\begin{bmatrix} \dot{r} \\ r \cdot \cos \delta \cdot \dot{\lambda} \\ r \cdot \dot{\delta} \end{bmatrix} = \begin{bmatrix} V_{rel} \cdot \sin \gamma \\ V_{rel} \cdot \cos \gamma \cdot \sin \chi \\ V_{rel} \cdot \cos \gamma \cdot \cos \chi \end{bmatrix} \quad 2-3$$

2.1.2 Earth's Form and Gravity Field

The shape of earth is considered here as an Ellipsoid, which is a simple mathematical figure that closely matches the earth shape. An ellipsoid is a surface of revolution described by the rotation of ellipse about its minor axis or the Earth Axis. WGS 1984 [20], is used as reference ellipsoid for this thesis and some of its important parameters are given in Table A-1

Latitude of Earth (see Figure 2-1) is usually defined by Geocentric Latitude δ and Geodetic Latitude ϕ . For a point on the surface of earth the relation between δ and ϕ is,

$$\tan \phi = \frac{\tan \delta}{(1-f)^2} \approx (1+2f) \tan \delta \quad 2-4$$

Where, f is the flatness of Earth as defined in Table A-1.

For a point s in space, the geodetic latitude ϕ of sub point s' (Figure 2-1) and the height h over the surface are expressed in terms of geocentric position vector r and geocentric declination ϕ' as,

$$\sin(\phi - \phi') = \frac{R_e}{r} \left[f \sin(2\phi') + f^2 \sin(4\phi') \left(\frac{R_e}{r} - \frac{1}{4} \right) \right] \quad 2-5$$

$$h = r - R_e \left[1 - f \sin^2 \phi' - \frac{f^2}{2} \sin(2\phi') \left(\frac{R_e}{r} - \frac{1}{4} \right) \right] \quad 2-6$$

Local Radius of Earth i.e. the distance between a point on ellipsoid surface and the earth centre is,

$$R_l = R_e \frac{1-f}{\sqrt{1-f(2-f)\cos^2 \delta}} \quad 2-7$$

If U is the function which represents the earth's gravitational potential field, then the best way to express it by considering the earth as sphere and then including the effects of non-spherical mass distribution. Due to the fact that Earth is assumed as a body of revolution, leads to express U , independent of longitude. Thus, the following is the expression for such potential field as given in [20].

$$U = \frac{\mu}{r} \left\{ 1 - \frac{J_2}{2} \left(\frac{R_e}{r} \right)^2 [3 \sin^2 \delta - 1] - \frac{J_3}{2} \left(\frac{R_e}{r} \right)^3 [5 \sin^3 \delta - 3 \sin \delta] \right. \\ \left. - \frac{J_4}{8} \left(\frac{R_e}{r} \right)^4 [35 \sin^4 \delta - 30 \sin^2 \delta + 3] - \dots \right\} \quad 2-8$$

Where, μ is the gravitational parameter of earth, and J -terms are known as Jeffery constants. These values are given in Table A-2.

Since the Earth is taken as an ellipsoid of revolution, therefore the gravitational potential of earth is limited only up to the 2nd order Jeffery constant.

Thus, the gravitational acceleration in geocentric rectangular coordinates system [20] may be found, by taking the gradient of U as follows,

$$g_r = \frac{\partial U}{\partial r} = \frac{3\mu}{r^2} \left[1 - \frac{3}{2} J_2 \left(\frac{R_e}{r} \right)^2 (3 \sin^2 \delta - 1) \right] \quad 2-9$$

$$g_\lambda = \frac{\partial U}{\partial \lambda} = 0 \quad 2-10$$

$$g_\delta = \frac{\partial U}{\partial \delta} = -\frac{\mu}{r^3} \left[\frac{3}{2} J_2 \left(\frac{R_e}{r} \right)^2 \sin(2\delta) \right] \quad 2-11$$

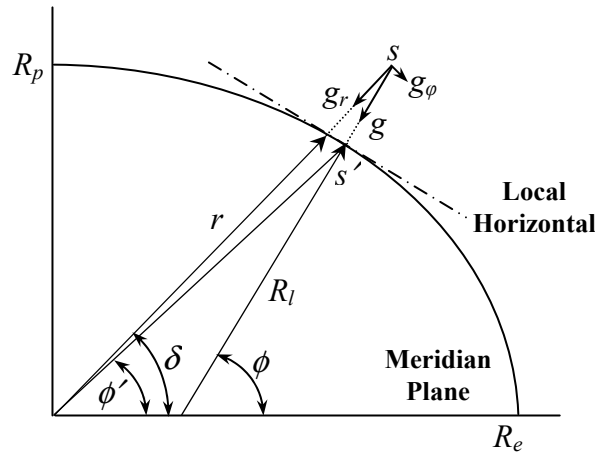


Figure 2-1: Gravity and shape of ellipsoidal Earth

2.1.3 Earth Atmosphere

Among the forces and moments applied to a spacecraft during its flight, the aerodynamic forces and moments play a significant role in the dynamical behaviour of spacecraft. These aerodynamic forces and moments depend upon the properties of the local atmosphere (density, pressure, temperature). The state of atmosphere varies with altitude, geographical latitude, season and time. Currently there are several measurement based atmosphere models that may be used.

Several models of atmosphere are available and can be used for the simulation, optimization as well guidance of aerospace vehicles e.g. Mass Spectrometer Incoherent Scatter Extended (MSIS-E 93) [23], US Standard Atmosphere 1962 [20], and Exponential Atmosphere [20].

The MSIS-E 93 is a complex model and requires considerable computational effort but on the other hand it gives atmospheric properties on the basis of altitude, geographic coordinates, calendar date, time of a day and solar activity. In

comparison, US Standard atmosphere uses only altitude to produce density, pressure and temperature of atmosphere. Therefore MSIS-E 93 is used for the purpose of simulation and optimization of re-entry trajectories.

However in the guidance model the future trajectories are predicted with the help of exponential model of atmosphere [20] which uses an exponential equation to find the density of atmosphere as a function of height.

$$\rho(h) = \rho_o \cdot e^{-\frac{h}{H}} \quad 2-12$$

Where, $\rho_o = 1.225 \text{ kg/m}^3$ and $H = 8.434 \times 10^3 \text{ m}$, is known as the atmospheric scale height.

The atmosphere is not isothermal through most of its altitude range; however, the two parameters can be adjusted to give a better fit over the attitude range of interest, say from 5 to 40 km. Acceptable parameters would be $\rho_o = 1.752 \text{ kg/m}^3$ and $H = 6.7 \times 10^3 \text{ m}$.

A table of various atmospheric properties usually required for the computation of other atmospheric properties like temperature, pressure, and local sonic velocity, is given in Table A-3.

2.1.4 Re-entry Heating

A vehicle entering a planetary atmosphere from space possesses a large amount of kinetic energy due to its speed. When it enters the atmosphere, a shock wave is formed ahead of the nose of the vehicle, heating the atmosphere in this region to a very high temperature. The velocity of the vehicle is continuously reduced due to the drag force of atmosphere. In this way the kinetic energy is converted into heat. This substantial amount of heat energy is transferred to the vehicle mainly through convection. At higher speed and high temperatures, however, radiation from the shock layer also constitutes a considerable portion of total heat transferred to the vehicle. If all the energy in the form of heat is transferred to the vehicle, it would be enough to vaporize the entire vehicle. But in actual a large amount of energy is diverted away from the vehicle to the atmosphere. This is done either by the action of strong shock wave, or by rejecting the heat back to the atmosphere.

The calculation of total heat transfer rates available to the vehicle is divided into convective heat transfer in the stagnation point region and the radiation heat transfer.

Stagnation Point Convective Heat Rate

Many correlations exist for the estimation of convective heat transfer in the stagnation region namely the optimized Kemp correlation [18], Verant Sangier correlation [18], which involves the computation of a number of aerothermodynamic properties behind the shock wave region as well as the computation of temperature at the surface of vehicle. A large computational effort is needed for the solution of such correlations. It is better to use an empirical relation at this stage to estimate the convective heat transfer rate at stagnation

points e.g. by using a simple and well known empirical relation given by Anderson [3].

$$q_c = 1.83 \times 10^{-8} V_\infty^3 \sqrt{\frac{\rho_\infty}{R_N}} \quad 2-13$$

Where ρ_∞ and V_∞ are the free air density and speed and R_N is the nose radius. According to this relation convective heat transfer to the vehicle is inversely proportional to the nose radius, i.e. a vehicle having larger nose radius will experience lower convective heat rate as compared to vehicle with smaller nose radius, at an instant when both have same velocity and atmospheric condition. Since atmospheric density directly influences the convective heat rate, therefore an entry at a steep entry angle result in higher convective heat rate since the vehicle penetrates deep into the dense atmosphere.

Radiation Heat Rate

Intense radiative heat transfer from high temperature shock layer to the surface of super-orbital re-entry vehicle is also an important engineering consideration in the design of thermal protection system. In orbital and sub-orbital re-entry vehicles the radiation heat transfer is negligibly small. A simplified method to calculate radiative heat transfer rate given by Tauber and Sutton [45] is adopted here.

$$q_r = 4.736 \times 10^4 R_N^a \rho_\infty^b f(V_\infty) \quad 2-14$$

Where exponent a and b are as follows and $f(V_\infty)$ are tabulated values (Table A-4).

$$a = 1.072 \times 10^6 V_\infty^{-1.88} \rho_\infty^{-0.325} \quad 2-15$$

$$b = 1.22 \quad 2-16$$

Blunt re-entry vehicle with large frontal area i.e. large nose radius, will definitely absorb more radiation, which is also clear in the Equation 2-14 where the nose radius is directly proportional to radiation heat transfer. This is exactly opposite to convective heat transfer where the heat transfer is lesser for blunt vehicles. Since radiation heat flux become negligible at velocities lower and 9 km/s, therefore a compromising solution is to select larger nose radius e.g. in case of a lunar return mission with entry velocity of about 11 km/s. This is because during the re-entry flight phase when the radiation heat transfer is considerable, the time of flight is shorter and the atmospheric density is lower as compared to remaining flight.

Anderson [4] compared radiative and convective heat transfer rates of a re-entry vehicle with nose radius of 4.57m at an altitude of about 61 km as a function of velocity, which is shown below in Figure 2-2. The limitation of Tauber's model that it does not calculates radiation heat flux for vehicle velocity lower than 9 km/s is clear in this figure, where it can be seen that near a velocity of 10 km/s, the radiation heat flux decreases rapidly with velocity.

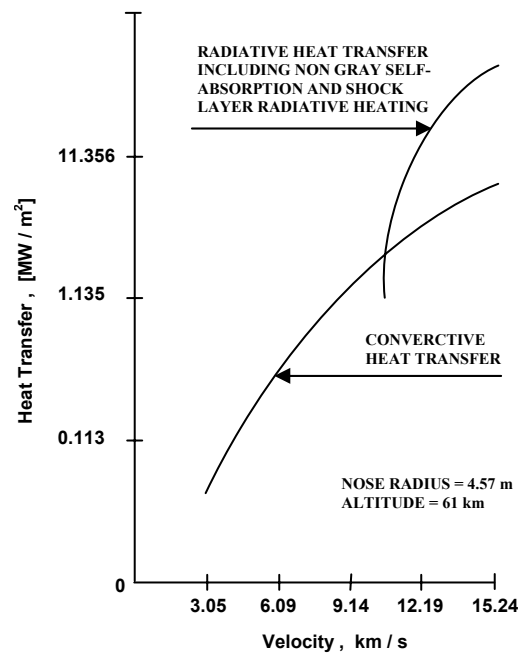


Figure 2-2: Comparison of radiative and convective stagnation point heat transfer [4]

2.2 Vehicle Model

Figure 2-3 represents a vehicle model in general. The origin of body coordinate system, which is also explained in section A.1, is at centre of gravity (CG) of the vehicle. The aerodynamic forces, which are defined in the aerodynamic coordinate system in section A.2, act on the centre of pressure (CP) of the external surface of vehicle.

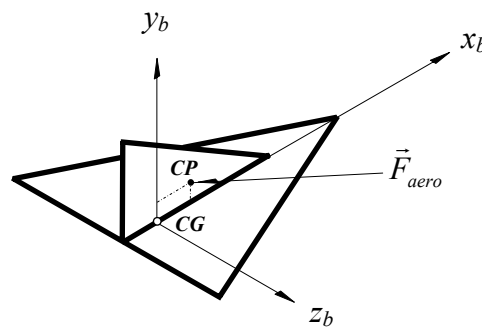


Figure 2-3: Generic vehicle model

In order to simplify the vehicle description, the following assumptions are made:

1. The vehicle maintains constant mass throughout re-entry (i.e. any effects of fuel usage and ablation are ignored).
2. The vehicle produces no thrust.

3. The vehicle experiences no side forces (i.e. there is no sideslip angle).
4. Air frame is assumed to be rigid, i.e. aero-elastic effects are not included in equations of motions. Hence all mass bound by the surface of the spacecraft forms an un-deformable body, so called “rigid” body.
5. Since dynamical equations for rotational motion of the vehicle is not considered in the 3DOF simulation model, it can be assumed that the *CP* and *CG* lie at same point.

Using the above simplifications the forces acting on the vehicle are defined with the help of various coordinates systems in section A.3.

2.3 Optimization Models

An optimization problem begins with the statement of the task to be accomplished. As an integral part of this task statement, the problem is usually defined by a set of goals or objectives and a set of constraints (either inherent in the system or artificially imposed).

In case of re-entry vehicle, several possibilities exist for modifying re-entry trajectory by controlling bank angle and/or angle of attack. Thus, for a given set of end-conditions, infinite trajectories exists which are mathematically and physically possible. Among them, it is of engineering interest to seek those special paths which meet some optimum requirement.

Generally speaking, the problem of the best operational performance in case of re-entry flight can be stated as the problem of finding a suitable flight path of engineering interest in such a way that an arbitrarily specified function, so called *cost function* is minimum. In practical cases a cost function can be, for instance, instantaneous heat load or total heat load, mechanical load, or dynamic pressure.

In general the selection of the optimum re-entry flight path is a complex variational problem. The solution to this problem by classical Euler-Lagrange methods [38] is burdened with severe difficulties. Even in the simple cases these methods lead to the necessity of solving a boundary value problem of a complex system of differential equations. For the atmospheric flight phase the problem becomes still lengthier due to the necessity, of selecting a flight program taking into account the constraints imposed on the control system and the vehicle design (for example, on the angle of attack, in the region of high dynamic pressures, etc.). Actually these constraints in the individual phases of a flight program design will so narrow the sphere of the possible variations in the control programs, that for these phases the solution to the variational problem by classical methods of the calculus of variations does not have practical significance.

The considerations presented above lead to the use of optimization methods for selecting optimum trajectory, on the basis of ideas of the direct methods of solving variational problems. In this connection, the numerical methods [67] can be used to find a finite number of discrete parameters which leads to the optimum

trajectory. A summary of numerical optimization methods for trajectory optimization is presented by Betts [9]. Classical gradient methods, which employ a search along the gradients of the objective function, have been widely used for optimization of large variety of problem. However, these methods have the disadvantage that they fail at singularities where no derivative of the function exists. Linear fitting procedures to mathematical functions which may be applied to non-linear problems were defined as Simplex methods by Nelder and Mead [53]. It uses linear adjustment of the parameters until some convergence criterion is met. It does not use derivatives, which confers safer convergence but the convergence because of linear adjustments is relative slow as compared to Gradient methods.

An optimization model in general finds the minimum of a function called the cost function while satisfying a set of constraints (either inherent in the system or artificially imposed). Thus an optimization problem can be written mathematically as:

$$\begin{array}{ll} \text{Minimize a cost function} & F(\vec{u}(t)) \\ \text{subject to final constraints} & \vec{g}_i(\vec{u}(t))=0 \\ \text{and in flight boundary constraints} & \vec{g}_j(\vec{u}(t))\leq 0 \end{array}$$

In case of re-entry flight equations of motion written in the form of differential equation below should be solved.

$$\dot{\vec{X}} = f(\vec{x}(t), \vec{u}(t)) \quad \text{2-17}$$

The state vector $\vec{X}(t)$ represents state vector including components of position and velocity of the vehicle, defined by r the distance to earth centre, λ and δ the geocentric longitude and latitude respectively, V the vehicle velocity, γ and χ the flight path angle and the flight azimuth respectively. The continuous control vector $\vec{u}(t)$ of equation 2-17 is approximated by a set of parameters \vec{p} of the control model discussed before.

The function of control model is to give a continuous time history of control commands during the complete flight time. To solve the problem of finding a continuous control history, guiding the vehicle to its desired target state, the profile is approximated by a set of linear and constant pieces, which is called parameterization or control model. The problem is thereby reduced to find sets of parameters $(t_i ; p_i)$ characterizing the control history (parameter optimization problem).

The optimization and guidance programs used for this thesis utilise non linear programming techniques combined with steering command parameterisation to generate and evaluate trajectories. The optimization program makes use of a complex optimization routine, sequential quadratic programming algorithm NLPQL method contained within the International Mathematics Standard Library (IMSL) [64], to find an optimized set of control parameters for a prescribed cost function

and restrictions only once at the beginning of a mission phase, whereas the guidance program makes use of a simplified and fast routine of a Gradient Projection Algorithm (GPA) [31] in order to have less computation load onboard during the entry flight.

2.3.1 NLPQL Subroutine

The NLPQL routine [64] contained within IMSL is used for the purpose of optimization of entire re-entry flight path before the vehicle actually re-enters the Earth atmosphere. This routine uses sequential programming method since it generates and successively a sequence of quadratic programming (SQP) sub-problems. SQP is one of the most popular and robust algorithms for nonlinear continuous optimization. The NLPQL routine is utilized only as a black box for this application, passing the required inputs to the routine. References [43,64] may be consulted for more detail.

2.3.2 Gradient Projection Algorithm

Gradient projection algorithm [31] is used for the purpose of future trajectory regeneration during the guidance loop. This algorithm is a parameter optimization scheme which combines, on each iteration, a constraint restoration step and an optimization step. The guidance program uses only the restoration step to conform the constraints. The optimization step is skipped because an optimized solution was already found by NLPQL during the optimization phase before re-entry. Following relations are used to update the parameterized control vector \vec{p} in order to restore the trajectory in a direction where all the constraints are satisfied.

$$\vec{p}_{k+1} = \vec{p}_k + \Delta p_k \quad \mathbf{2-18}$$

Where,
$$\Delta p_k = -\vec{H}_k \cdot \vec{G}_k \left[\vec{G}_k^T \cdot \vec{H}_k \cdot \vec{G}_k \right]^{-1} \cdot \vec{g}_k^T \quad \mathbf{2-19}$$

\vec{H}_k is a Quassi-Newton matrix which is approximated as unity matrix. \vec{g}_k is the vector containing all the constraint violations. \vec{G}_k is the Jacobian matrix containing the constraint violation gradients with respect to parameter variation found by a single flight path prediction with forward perturbation of single parameter performed separately for each individual parameter.

$$\vec{G}_k = \nabla \vec{g}(\vec{p}_k) \quad \mathbf{2-20}$$

Since only restoration step is used in guidance, the solution found by this approach is sub-optimal. The minimization of the cost function is not a primary concern as the final flight path is only a slight modification of the pre-optimized trajectory.

2.4 TDS Simulation Tool

Trajectory Dynamics Simulation (TDS) is an IRS in-house simulation tool, which is gradually developed over the past few years under different name and used for different projects to optimize and simulate trajectories of space flight vehicles entering into planetary atmosphere. The program is written in FORTRAN language and simulates the motion of a vehicle as a point mass in a three dimensional space using three degrees of freedom 3-DOF. The layout of the program is such that it is comparatively easy to extend it for the models required for the guided simulations of hyperbolic re-entry vehicles. The original version of TDS had the capability to simulate the open-loop behaviour of the re-entry vehicles in 3-DOF. With open loop it is meant that no guidance is included. A non linear programming method (NLP) method is included to find optimum trajectories for a given cost function as a function of a finite number of control parameters with upper and lower bounds and subjected to equality and inequality constraints. Aerodynamic models of several known vehicles are already available in the program and can be easily used. Various models of Earth gravitation, atmosphere, and geometry are already available in the program. The data of these models can be changed, for entry into other planet. The mission environment can also be extended for simulations on planets other than Earth if the geometric, gravitational and atmospheric data of the planet is known.

The software tool was used throughout this research for the mission and system analysis of various vehicle configurations. For the mission analysis of the hyperbolic re-entry vehicle, several extensions to TDS were required. Radiation heat transfer can not be neglected for such missions as compared to sub-orbital and orbital missions where it is negligibly small [4,45] Therefore, A simple model of Tauber and Sutton [45] based on empirical relations was added to the simulation program. The guidance strategy, which was designed and proposed for such mission, was implemented in FORTRAN and in order to generate guidance commands, TDS tool was used as a sub-program for the prediction of future trajectories. Furthermore, to do a sensitivity analysis in an efficient manner, the definition sensitivity parameters and execution of guided simulations and the post processing of the results were incorporated outside the simulation environment with the help of MATLAB codes.

2.5 Performance of Simulation Tool

In this section the Trajectory Dynamics Simulation program will be evaluated in order to see that the simulated outputs are good approximation of reality. The best way to evaluate a flight simulation program is to simulate it for existing vehicle and mission.

The TDS program was developed at IRS over the past few years and used on different projects for simulation and optimization of trajectories of various space flight vehicles returning from *sub-orbital* and *orbital* missions. For this thesis, this simulation program is used as a basic tool for the mission and system analysis of

various re-entry vehicles returning from *interplanetary* missions, where the issues like heat load, deceleration load and the problem of skip-out become more prominent. Further more the simulation program is used as trajectory simulator and trajectory predictor, while setting up the guidance scheme for these missions.

Therefore, before this simulation program is used for complex missions of interplanetary re-entry and for the development of guidance scheme, a simple vehicle and mission is first studied with this program. A summary of mission analysis of Stardust re-entry vehicle is given in the following section. This vehicle and mission is simple in a sense that it used a purely ballistic re-entry method to enter the Earth atmosphere and does not generate aerodynamic lift. The vehicle is not controlled by any means and it travels through the atmosphere only under the influence of gravity and drag forces. Therefore it will be best to study the simulation tool for this mission, since no control is required. Daniela Bolz [14] has also performed analysis of various re-entry mission (including Stardust) using this simulation tool.

2.5.1 Comparison with Stardust Data

The Stardust spacecraft was launched on February 7, 1999 with Delta II rocket and returned safely to Earth on Jan. 15, 2006. The primary goal of Stardust was to collect dust and carbon-based samples from Comet Wild 2. The capsule carrying cometary and interstellar particles was the fastest ever entry of a man made object into the Earth atmosphere. The outer profile of Stardust re-entry capsule is shown in Figure 2-4. The conditions at entry [55,56] of the capsule into the earth atmosphere were:

- Altitude = 125 km
- Entry angle = -8.2° (inertial)
- Entry velocity = 12.8 km/sec (inertial)
- Mass = 45.8 kg
- Ballistic Coefficient = 60 kg/m^2
- Node radius = 0.23 m
- Base Area = 0.52 m^2

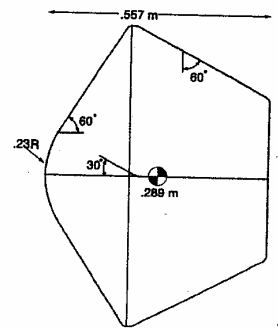


Figure 2-4: Stardust re-entry vehicle [55]

Lift coefficient is taken as zero for simulation, as the flight is purely ballistic. A value of ballistic coefficient β of 60 kg/m^2 [55], is used to find the drag coefficient C_D of re-entry capsule by using following equation.

$$C_D = \frac{m}{\beta \cdot S_{ref}} = 1.468 \quad 2-21$$

Where; m = Mass of re-entry capsule

and, S_{ref} = Reference area (base area)

Stardust, being a ballistic re-entry vehicle i.e. with zero lift to drag ratio, enters directly into the Earth atmosphere experiencing high heat and deceleration loads. Simulated trajectories with TDS Simulation tool for given entry conditions are compared with Stardust re-entry trajectory data [62]. Figure 2-5 and Figure 2-6 for example compare histories of velocity and stagnation point convective heat flux with respect to height.

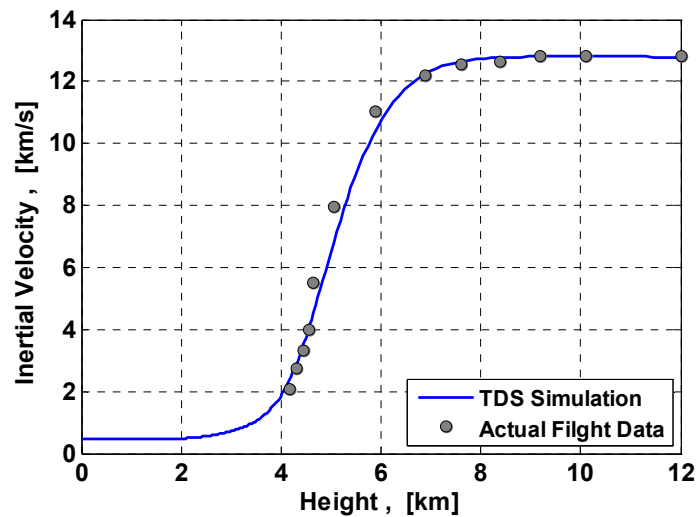


Figure 2-5: Stardust: Velocity profiles of simulation and actual data

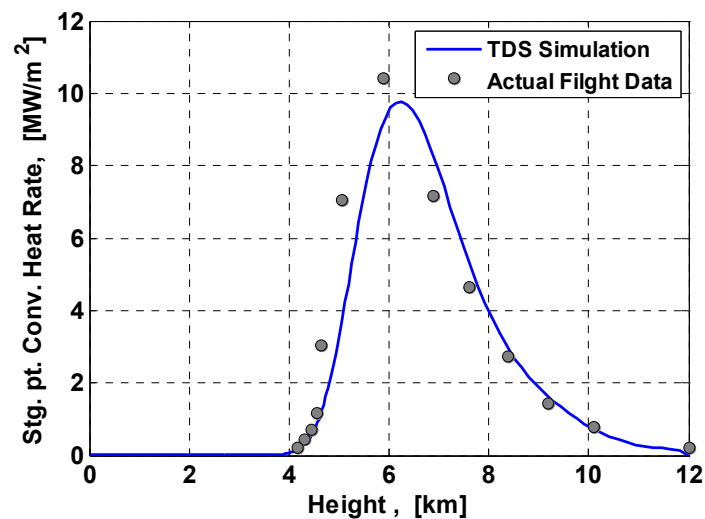


Figure 2-6: Stardust: Heat transfer profiles of simulation and actual data

The simulation results seem to be in a good agreement with actual data. Peak value of heat flux in both profiles arrives nearly at the same altitude. A closer look at the velocity profile reveals that in actual data the velocity at a point of peak value of heat flux has a slightly higher value as compared to simulation results, which also results in a slightly higher value of peak heat flux.

2.5.2 Qualitative Performance

In order to prove the functionality of the simulation tool and to investigate the qualitative behaviour of different trajectory parameters, several trajectories with different entry conditions, different atmospheric conditions and different vehicle properties were simulated. A similar analysis was also done by Daniela Bolz [14] and presented here to see the performance of simulation tool.

At first, trajectories at an inertial velocity of 12.8 km/s at entry point was simulated with a variation in flight path angles to see the effect on range and also to find out the maximum entry angle at which vehicle once enters dense atmosphere, does not skip out again. Figure 2-7 shows the trajectories in vertical plane for different entry angles.

An entry angle of -6.3° is found to be the maximum angle for 12.8 km/s of entry velocity at which vehicle descends continuously without any skip. An angle slightly higher than this value e.g. -6.14° causes the vehicle to ascend again and re-entering for the second time till touchdown at a distance of more than 3500 km from the landing point of trajectory with highest entry angle without skip. A line crossing all the trajectories in this figure shows the points of maximum stagnation point heat flux. It is clear that steeper the trajectory is; deeper in atmosphere is the occurrence of this point.

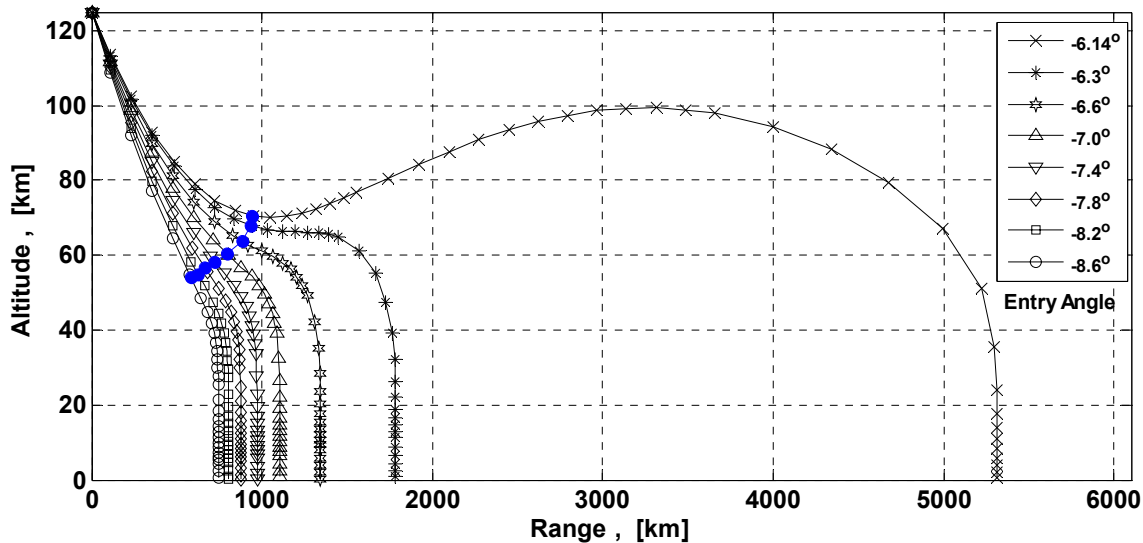


Figure 2-7: Stardust re-entry trajectories; range versus altitude at different entry angles

Because of very fast re-entry into the earth atmosphere, aerodynamic heating is very important parameter while selecting suitable entry conditions. Deceleration is also equally important for such missions but because of unmanned re-entry vehicle decelerations of more than 30 g's are accepted for this mission. Figures below present variation of maximum stagnation point heat flux and integral load (Figure 2-8) and variation of deceleration load (Figure 2-9) for different entry velocities and entry angles.

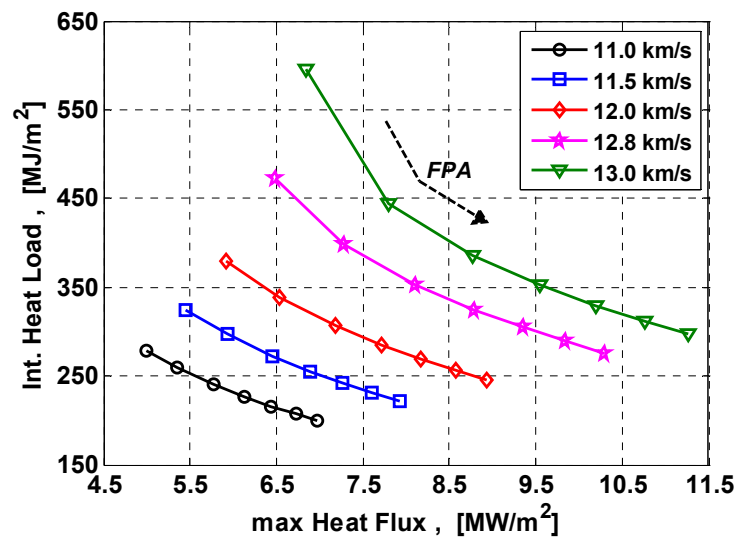


Figure 2-8: Stardust: Effects of entry velocity and entry angle variations on max stagnation point heat flux

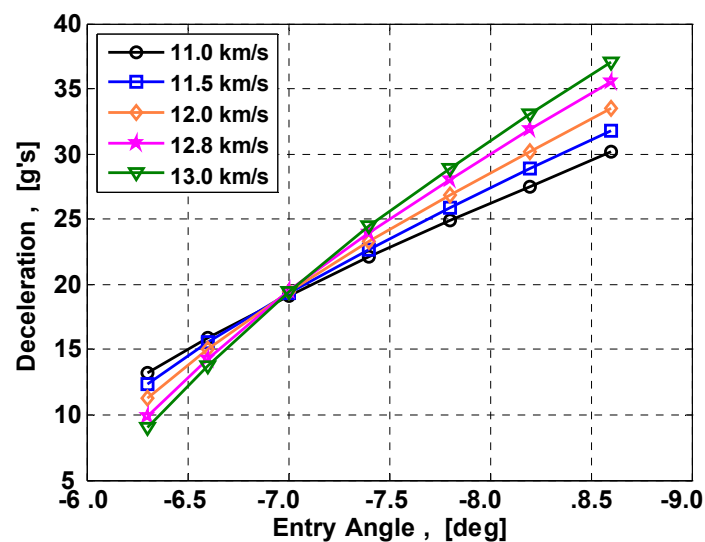


Figure 2-9: Stardust: Effects of entry velocity and entry angle variations on deceleration level

Vehicle mass and atmospheric density is then taken as parameters with a variation of $\pm 10\%$ to investigate their influence on trajectory parameters. A significant influence of variation of vehicle mass on maximum stagnation point heat flux is observed, whereas there is only a little variation of deceleration loads (Figure 2-10, Figure 2-11). It is observed that the variation of atmosphere does not influence the trajectory to a greater extent as compared to variation of vehicle entry velocity and entry angle, which cause a large variation in aerodynamic and aero-thermal loads.

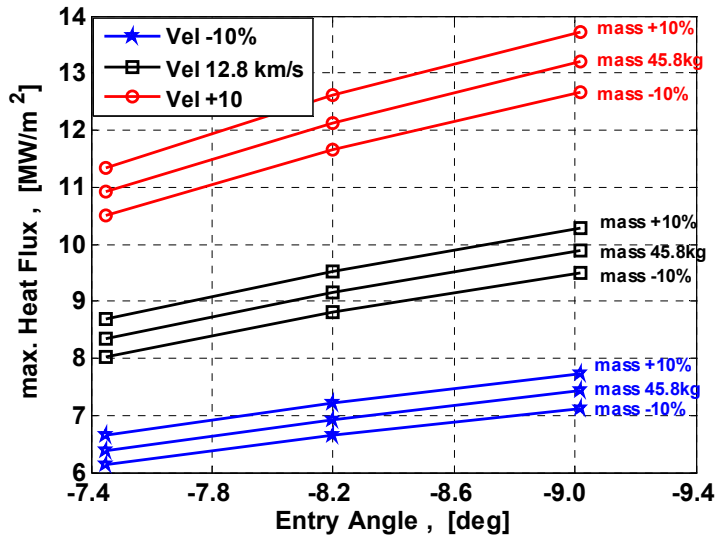


Figure 2-10: Stardust: Effects of different entry mass on max stagnation point heat flux

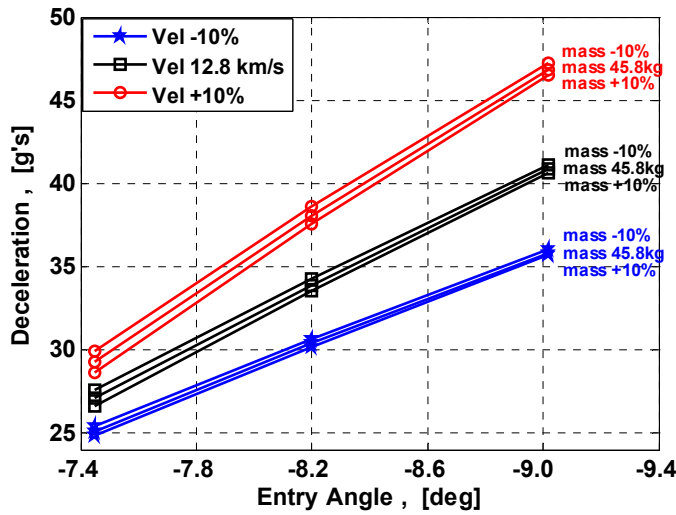


Figure 2-11: Stardust: Effects of different entry mass on deceleration level

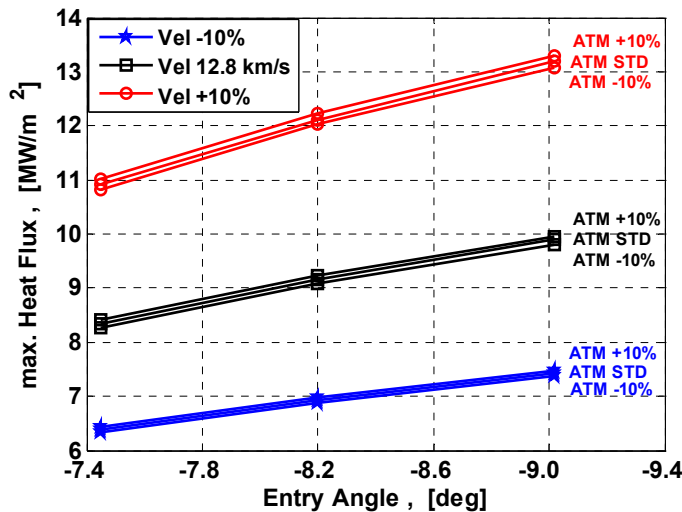


Figure 2-12: Stardust: Effects of atmospheric density variations on max stagnation point heat flux,

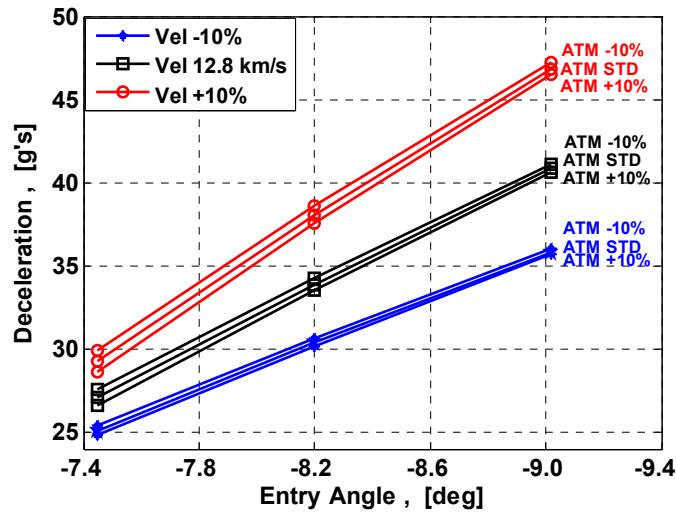


Figure 2-13: Stardust: Effects of atmospheric density variations on deceleration level

2.6 Summary

Re-entry trajectories of Stardust re-entry missions were simulated in order to evaluate the simulation environment. Firstly the simulated trajectory results with actual entry conditions are found to be closer to the flight data. Secondly the results of TDS simulation tool is found to be in agreement with dynamics and aerothermodynamics, i.e. the variations of aerodynamic and aero-thermal loads and deviation of trajectories from standard conditions are found to be in accordance with the variation in input conditions. All the trajectories are simulated for uncontrolled direct entry into the atmosphere with lift to drag ratio equal to zero.

The influence of variations of entry conditions, variation of atmospheric density and variation of vehicle mass on deceleration and heat loads investigated in the previous section, can be summarized with the help of following figures (Figure 2-14). Both heat flux and deceleration load are more sensitive to variations of entry velocity and entry flight path angle as compare to variations of mass and atmosphere.

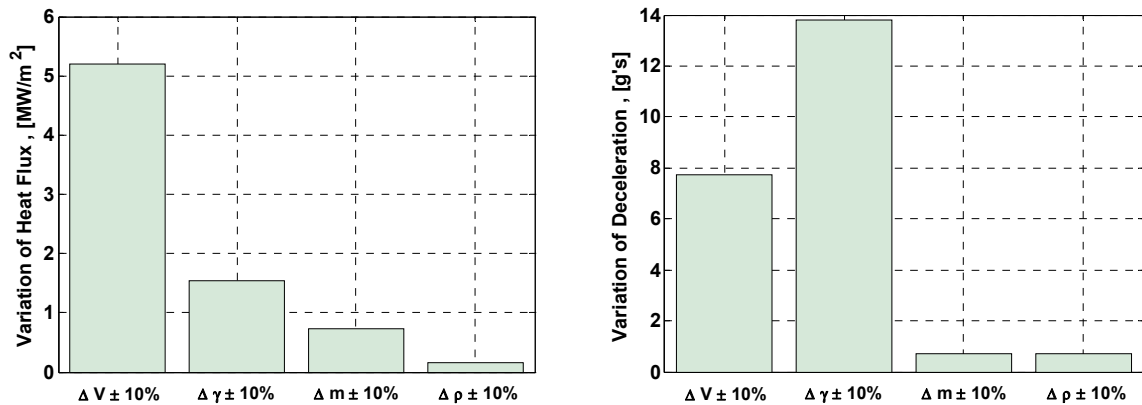


Figure 2-14: Stardust: Influence of variations on heat flux and deceleration loads

3 Mission and Vehicle Analyses

Mission and system analysis is done for three different kinds of vehicles; an Apollo like capsule [5,6,7], a flattened bi-conic [68] and a winged vehicle [58]. The reference mission for the investigation is Earth capture and re-entry phase of lunar return mission with crew inside. Two kinds of re-entry approaches are considered for investigations; direct re-entry with steep entry angle for low lift to drag vehicles and re-entry with constant altitude phase for lifting vehicles, which utilize their lift to maintain a constant altitude.

3.1 Reference Mission

The reference mission for this analysis is a lunar return mission with an orbital inclination of return trajectory of 28.5° with respect to earth equator. For this analysis a Kepler orbit is considered with assumed apogee of 385,000 km, which is the average distance of Moon from centre of Earth. The velocity at Earth atmospheric interface of 120 km above Earth surface (Figure 3-1) is approximated to 11.0 km/sec. (Lunar return missions usually return at velocities ranging between 10 to 12 km/sec). Re-entry capsule of Apollo-8 mission entered the Earth atmosphere at an angle of -6.5° , which is also selected here as an entry angle for mission analysis of Apollo like capsule. In case of flattened bi-conic and lifting vehicles the perigee of the return orbit is selected in such a way that during atmospheric re-entry phase the vehicle attains enough lifting capability to maintain a constant altitude flight phase. After a number of simulations, the angles of -5.1° and -4.0° at for flattened bi-conic and lifting vehicles respectively, found to be suitable for flying such a mission with significant margin.

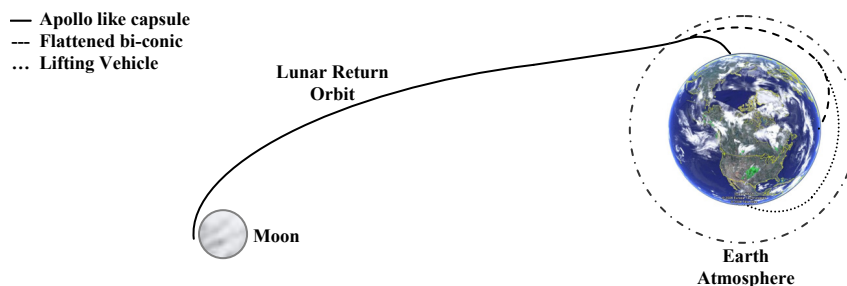


Figure 3-1: Reference Mission

The target landing location for the reference mission is selected on the surface of sea, located approximately 400 km from the westerns coasts of Australia (Figure 3-2). The latitude and longitude of target point are 112° and -30° . This target location is selected because if it will be required in future to aim a target on land instead of sea, then the mission can be easily extend or change to aim for targets somewhere on Australian terrains, e.g. *Woomera* in South Australia, which was also selected for guided simulations of experimental spacecraft *X-38* by M. H. Graesslin [47].



Figure 3-2: Aimed target location for reference mission

3.2 Re-entry Strategy

Two kinds of re-entry approaches are considered for re-entry trajectory simulations Figure 3-3; *direct re-entry* for Apollo-8 re-entry module because of its low lift to drag ratio and *re-entry with constant altitude phase* for lifting vehicles, which utilize their lift to maintain a higher constant altitude in order to decelerate at low heat flux levels. Figure 3-3 shows a simulated trajectory profile of Apollo-8 re-entry [55] (*direct re-entry*) having L/D ration 0.3 and entry angle of -6.9° , and a simulated trajectory profile of a high lifting vehicle [58] (*re-entry with constant altitude phase*) having L/D ration 2.2 and entry angle of -4.0° .

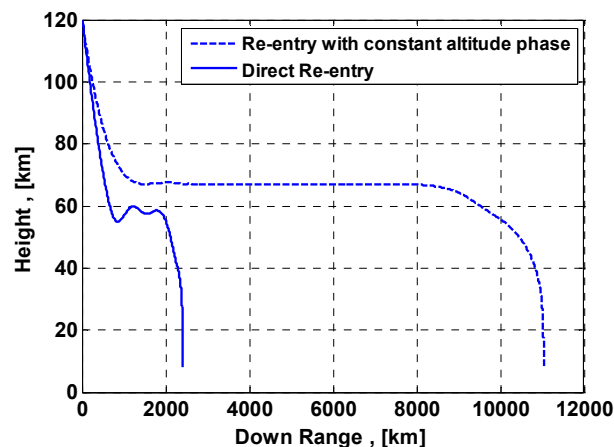


Figure 3-3: Different re-entry strategies

3.2.1 Direct Re-entry

In general, spacecrafts returning to the Earth from an interplanetary mission adopt a direct re-entry strategy. The direct entry trajectory offers the advantage of a “no-miss” scenario which starts at steep entry angle, quickly dissipating excessive kinetic energy, which results in a very high level of deceleration and heat loads. The main parameter that drives a trajectory to “direct” is the perigee of the lunar return orbit. In many unmanned re-entry missions, a ballistic entry method is adopted, where only drag force slows down the vehicle. A purely ballistic entry, in which deceleration levels during re-entry are extremely high, is not survivable by human crew. A semi-ballistic approach is useful in this case, where appropriate control method is used to generate lift in order to reduce deceleration and heat loads.

3.2.2 Re-entry with Constant Altitude Phase

Exploiting lift forces during interplanetary re-entry is being considered by researchers around the world to get more control over the trajectory and guide the spacecraft more precisely to a landing site. Vehicles concepts other than a blunt body, like winged, bi-conic, inflatable ballute design etc. were presented from time to time at various platforms [51,52,58,61,68].

The orbit of the return trajectory is so designed that the vehicle intercepts the outer atmosphere and then exploits vehicle lift to fly at constant altitude and dissipating excess energy using aerodynamic drag. The trajectory from space to ground is divided into three phases:

1. **Hyperbolic approach phase;** which starts with the entry of vehicle into the Earth atmosphere at 120 km above mean sea level, at entry velocity of 11.0 km/s, entry angle of -4.0° for lifting vehicle and -5.1° for flattened bi-conic vehicle, and entry mass of 5000kg. Vehicle at super-orbital speed generates enough centrifugal force to skip out of upper atmosphere. To balance this centrifugal force vehicle enters at an initial bank angle of 180° at atmospheric interface (i.e. upside down) in order to have a component of lift in a direction to Earth centre. In this way vehicle is able to be captured by earth atmosphere.
2. **Constant altitude phase;** with a control law the lift is controlled by angle of attack variation and also bank angle modulation, in order to keep the altitude constant. Vehicle’s drag slowly decelerates the vehicle during this phase and hence required angle of attack also reduces to maintain the altitude. Practically the vehicle is required to be insulated mostly on one side i.e. on the side of stagnation point. In this regards a control law find values of angle of attack not lower than a certain value. Bank angle is modulated to get the desired lift in vertical plane when the angle of attack requirement is lower than the specified lower limit. Bank angle is gradually reduced from 180° to 90° (or 270°) where speed become equal to instantaneous orbital speed and then further reduced to 0° as the speed also gradually reduces.

3. **Final descend phase;** starts when the speed of the vehicle is reduced during constant altitude phase to such a level that it can safely bring down to the Earth surface. Bank angle is again modulated during this phase to reach desired landing site.

3.3 Vehicle Configurations

Three different configurations of re-entry vehicles were considered to perform mission and system analysis. Apollo like capsule [5,6,7] with an L/D ratio of about 0.3, flattened bi-conic [68] with an L/D ratio of about 0.7 and winged vehicle [58] with an L/D ratio of about 2.2 are categorised as low, medium and high lifting vehicles. Assessment of various performance parameters were done for these configurations, which will be presented in section 3.5.

3.3.1 Apollo Re-entry Vehicle

Apollo-8 was the second manned mission of the Apollo space program, launched on Dec. 21, 1968. The command/service module returned back to the Earth after orbiting the moon. Command module/service module separated 17.4 minutes before the entry of command module into the Earth atmosphere. The re-entry module (Figure 3-4) followed a guided entry profile and landed on Dec. 27, 1968, in the Pacific Ocean at 8 degrees 8 minutes north latitude and 165 degrees 1 minute west longitude. The actual conditions at entry interface are presented below:

- Altitude = 120.0 km
- Entry angle = -6.5° (inertial)
- Entry velocity = 11.0 km/sec (inertial)
- Mass = 5806 kg
- Latitude = 20.7268°
- Longitude = 176.9056°
- Node radius = 4.69 m
- Base Area = 12.02 m²

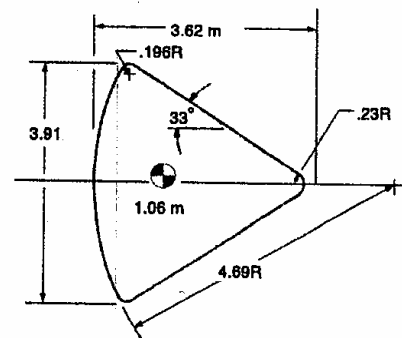


Figure 3-4: Apollo Re-entry Module [55]

Aerodynamic force coefficients for Apollo-8 re-entry module are calculated by following equations, derived by *Sforza* [54] based on *Newtonian* method.

$$C_{D,0} = \left(2 - \frac{k-1}{k+1}\right) \frac{(1 + \cos^2 \theta)}{2} \quad 3-1$$

The quantity θ is half cone angle k is the ratio of specific heats: $k=1.4$, the standard air value, and $k=1.2$, a value more representative of the hot gas around a re-entering space capsule. Lift and drag coefficients for a capsule orientation (Figure 3-5) can be calculated as follows. Aerodynamic coefficients calculated from these

equations (Figure 3-6) found to be in agreement with CFD and experimental results of *Padila and Boyd* [35].

$$C_L = \left[2(1 - C_{D,0}) - \left(3 - \frac{5}{2} C_{D,0} \right) \sin^2 \alpha \right] \sin \alpha \quad 3-2$$

$$C_D = C_{D,0} + 12(1 - C_{D,0}) \sin^2 \frac{\alpha}{2} - 6(6 - 5C_{D,0}) \sin^4 \frac{\alpha}{2} + 4(6 - 5C_{D,0}) \sin^6 \frac{\alpha}{2} \quad 3-3$$

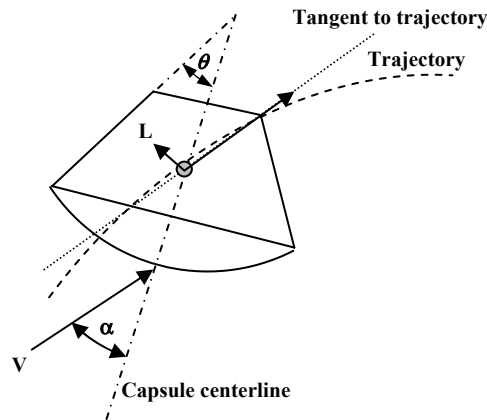


Figure 3-5: Orientation of Capsule for Positive Lift Coefficient

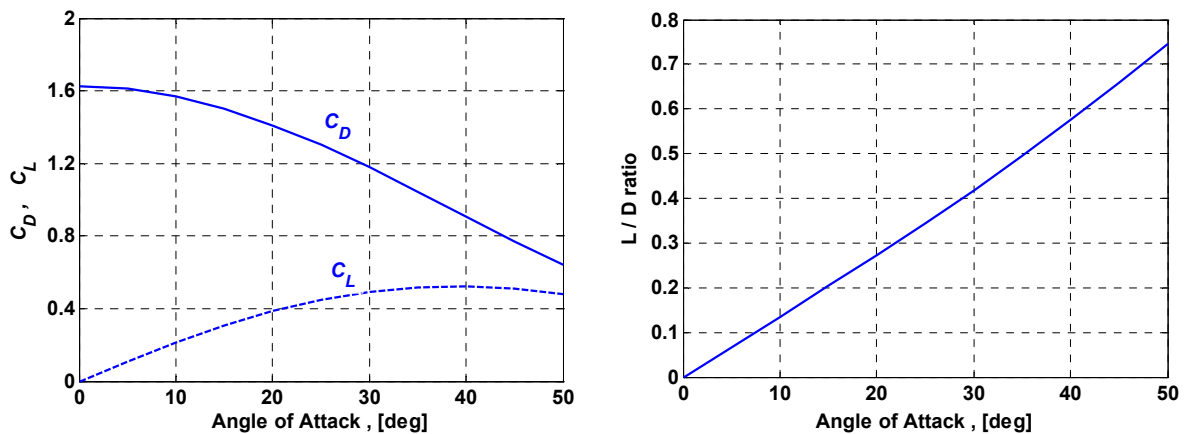


Figure 3-6: Aerodynamics of Apollo-8 re-entry module (a) lift and drag coefficients (b) lift to drag ratio

Aerodynamic properties of Apollo-8 re-entry module are investigated [35,54], and an average value of 1.4 for drag coefficient and 0.3 for L/D ratio can be taken for a fixed angle of attack of 20° . TDS program is also restricted to stop at an altitude of 8.125 km, where the drogue was actually deployed to Apollo re-entry module. To reach landing site, equality constraints on geodetic latitude and longitude at the end of flight are used.

3.3.2 Lifting Re-entry Vehicle

Exploiting lift forces for manned interplanetary re-entry missions has been an interesting research topic, because of high deceleration loads of more than 7 g's during re-entry of early Apollo missions. Different re-entry strategies like aerocapture, aero-breaking and different vehicle concepts were studied from time to time by people. A concept of winged vehicle with high aerodynamic efficiency (Figure 3-7) entering Earth atmosphere at hyperbolic velocities was proposed by *Monti, et al.* [58]. This vehicle is considered here as a candidate for comparative analysis. The conditions at entry of the vehicle into the earth atmosphere are:

- Altitude = 120 km
- Entry angle = -4.0° (inertial)
- Entry velocity = 11.0 km/sec (inertial)
- Mass = 5000 kg
- Wing tip radius = 0.1 m
- Wing planform area = 50 m²

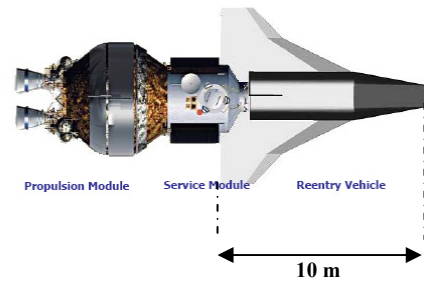


Figure 3-7: High-lift vehicle [58]

Newtonian flow approximation is considered to calculate drag and lift forces, because it is a simple and attractive method for developing simple relationships to predict the aerodynamic properties of bodies at hypersonic speed. Following relations given by Anderson [2] for drag and lift coefficient are considered.

$$C_D = \sin^3 \alpha + 0.1 \quad 3-4$$

$$C_L = 2 \cdot \sin^2 \alpha \cdot \cos \alpha \quad 3-5$$

Second term in Equation 3-4 accounts for zero lift drag. Aerodynamic coefficients and lift to drag ratio calculated from above equations are shown in Figure 3-8

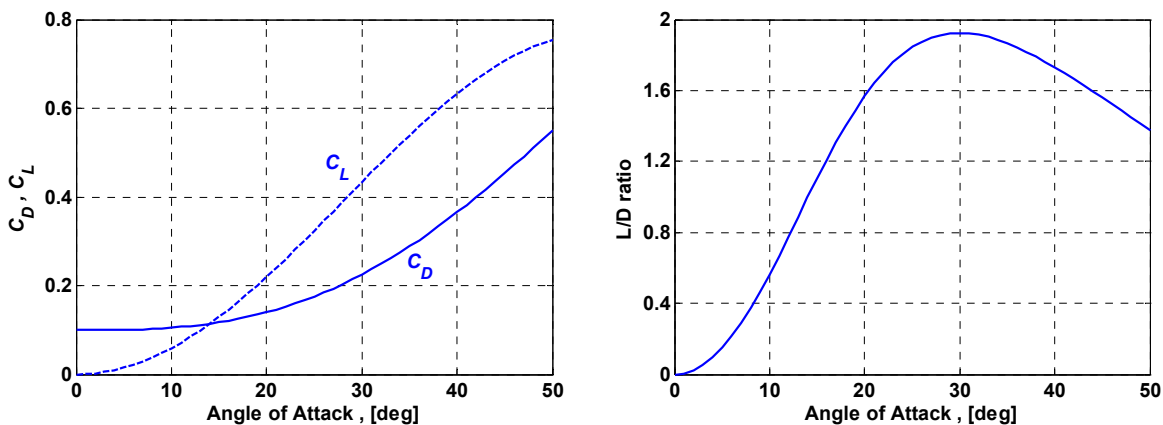


Figure 3-8: Aerodynamics of high lifting vehicle (a) lift and drag coefficients (b) lift to drag ratio

Re-entry approach with constant altitude phase is used with a trajectory that has a higher perigee of lunar return orbit only intercepts the outer atmosphere. The trajectory from space to ground is divided into three phases, i.e. *hyperbolic approach phase*, *constant altitude phase* and *final descend phase*.

3.3.3 Flattened Bi-conic Re-entry Vehicle

Apollo like capsule having an advantage of the simplest design enters at high deceleration levels. This is exactly opposite for high lifting vehicle which despite experiences very low deceleration load is very complex in design. Flattened bi-conic vehicle (Figure 3-9), presented by Whitmore, et al. [68] lies in between the two, is comparatively simple in design and it is selected as third candidate vehicle for comparative analysis here but scaled down for a total mass of 5000kg. The conditions at entry of the vehicle into the earth atmosphere are:

- Altitude = 120 km
- Entry angle = -5.1° (inertial)
- Entry velocity = 11.0 km/sec (inertial)
- Mass = 5000 kg
- Nose radius = 0.75 m
- Flattened area = 6.9 m^2

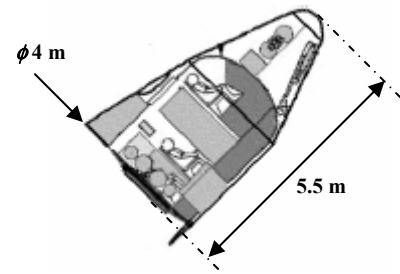


Figure 3-9: Flattened bi-conic vehicle [68]

Aerodynamics coefficients for a reference area of 6.9 m^2 as shown in figure below (Figure 3-10) are assumed to be same as trimmed longitudinal aerodynamic data by Whitmore, et al. [68]. The following relations were deduced to find aerodynamic coefficient for flattened bi-conic vehicle, instead of data interpolation. These relations give approximately the same results.

$$C_D = 2.4 \cdot \sin^{2.2} \alpha + 0.5 \quad 3-6$$

$$C_L = 1.6 \cdot \sin \alpha \cdot \cos \alpha \quad 3-7$$

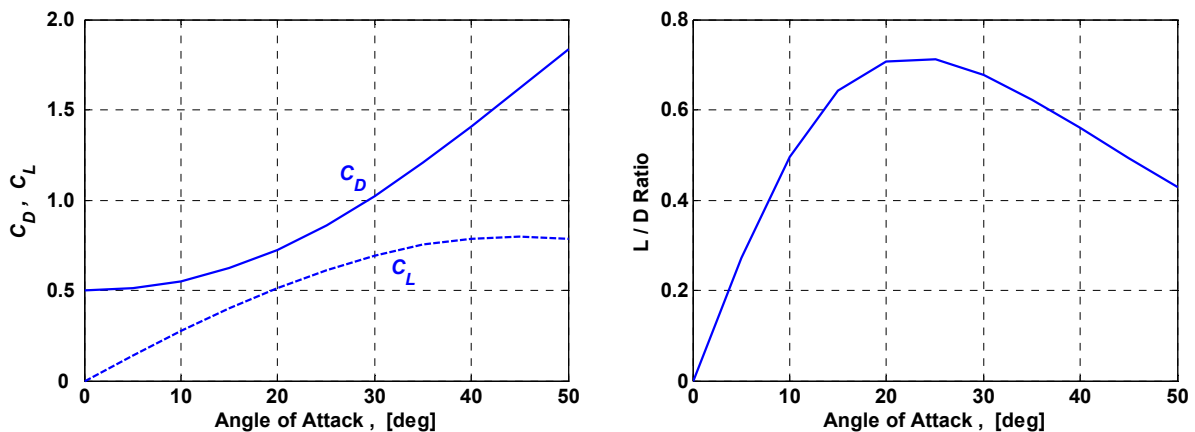


Figure 3-10: Aerodynamics of flattened bi-conic vehicle (a) lift and drag coefficients (b) lift to drag ratio

3.4 Trajectory Simulations

3.4.1 Apollo Vehicle Re-entry Simulation

Re-entry trajectory of Apollo-8 [55] module was simulated for entry velocity of 11 km/s, entry angle of -6.5° and entry mass of 5806 kg, with bank angle modulation to use the lift in order to minimize stagnation point heat flux as well as to reach target point. Because of its low lift to drag ratio of 0.3, this vehicle is incapable of flying at constant altitude for a long duration of time. According to original Apollo guidance algorithm the bank angle during the initial descent phase is so modulated to ensure the atmospheric capture followed by an upward skip (see section A.6) to extend the range if required. In case of Apollo-8 an upward skip was not needed and the vehicle started descending after a few up and down manoeuvres to meet the target point. The simulated trajectory in Figure 3-11 is a result of trajectory optimization of Apollo-8 re-entry module for minimum heat flux as cost function, desired target point as end constraints, and bank angle commands as control parameters. Altitude and flight path angle profiles are compared in Figure 3-11 with actual data of Apollo-8 re-entry as given in post flight mission reports [5,6,7].

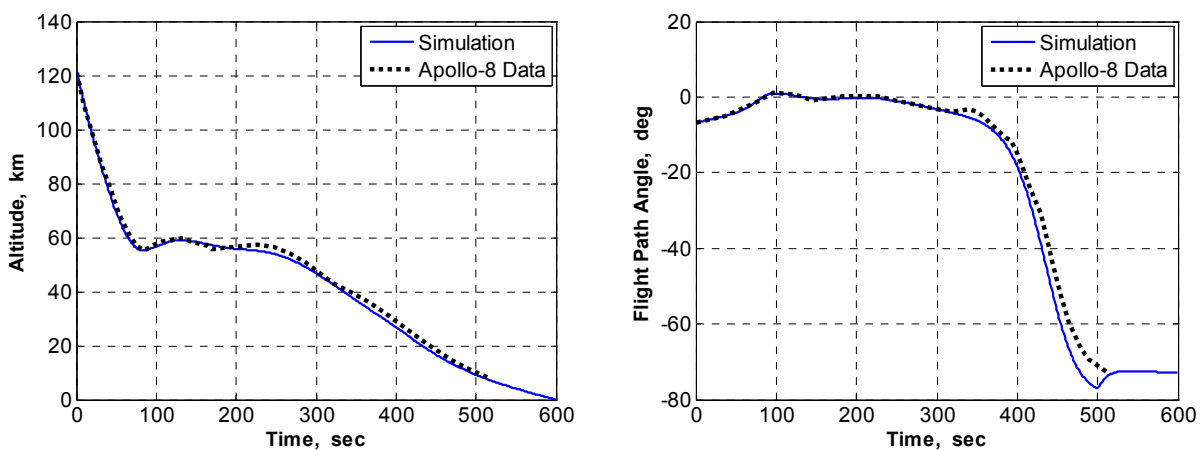


Figure 3-11: Altitude and flight path angle histories simulated and actual flight data of Apollo re-entry trajectory.

Because of steep entry into the Earth atmosphere the vehicle experiences high heat and deceleration loads. A comparison of stagnation point heat transfer rates for both convection and radiation is shown in figures below. Peak radiation heat flux is found to be 39%, of the peak total heat flux. Apollo capsule also experiences high deceleration loading of more than 7 g's (Figure 3-12), which is more than the current safety standards for astronauts [40].

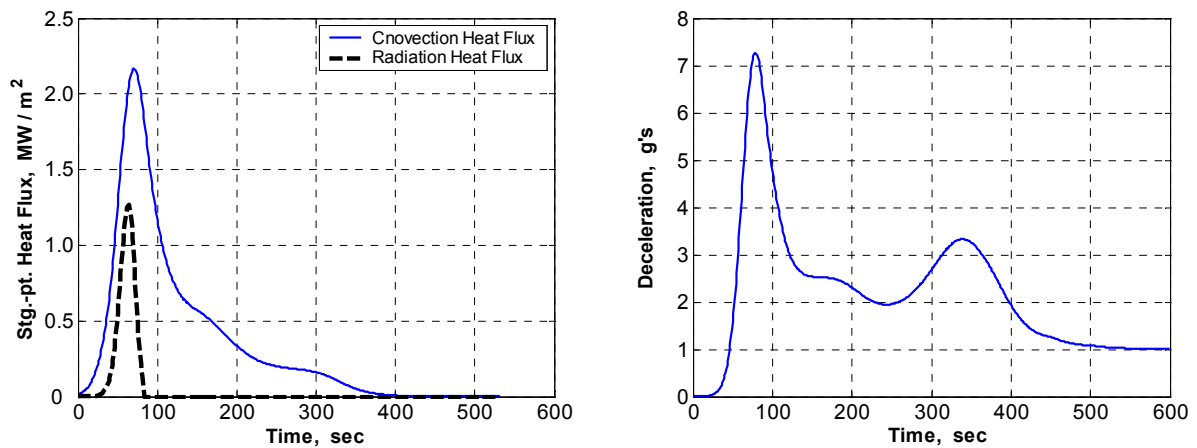


Figure 3-12: Stagnation point convective and radiative heat flux and deceleration load of Apollo re-entry

3.4.2 Lifting Vehicle Re-entry Simulation

Trajectory of high lift vehicle [58] is simulated for a re-entry strategy with constant altitude phase as described in section 3.2.2 and for re-entry conditions as described in section 3.3.2. The trajectory during the initial descend phase is optimized for minimum heat flux as cost function, and angle of attack commands as control parameters. Afterwards, the motion of vehicle is governed by a control law to keep it flying at constant altitude, which can be defined by an equilibrium flight in vertical plane under the hypotheses of flight path angle equal to zero (constant altitude flight) and bank angle equal to 180° (downward lift). Under this hypothesis the constant altitude can be maintained when the maximum available acceleration due to lift force in vertical plane is greater than the sum of the accelerations due to centrifugal force and gravitational force. The final descend phase is also a result of optimization for minimum heat flux as cost function, desired target point as end constraint and angle of attack and bank angle commands as control parameters. As shown in Figure 3-13, the vehicle, after initial descend phase, maintains a constant altitude flight phase at about an altitude of 83 km for a long duration of time.

As seen in bank angle profile (Figure 3-14) that vehicle enters upside down until a point where angle of attack is reduced to a lower limit of 20° . There after angle of attack does not reduce further and bank angle is modulated to compensate for lift requirement. Once the excess lunar-return kinetic energy has been dissipated the vehicle gradually rolls upright and proceeds further with upward lift vector to maintain the altitude and reduce further energy. Monti et al. [58] do not use bank angle modulation but modulate only angle of attack between -45° and $+45^\circ$. Whereas in this research work, the angle of attack always remains positive whereas the bank angle is modulated when the required angle of attack is negative of below a specified lower limit. This difference is also visible in Figure 3-14. The instance, where the vehicle achieves a speed of circular orbit at the local height, occurs shortly after 2000 seconds in both cases. In case of TDS simulation this instant occurs where the bank angle is equal to 90° whereas this instant is seen in the result of Monti et al. at a point where angle of attack is equal to zero.

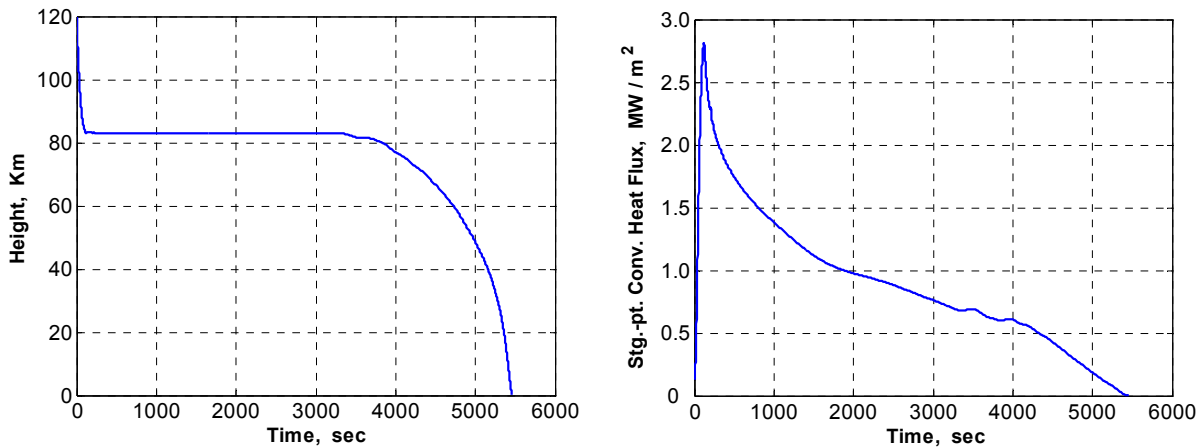


Figure 3-13: Trajectories of high-lift vehicle; (a) time versus altitude, (b) time versus stagnation point heat flux

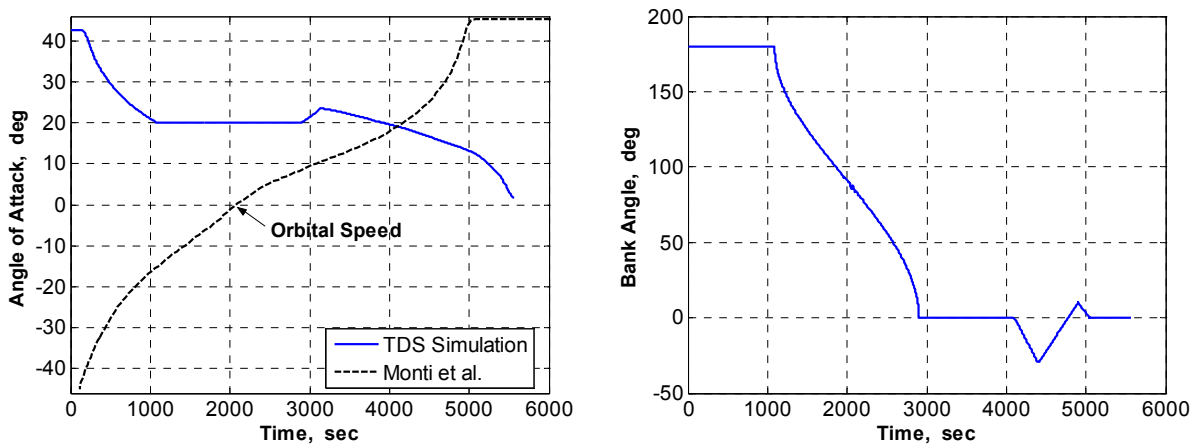


Figure 3-14: Trajectories of high-lift vehicle; (a) time versus angle of attack, (b) time versus bank angle

3.4.3 Flattened Bi-conic Vehicle Re-entry Simulation

Like high lifting vehicle, similar re-entry approach with constant altitude phase is used for flattened bi-conic vehicle [68], with a trajectory that has an entry angle lower (steeper) than the case of high lifting vehicle but higher (shallower) than Apollo re-entry module. Following the same strategy for angle of attack control and bank angle modulation as of high lifting vehicle and the same optimization approached during initial and final descend phases, the re-entry trajectory of flattened bi-conic vehicle is simulated and presented below (Figure 3-15). The vehicle enters the Earth atmosphere at an inertial velocity of 11 km/s with an initial flight path angle of -5.1° . At about an altitude of 67 km the motion of vehicle is governed by a control law to keep it flying at constant altitude.

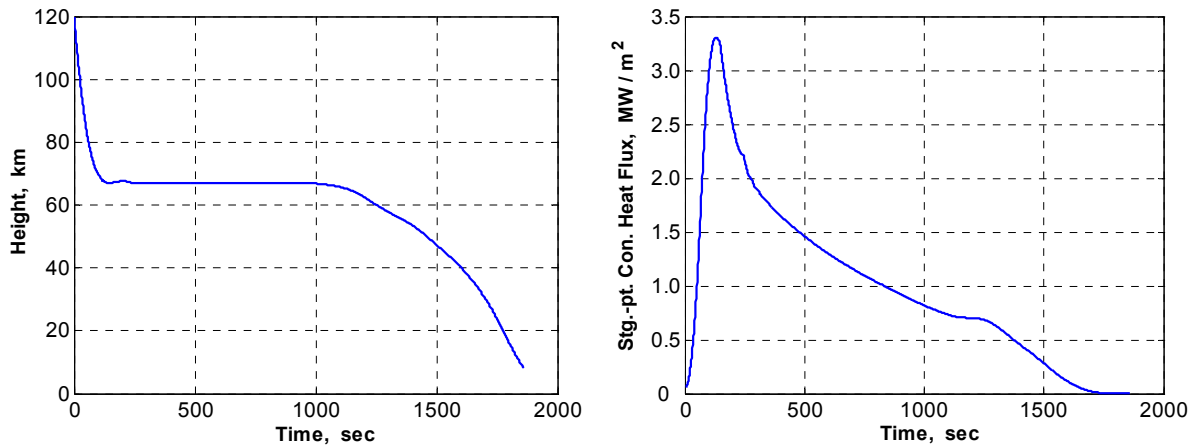


Figure 3-15: Trajectories of flattened bi-conic vehicle; (a) time versus altitude, (b) time versus stagnation point heat flux

As seen in bank angle profile (Figure 3-16) that vehicle enters upside down until a point where angle of attack is reduced to a lower limit of 10° . There after angle of attack does not reduce further and bank angle is modulated to compensate for lift requirement. Once the excess lunar-return kinetic energy has been dissipated the vehicle gradually rolls upright and proceeds further with upward lift vector to maintain the altitude and reduce further energy.

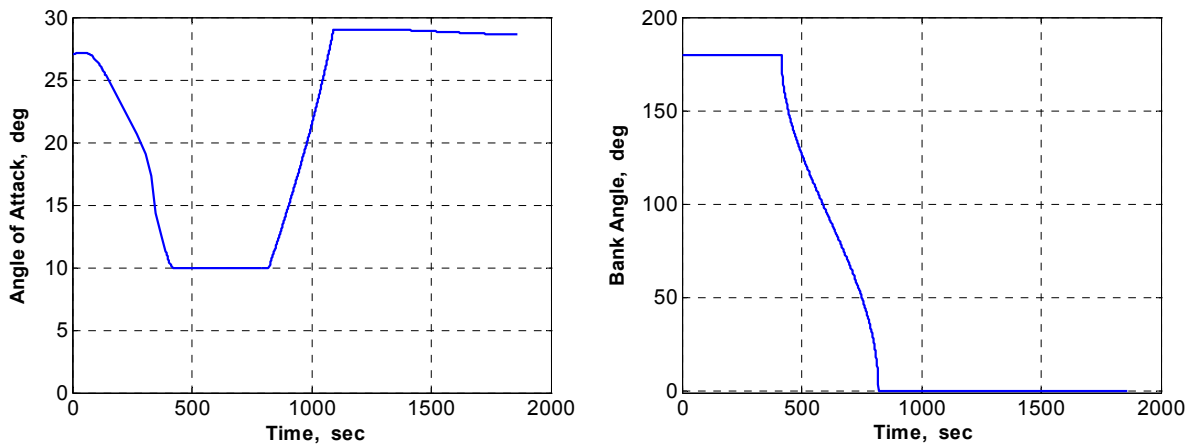


Figure 3-16: Trajectories of flattened bi-conic vehicle; (a) time versus angle of attack, (b) time versus bank angle

3.5 Assessment of Performance Parameters

A comparative analysis is performed using five performance parameters; 1- *volumetric efficiency*, 2- *controllability*, 3- *peak deceleration during re-entry*, 4- *stagnation point heating rates*, and 5- *total heat load during re-entry*. These five parameters will be weighted to compare the configurations and the results of this performance analysis will be presented. Each configuration will be assigned a score from 1 to 5 for each performance parameter, 1 being lowest score, and 5 being highest. The selection of these five performance parameters are described in the following paragraphs.

3.5.1 Volumetric Efficiency

Volumetric efficiency is a critical packaging parameter and is defined as *volume of the vehicle divided by the cube of the largest external dimension*. In general the blunter the vehicle, the higher is the volumetric efficiency.

This section presents a comparison of the volumetric efficiency of vehicles under consideration. Vehicle design of Apollo capsule [55], high lifting [58] and flattened bi-conic vehicles [68] are already shown in Figure 3-4, Figure 3-7 and Figure 3-9 respectively. The diameter of Apollo like capsule, length of flattened bi-conic vehicle and wingspan of high lifting vehicle are the largest external dimension of these vehicles.

Table 3-1 is presented below to shows that Apollo capsule is having the highest and high lifting vehicle is having the lowest volumetric efficiency. The volumes are calculated by approximating various geometrical segments of the vehicles for the volumes of spherical caps, cylinders, cones and conical frustums. The volume of wings is not considered here.

Table 3-1: Comparison of volumetric efficiency

		Capsule [55]	Bi-conic [68]	High-lift [58]
Largest External Dim. (L)	m	<i>diameter-</i> 3.9	<i>length-</i> 5.5	<i>wingspan-</i> 10.0
Approx. Volume (V)	m ³	14	25	30
Volumetric Eff. (V / L ³)		0.23	0.15	0.03
Score		5	3	1

3.5.2 Controllability

The controllability of the vehicles is considered in this section which is the key elements that allows a real vehicle to successfully enter the earth atmosphere from capture till landing. It is practically useless, if a vehicle has a maximum high-lift to drag ratio but is unable to trim at that condition, or if the vehicle is unstable at the angle of attacks which are required to achieve an optimized trajectory. A comparison of trim angle of attack range of each vehicle is presented in Table 3-2. In case of Apollo like capsule trim angle of attack is achieved by the adjustment of centre of gravity (CG) in vertical plane. CFD results by Whitmore [68] shows that Apollo like vehicle is trim able between -23° and 8° of angle of attack under allowable limits of CG variation, whereas the flattened bi-conic has a relative larger range of trim angle of attack from -17° to 51°, which uses trim flaps for this purpose. Fumo [42] has performed CFD analysis of high lifting vehicle for Mach number from subsonic to hypersonic and for angle of attack from -20° to 20°. The results show that the vehicle is longitudinally stable between 5° and 20° at hypersonic speed. But since Monti et al. [58] has performed trajectory simulation with a maximum angle of attack of 45°, we also assume this value as maximum trim angle of attack. The larger range of trim conditions for flattened bi-conic scores it better than other candidates.

Table 3-2: Comparison of trim angle of attack range

	Capsule	Bi-conic	High-lift
Trim Angle of Attack Range deg	-23° – 8°	-17° – 51°	5° – 45°
Score	3	5	3

3.5.3 Deceleration

Deceleration load during re-entry is also an important parameter, especially for safety and comfort of the crew in case of manned mission. Man-Systems Integration Standards [40] defined by NASA for physically de-conditioned astronauts are considered here, which states that: 1- peak deceleration level during re-entry can not exceed 4.0 g's for a de-conditioned astronaut sitting upright position, 2- peak deceleration level during re-entry can not exceed 4.0 g's for a de-conditioned astronaut sitting reclined position. A de-conditioned astronaut is defined as a person who has been exposed to zero-g or micro-gravity conditions for a period of two weeks or more.

Apollo capsule enters directly into the atmosphere with steep entry angle, decelerates at high loading of more than 7 g's (Figure 3-17), which is more than the current safety standards for astronauts. Lift force in case of flattened bi-conic and high-lift vehicles is exploited to keep them flying at constant altitude where atmospheric density is lesser and thereby decelerating at much slower rate until they enter sub-orbital speed regime. Peak deceleration for flattened bi-conic and high-lift vehicles noted from re-entry trajectory simulations are 1.5 g's and 1.2 g's respectively. Figure 3-17 shows histories of deceleration rate for all three candidate vehicles. The scores of vehicles for deceleration load are given in Table 3-3.

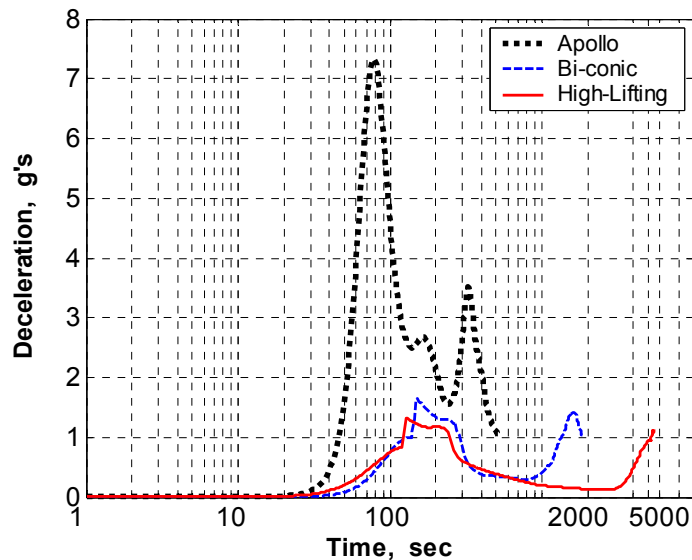


Figure 3-17: Comparison of deceleration load

Table 3-3: Comparison of deceleration load

		Capsule	Bi-conic	High-lift
Peak Deceleration Load	g's	7.3	1.6	1.3
Score		1	5	5

3.5.4 Maximum Heat Rate

A comparison of stagnation point heat transfer rates for both convection and radiation based on above mentioned methods is shown in figures below (Figure 3-18 and Figure 3-19). The convective heat transfer at stagnation point in the adopted method is directly proportional to the square root of atmospheric density and inversely proportional to the square root of nose radius. High-lift vehicle maintain a higher constant altitude, where the density is comparatively very low, but due to very small wing tip radius it is subjected to a higher stagnation point convective heat flux as compared to Apollo capsule (Figure 3-18). Flattened bi-conic vehicle, because of its small nose radius and lower constant altitude flight experiences the highest convective heat rate at stagnation point among three vehicles.

The radiative heat transfer at stagnation point in the adopted method is proportional to both atmospheric density and nose radius of the vehicle. This is the reason that high lift vehicle having very small wing tip radius and high constant altitude flight experiences very low stagnation point radiative heat flux. Apollo capsule, in this manner experiences the highest stagnation point radiative heat flux among three vehicles. Total heat flux is also presented in a figure below (Figure 3-20). Peak radiation heat flux is found to be 39%, 13%, and 1% of the peak total heat flux for Apollo, bi-conic and high-lift vehicles respectively. The scores of vehicles for stagnation points heat rate is given in Table 3-4.

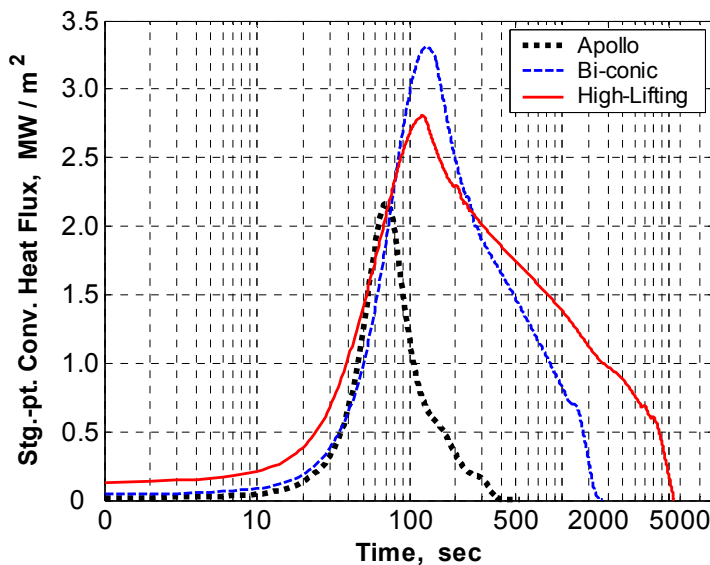


Figure 3-18: Comparison of convective stagnation point heat transfer

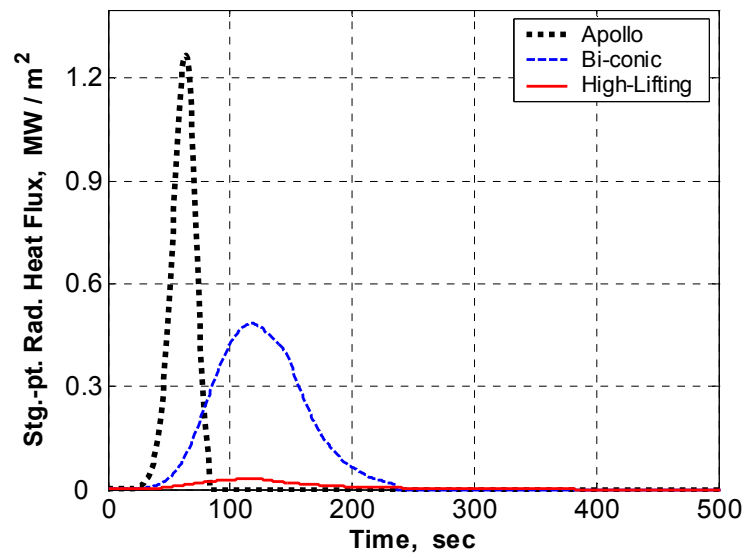


Figure 3-19: Comparison of radiative stagnation point heat transfer

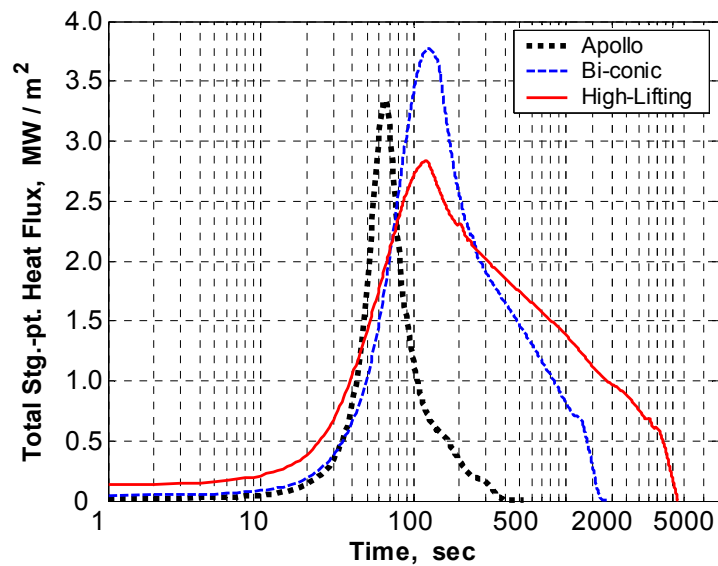


Figure 3-20: Comparison of total stagnation point heat transfer

Table 3-4: Comparison of stagnation point heat transfer rate

		Capsule	Bi-conic	High-lift
Peak Stg.-pt. Heat Flux (Convective + Radiative)	MW/m ²	3.34	3.77	2.84
Score		4	3	5

3.5.5 Integral Heat Load

Integral heat load is calculated by integrating the sum of stagnation point convective and radiative heat fluxes over entire flight time.

$$\bar{q} = \int_0^t (q_c + q_r).dt \quad 3-8$$

High-lift vehicle although experiences lowest stagnation point heat flux among three vehicles, due to its long constant altitude flight, total heat absorbed by the vehicle is much greater. Table 3-5 compares maximum stagnation point heat rate, integral heat load and total flight time for nominal entry and environmental conditions.

Table 3-5: Comparison of integral heat load

		Capsule	Bi-conic	High-lift
Flight Time	<i>sec</i>	532	1858	5456
Integral Heat Load	<i>MJ/m²</i>	225	1906	4908
Score		5	3	1

3.5.6 Result of Performance Analysis

Each performance parameter is already analysed and respective scores are assigned to the three vehicles. Since not all the performance parameters weigh equal to each other, so multiplication factors are assigned to each parameter to weigh each parameter with respect to other. The sum of multiplication factor is equal to one, thus the weighted average of performance parameters of each configuration will again range between 1 and 5 with 1 as the lowest score and 5 as the highest. Since the research is focused around hyperbolic re-entry with crew inside, the deceleration load and total heat load to the vehicle weigh higher in order not to endanger the crew. Then controllability is also important to have control margins available through out re-entry phase. Since the difference of stagnation point heat rate for all three vehicles is not large, the importance to rank them with each other on the basis of this parameter is also reduced. Volumetric efficiency is an important packaging parameter as far as launcher is concerned, but from the aspect of safe re-entry it is not as important as other parameters. Weighted average is calculated as:

$$\text{Weighted Average} = \sum_{i=1}^5 x_i \cdot p_i \quad 3-9$$

Table 3-6 shows a comparison of weighted average calculated by using above relation. Flattened bi-conic vehicle gained a highest score mainly because its performance is better for those parameters which are considered to be more important in this research.

Table 3-6: Comparison of weighted average

Performance Parameter 'p'	Factor 'x'	Capsule	Bi-conic	High-lift
Volumetric Efficiency	0.15	5	3	1
Controllability	0.20	3	5	3
Peak Deceleration Load	0.25	1	5	5
Peak Stg.-pt. Heat Load	0.15	4	3	5
Integral Heat Load	0.25	5	3	1
Weighted Average		3.45	3.90	3.00

3.6 Summary

Re-entry trajectories are simulated for three different configurations of re-entry vehicles returning Earth from a lunar mission. A comparison of vehicle volumetric efficiency is presented and an assessment of simulation results is done for controllability, stagnation point heat rate, integral heat load, and deceleration load. Whitmore [68] has also done an assessment of various re-entry vehicles for the selection of crew entry vehicle for NASA's constellation program. His assessment includes a performance parameter or rather a selection parameter of technology readiness level, which is more important and has more weighing factor, because US government plans to launch this mission by 2018. This selection criterion is not very important for this research, as this research is not a part of NASA's program. So the assessment done in the above sections is summarized below.

Apollo like capsule is analysed and the advantages of this configuration are lower integral heat load, simplest adaptability in the launcher system and maximum volumetric efficiency. This configuration despite being the simplest design, enters into the atmosphere with steep entry angle, following a direct entry strategy and decelerates at high loading of more than 7 g's which is more than the current safety standards for astronauts [40]. High deceleration load is the main disadvantage of this type of vehicle and this is the reason that alternate vehicle configurations are studied and compared here.

High-lift vehicle keeps a constant altitude where the atmospheric density is much less and therefore flying at much lower deceleration loads. Comparative sharp wing tips are subjected to high heat rate, for which ceramic material is proposed by *Monti, et al.* [58]. Total heat input to the vehicle is almost 22 times the integral heat load of Apollo capsule. Already having low volumetric efficiency, a large amount of thermal protection would be required to protect the vehicle itself, and astronauts and instruments inside it. Requirement of large wing span make it difficult to integrate with the launcher system.

Flattened bi-conic has the advantages of better controllability, launcher system adaptability, better volumetric efficiency and lesser integral heat load as compared to high lifting vehicle. It re-enters at lower deceleration load of around 2 g's but with higher stagnation point and higher total heat load, about 8 times the integral heat load of Apollo like capsule. Total heat input to the vehicle requires more

thermal protection system to be applied, which would reduce the space required for the astronauts and instruments inside.

Flattened bi-conic vehicle found to be most suitable among three vehicles which gained highest score in the assessment of performance parameters since; its design is simple it does not experience very high integral load when compared with high-lift vehicle, it does not experience very high deceleration load like Apollo capsule, and it has better controllability.

4 Guidance Algorithm

Manned vehicles returning from interplanetary missions enter the Earth atmosphere at super-orbital speeds. Major guidance problems of the missions at such a high entry speed are safe capture of the vehicle into the Earth atmosphere keeping the aerodynamic heating as well as deceleration levels within limits and finally assuring arrival at a desired landing site. So the guidance system must provide control commands to control the spacecraft in such a way to reach the desired landing point with specified accuracy without compromising the vehicle structural integrity or endangering the crew. Improper guidance during entry can cause large deviations from the desired touchdown area, excessive aerodynamic heating of the vehicle, deceleration in excess of crew tolerance limits, or, in the extreme, the loss of the spacecraft and its crew.

Practically to ensure the mission success, the vehicle is to be equipped with Navigation system and Control system in addition to Guidance system, so-called GNC system. The task of guidance system is to find a set of control vector in order to guide the vehicle to its target end conditions by numerically solving an optimal control problem. The future trajectories during the guidance loop are also predicted numerically. For this task, the inputs are needed from the outside world, e.g. the current actual state. These data has to be provided by navigation system, using sensor information and pre-defined theoretical models. The control system has to take care that the steering commends are carried out (e.g. the actual attitude approaches the commanded attitude) with a certain tolerance in a finite time. Since modelling of navigation and control systems are out of scope of this thesis, therefore a perfect navigation system is assumed that provides all the relevant data that are required for the execution of guidance. It is also assumed that the control system can perfectly generate the required moments to change the attitude of the vehicle, and that the attitude changes take place instantaneously.

Uncertainties in vehicle characteristics, e.g. in the lift-drag (L/D) ratio and vehicle mass properties, uncertainties in atmospheric variations as well as errors in vehicle states at entry interface affect guidance performance. Therefore a guidance system should be as insensitive as possible to uncertainties in those parameters over which the guidance designer has no control, in particular, vehicle.

Re-entry guidance is simply a specific application of general guidance principles, so guidance methods used for similar purposes may easily be applicable to re-entry guidance. It is already discussed in preceding chapters that a combination of direct entry and aero-capture of the vehicle till touch down is possible by properly modulating the lift force. So the re-entry strategy proposed includes a constant altitude phase which is maintained with the help lift vector in the direction of Earth (negative lift) until orbital speed and positive lift afterwards. The guidance design for a re-entry vehicle with proposed re-entry strategy may benefit a great deal from recent aero-capture research. A spacecraft performing aero-capture dives into the atmosphere as it is passing by a planet in order to change its trajectory into an orbit about that planet. Just like a re-entry algorithm, an aero-capture algorithm must perform:

1. Capture into the atmosphere,
2. Manage energy by removing excess velocity through drag management, and
3. Steer to a target. For re-entry the target is a landing site, and for aero-capture the target is a set of atmospheric exit conditions.

4.1 IRS Guidance Concept

The proposed guidance method is an evolution of IRS guidance algorithm, which is based on predictive guidance method (explicit guidance) [15,16,27,28,29,32,36,37, 46-50,62,65]. The development of guidance algorithms at the Institute of Space Systems (IRS) focused on an algorithm that offers a high degree of autonomy and generality. Originally intended for the COLIBRI capsule [65] the core of the guidance algorithm was further developed and under investigation in the last years within the German TETRA and ASTRA technology programs (technology for future space transportation systems [69]; advanced systems and technologies for future space transportation applications [66]). The reference missions have been the X-38 [15,16,32] demonstrator and the Hopper vehicle [29,36,48]. For X-38 the guidance algorithm was not only applied to the hypersonic [47,49] but also to the terminal area flight phase (known as terminal area energy management; TAEM) [27,28,29]. This guidance algorithm is now adapted and applied to a flattened bi-conic re-entry vehicle, returning from a lunar mission, which demands special guidance solutions to ensure a safe capture at super-orbital speeds. This vehicle has a medium L/D ratio and which is selected on the basis mission requirements as assessed in section 3.5

The concept of guidance algorithm is same as basic optimization problem i.e. the problem of finding the best solution from all feasible solutions. A prescribed cost function (objective) is minimized by finding a parameterized set of control vector with the help of Non linear programming (NLP) methods. An optimization problem in general can be stated as:

$$\begin{array}{ll}
\text{Minimize a cost function} & F(\vec{u}(t)) \\
\text{subject to final constraints} & \vec{g}_i(\vec{u}(t))=0 \\
\text{and in flight boundary constraints} & \vec{g}_j(\vec{u}(t))\leq 0 \\
\text{subject to the differential equation} &
\end{array}$$

$$\dot{\vec{X}} = f(\vec{x}(t), \vec{u}(t)) \quad 4-1$$

The flight path of the vehicle based on the set of control parameters is computed by numerical integration of a set of equations of motion in three dimensional space using three degrees of freedom. The advantage of this in respect to older approaches is that down range and cross range are not decoupled. Therefore the future state of the vehicle can be predicted very accurately in the order of model uncertainties. The continuous control vector $\vec{u}(t)$ of Equation 4-1 is approximated by a set of parameters \vec{p} of the control model discussed before. The state vector (Equation 4-2) represents position and velocity vector of the vehicle, defined by r the distance to earth centre, λ and δ the geocentric longitude and latitude respectively, V the vehicle velocity, γ and χ the flight path angle and the flight azimuth respectively.

$$\vec{X} = [r \quad \lambda \quad \delta \quad V \quad \gamma \quad \chi]^T \quad 4-2$$

The function of control model is to give a continuous time history of vehicles attitude during the complete flight time. To solve the problem of finding a continuous control history, guiding the vehicle to its desired target state, the profile is approximated by a set of linear and constant pieces, which is called a parameterization or control model. The problem is thereby reduced to find sets of parameters $(t_i ; p_i)$ characterizing the control history (parameter optimization problem). Several different simple and complex models with varying number of parameters can be designed to adapt for different vehicles and missions. To stay within limits of onboard computation, the number of parameters should be as low as possible but at least as high as the number of final constraints defined, to have a solvable mathematical problem. However, during optimization the number of optimization parameters can be increased, because CPU time is not as restricted before flight or in a coasting arc. The parameter model is defined in a velocity, Mach number or time frame. Velocity has proven to be advantageous compared to time, because we know initial and final velocity of the vehicle more or less exactly and time may vary in a great range, depending on cross and downrange conditions for different missions.

The proposed guidance scheme is implemented in two steps: the optimization step and the guidance step. The first step begins before or during coasting arcs, in which time is used for the costly flight path optimization of the upcoming flight phase. For optimization step the problem is solved using the sequential quadratic programming algorithm NLPQL method contained within the International Mathematics Standard Library (IMSL) [64]. An optimized set of control commands

are found depending on the given entry conditions for a given target point on planetary surface, while at the same time minimizing a cost function and taking care of flight path restrictions. The control profile generated is used as basis for vehicle control commands. This optimization is done only once to obtain an initial guidance command solution for the complete re-entry flight. For the guidance step an accelerated Gradient Projection Algorithm (GPA) [31] is utilised to provide updates of the control history repeatedly to the onboard flight path predictor for the remaining flight segment by using a simplified restoration step. Only restoration step of GPA is used during the guidance phase because the objective of guidance phase is to find an acceptable trajectory instead of an optimized trajectory. Thus the computational burden onboard during the entry flight is reduced. This two step algorithm is presented in a figure below (Figure 4-1).

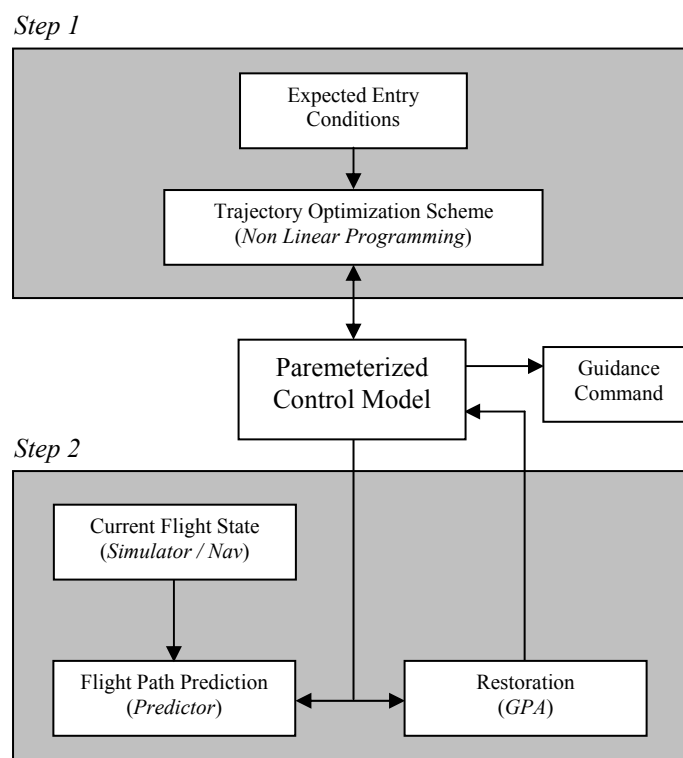


Figure 4-1: Predictive guidance algorithm

4.2 Re-entry Guidance Strategy of Flattened Bi-conic Vehicle

In section 3.2 the use of lift forces during interplanetary re-entry are considered for high lifting vehicles and a re-entry approach with a constant altitude flight phase is studied. This re-entry approach was then applied to re-entry trajectory simulation of flattened bi-conic vehicle. In correspondence to this re-entry approach the guidance algorithm also consists of three phases. In addition there is also a Pre-entry phase, which begins as soon as the guidance algorithm gains control of the vehicle. In this phase time is used for the costly flight path optimization of the upcoming flight phase. The attitude (upside down) of the vehicle is achieved and

maintained during this phase until a sensible atmosphere has been detected. A guidance cycle occurs once every two seconds.

The re-entry guidance strategy of flattened bi-conic is simpler in comparison with Apollo re-entry guidance strategy, since the complete guidance scheme is divided into three phases and each phase has its own objective and end conditions. The first phase of flight for example is completely independent of the later flight phases. In the guidance loop of this phase future trajectories are predicted only till the end of this phase and the only objective of this phase is to bring the vehicle to such a state that the vehicle achieve enough aerodynamic controllability to maintain a constant altitude in the later flight phase.

The first guidance phase starts once the sensible atmosphere is detected (at about 120 km above mean sea level). Vehicle at super-orbital speed generates enough centrifugal force to skip out of upper atmosphere. To counter this centrifugal force vehicle enters at an initial bank angle of 180° at atmospheric interface (i.e. upside down) in order to have a component of lift in a direction of Earth surface. In this way it becomes possible for the vehicle to be captured by earth atmosphere. The primary function of this phase is to ensure a safe capture, i.e. to bring the vehicle to such a state that it could produce enough lift in order to stay in the Earth atmosphere. Therefore there is only one channel in the guidance strategy: vertical and there is one control as well: angle of attack.

The function of second phase of guidance '*constant altitude phase*' is to maintain a constant altitude, which is achieved with the help of a control law. The control law controls the lift in vertical plane by varying the angle of attack as well as modulating the bank angle. Vehicle's drag slowly decelerates the vehicle during this phase and hence the requirement angle of attack also reduces to maintain the altitude. Practically the vehicle is required to be insulated mostly on one side, i.e. the windward side. In this regards a control law find values of angle of attack not lower than a certain value, e.g. 10° . Bank angle is modulated to get the desired lift in vertical plane when the angle of attack requirement is lower than 10° . Bank angle is gradually reduced from 180° to 90° (or 270°) where speed becomes equal to instantaneous orbital speed and then further reduced to 0° as the speed also reduces.

The third phase '*Final descend phase*' starts when the speed of the vehicle is reduced during constant altitude phase to such a level that it is safe to bring it down to the Earth surface. The target of guidance algorithm in this phase is to control the radial dispersion at the terminal conditions of this flight phase. We can say that this is the second re-entry phase in which the flattened bi-conic vehicle is guided to the desired landing point with the help of predicted guidance algorithm. Apollo re-entry vehicle also performs second re-entry, either with skip trajectory profile or without, but in contrast uses trajectory following guidance to follow a pre-stored reference trajectory. In case of Apollo re-entry there are two channels in the guidance strategy 'vertical' and 'lateral' to control the down range and cross range, whereas in case of proposed guidance strategy for flattened bi-conic vehicle only radial dispersion from the target end point at the end of this flight phase is

controlled. Hence the down range and cross range in this case are not decoupled. An overview of guidance strategy is also given in section A.6 for comparison.

4.3 Implementation of Guidance Algorithm

As mentioned in the previous section that the guidance algorithm is implemented in three phases namely, hyperbolic approach phase with predicted guidance, constant altitude phase with a control law, and final descend phase with predicted guidance. The state variables used for guidance information are acceleration, velocity, altitude and range, where acceleration is a basic measurement obtained from the inertial equipment onboard, velocity is a fundamental measure of spacecraft energy, and the range and altitude are the quantities to be controlled.

4.3.1 Hyperbolic Approach Phase with Predicted Guidance

This phase starts with the initial contact with the atmosphere until approximately horizontal flight is achieved. Models of stop criteria, end restriction, predictor update model, and control model for this flight phase will be described in this section.

Stop Criteria:

In general, different criterions to stop this phase of flight exist, e.g. at specified altitude, particular speed or dynamic pressure. These quantities fail as stop criterion and lead the vehicle either to uncontrolled skip out in case if the atmospheric density is less than expectation or the vehicle falls deep into the atmosphere with very high heat and g-loads if the density is higher. In order to set a stop criteria which guarantees a safe capture and lead the vehicle successfully to the next phase, first we have to see the requirement of next flight phase, which is to maintain a constant altitude. To maintain a constant altitude flight in the next phase the vehicle should be capable of producing enough force in vertical plane to counter the centrifugal force of the orbit. To see how this can be accomplished let's write the equilibrium equation in vertical plane under the hypotheses of flight path angle equal to zero (constant altitude flight) and bank angle equal to 180° (downward lift) and neglecting the Earth's rotation. According to the forces shown in Figure 4-2, the equilibrium flight is possible only if,

$$\frac{1}{m}L + g_r = \frac{V^2}{r} \quad 4-3$$

Hence the lift required for the equilibrium flight is:

$$\frac{1}{m}L = \frac{V^2}{r} - g_r \quad 4-4$$

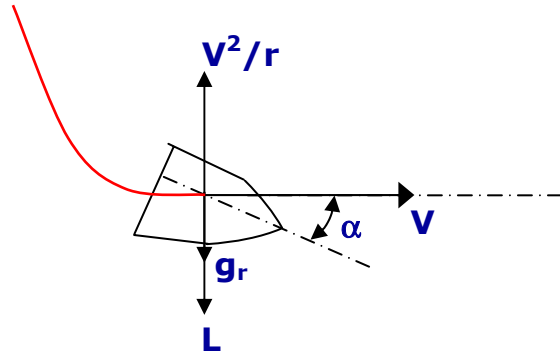


Figure 4-2: Forces acting on vehicle

From the Equation 4-4 we can say that the constant altitude can be maintained in the next phase only if the vehicle at the end of hyperbolic approach phase is in a state that the flight path angle is approximately zero and the maximum available acceleration due to lift force in vertical plane is greater than the sum of the accelerations due to centrifugal force and gravitational force, i.e.

$$\frac{1}{m} L_{\max} > \frac{V^2}{r} - g_r \quad 4-5$$

or

$$\frac{1}{m} L_{\max} - \frac{V^2}{r} - g_r > 0 \quad 4-6$$

As a safety margin, in order to avoid a possibility of skip out because of any unknown fluctuation, the flight phase is stopped only when the net acceleration in Equation 4-6 is greater than 0.5 m/s^2 .

End restriction:

Since after the end of this phase we need the vehicle to follow a constant altitude phase, therefore a restriction of flight path angle equal to zero at the end of this phase is necessary.

There are two possible trajectories other than the required trajectory that the vehicle can fly, i.e. either the vehicle is flying steeper trajectory or the vehicle is flying a shallower trajectory (Figure 4-3).

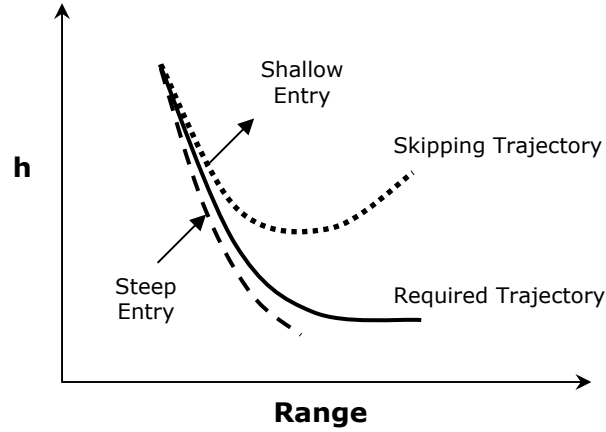


Figure 4-3: Shallow and steep entries in comparison to required trajectory

In case of steeper trajectory the vehicle achieves the above mentioned stop criteria at a state where the flight path angle is not equal to zero. From this point onward the vehicle descends further into the atmosphere and then it becomes difficult for the vehicle to control its trajectory and to maintain a constant altitude. So the value of the flight path angle at the point where the stop criteria is achieved is sent to the guidance scheme as a violation of end restriction (constraint violation). The restoration routine of GPA in the guidance loop takes care of this violation and brings back the vehicle to a trajectory which ends at approximately horizontal flight path by updating the control commands accordingly.

In case of a possibility of a shallower trajectory, the vehicle never comes to a state where the above mentioned stop criteria of Equation 4-6 is fulfilled as it starts skipping out of atmosphere because of insufficient aerodynamic lift force as compared to centrifugal force. A skip function in the guidance scheme is introduced, which stops the predictor to simulate the trajectory whenever the altitude of the vehicle starts increasing. The net acceleration from Equation 4-6 at this stage is certainly less than zero, which is sent to the guidance scheme as a violation. Again the restoration routine of GPA in the guidance loop takes care of this restriction by updating the control commands accordingly.

Predictor Update:

Acceleration due to aerodynamic drag and lift are the only accelerations sensed by inertial measurement unit of a re-entry vehicle if there are no propulsion elements. Both drag and lift accelerations are dependent on aerodynamic coefficients, atmospheric density, vehicle's mass and velocity.

$$a_{drag} = \frac{C_D \cdot \rho(h) V^2 \cdot S_{ref}}{2 \cdot m} \quad 4-7$$

and

$$a_{lift} = \frac{C_L \cdot \rho(h) V^2 \cdot S_{ref}}{2 \cdot m} \quad 4-8$$

The predictor at every guidance loop computes the future trajectories based on the navigation states, and pre-stored simulation models (which include aerodynamic coefficients, atmospheric density and vehicle's mass). A variation of one or more pre-stored quantities would lead to an incorrect computation of accelerations in the predictor. An example is illustrated in figure below (Figure 4-4). Starting at point '1', the guidance algorithm generates control commands to guide the vehicle to desired end conditions based on the future trajectories predicted by the predictor, which does not know if there are deviations in simulation models. In actual if the trajectory is extrapolated with deviated simulation models the flight would end at point '1*'. If this continues, a time will arrive e.g. at point 'n' where the guidance will be unable to guide the vehicle to the desired end conditions, which is called guidance error. Due to this error it is sometime not possible in the next flight phase to control the vehicle at desired constant altitude.

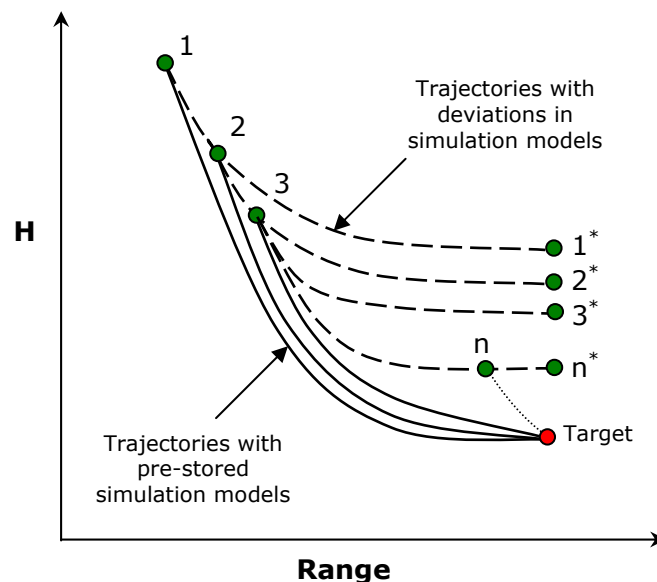


Figure 4-4: Predicted trajectories with pre-stored simulation models and assumed trajectories with deviations in simulation models

An idea to send an update of acceleration sensed by the inertial measurement unit to the predictor greatly improves the accuracy of the predictor for prediction of future trajectories, thus reducing the guidance error at the end. Actual accelerations from the sensors are divided with the computed accelerations at corresponding time of the last predicted trajectory and sent as a multiplication factor to predictor at next guidance loop (see Figure 4-5). This comparison can be done at regular intervals of time for example every 5 seconds.

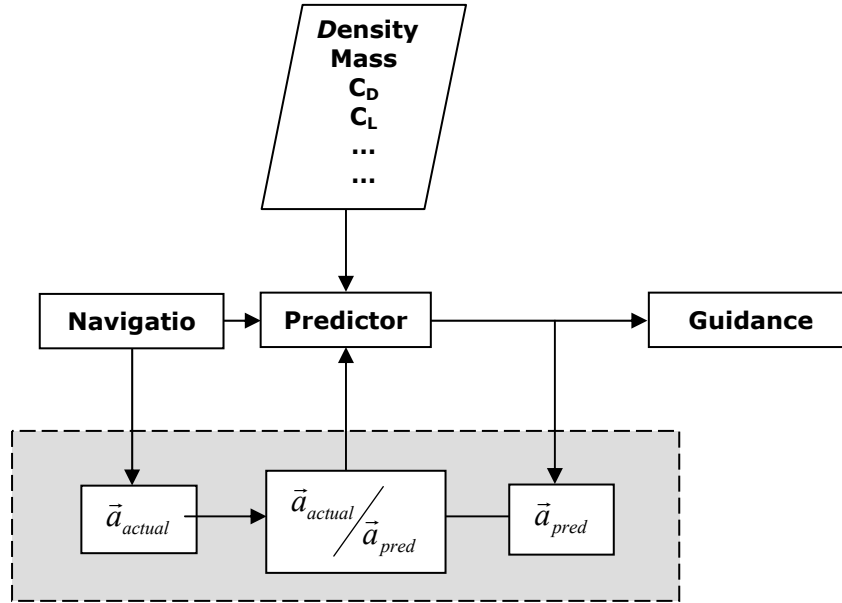


Figure 4-5: Predictor update model

Control Model:

The trajectory during this phase is controlled only with the help of angle of attack commands. The control model is defined as three parameters of angle of attack p_1 , p_2 , and p_3 as function of flight velocity (inertial) at three different points v_1 , v_2 , and v_3 (Figure 4-6). Angle of attack command at any instant during the flight is computed by linear interpolation between any two points. Point v_1 is equal to entry velocity and point v_3 is a velocity where this flight phase mostly ends. Any command outside the limits of these velocities is extrapolated. As the vehicle passes through the atmosphere its velocity is reduced and till it is less than v_1 , with which the influence of the variation of parameter p_1 on the trajectory is reduced till a point when the velocity is equal to v_2 . After this point parameter p_1 has no influence and the trajectory is controlled only by parameters p_2 and p_3 . The same applies when the velocity of the vehicle is less than v_3 and the trajectory is controlled with only one parameter p_3 .

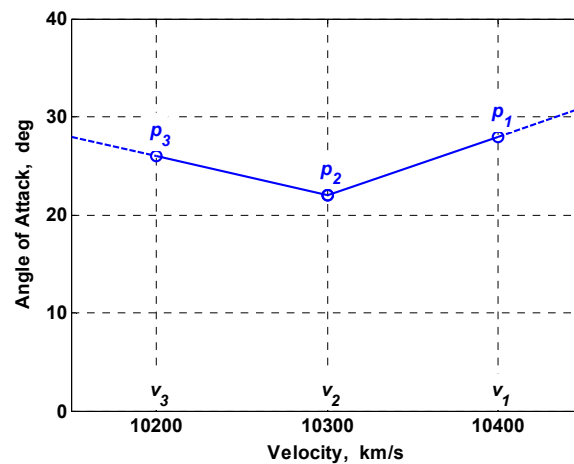


Figure 4-6: Parameterized control model during hyperbolic approach phase

CFD data by Whitmore, et al. [68] shows that the vehicle can be trimmed and remains stable over a wide range of angle of attack with the help of trim flaps (Figure 4-7). Practically the usage of available window of trim angle of attack is limited to positive values only because the vehicle is required to be insulated mostly on one side i.e. on the windward side, where the stagnation point exists. This window of angle of attack with positive values only, is further shrunk, in order to reduce the risks due to large movement of stagnation point over the vehicle of surface. So the lower limit of angle of attack is set to $+10^\circ$ and upper limit to $+45^\circ$ (Figure 4-8).

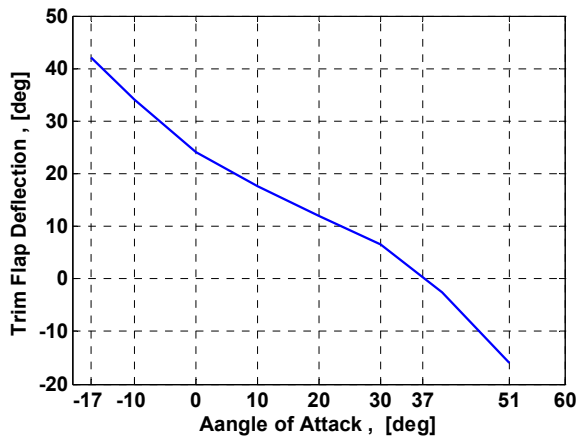


Figure 4-7: Trim Angle of attack range

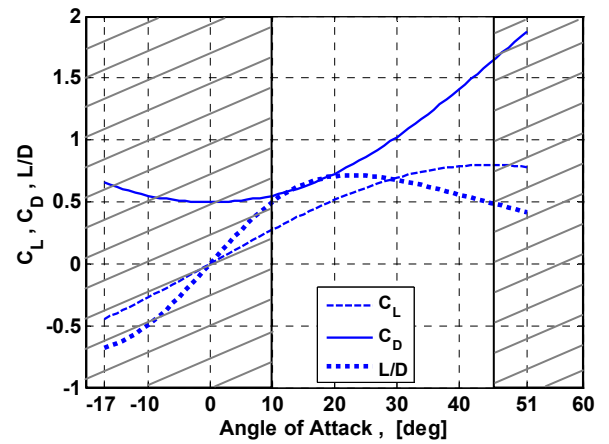


Figure 4-8: Useable window of angle of attack

It is required many times, during the guided simulations that the angle of attack requirement is lower than the specified lower limit and even in many cases an upward lift in vertical plane is required. In such situations the angle of attack is still restricted to its lower limit and the required amount of lift is generated by modulating the bank angle accordingly as per relation below.

$$\psi = \pi \pm \cos^{-1} \left(\frac{C_L(a)}{C_{L(\alpha=10^\circ)}} \right) \quad \forall \quad \alpha < 10^\circ \quad 4-9$$

The ratio of lift coefficients in the above expression is either added or subtracted from π , depending upon the direction of initial azimuth error. Bank angle should be in the range of 0 to 180° if the initial azimuth error is negative. In this case the above relation is used with negative sign. In other case with positive sign, bank angles are 180° to 360° . Figure 4-9 below shows the implementation of angle of attack commands versus required angle of attack. In this figure one can see that the implemented angle of attack command is restricted to a lower limit of 10° , if the required angle of attack varies between -10° and $+10^\circ$. Also the required angle of attack command below -10° is implemented with opposite sign provided that the bank angle is 0° . Figure 4-10 and Figure 4-11 show the modulation of bank angle for initial azimuth error of negative and positive respectively, when the requirement of angle of attack varies between -10° and $+10^\circ$.

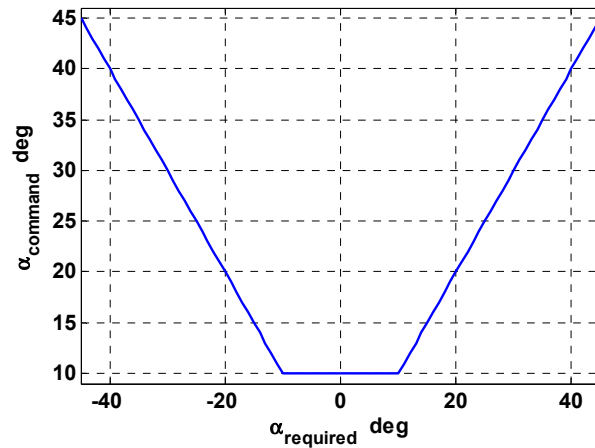


Figure 4-9: Command angle of attack versus required angle of attack

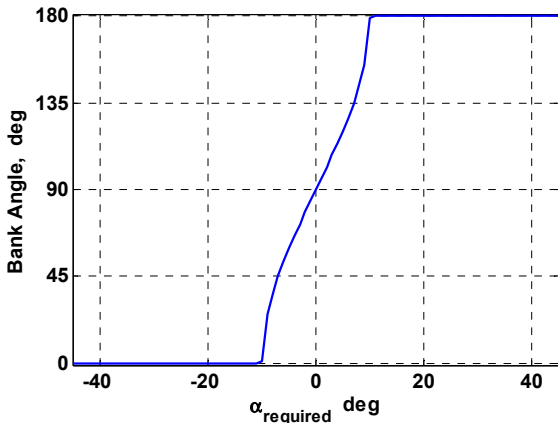


Figure 4-10: Bank angle adjustment for angle of attack less than 10° and negative azimuth error

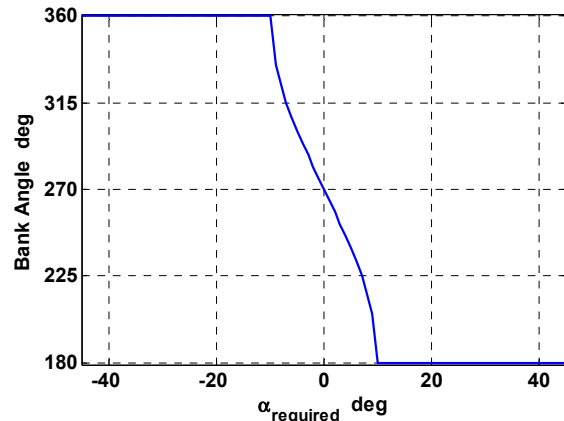


Figure 4-11: Bank angle adjustment for angle of attack less than 10° and positive azimuth error

4.3.2 Constant Altitude Flight Phase with Control Law

This phase starts at the end of hyperbolic approach phase where the vehicle is flying approximately a horizontal flight and having enough aerodynamic controllability to maintain constant altitude till the velocity of the vehicle is less than the orbital velocity and it is safe to start the next phase for final descend. Model of stop criteria, and control model for this flight phase will be discussed in this section.

Stop Criteria:

It was seen during the constant altitude phase that a number of termination points exist from where desired target can be achieved (Figure 4-12). The earliest point and the latest point along the constant altitude flight phase are shown in this figure, from where final flight phase can be started to achieve the desired target point. These points depend on the aerodynamic capability of the vehicle. A full lift

up will be required to achieve maximum range-to-go if the constant altitude flight is terminated at point 1. Similarly a steepest descent with full lift down will be required to achieve the target if the constant altitude phase is to be terminated at point 3. If a full lift up trajectory is selected then in case of any deviations the vehicle will not be able to produce more lift (if required). The same will happen in case if a full lift down trajectory is selected. So it is required to find a solution from where the vehicle will be having a maximum control margin in the final flight phase.

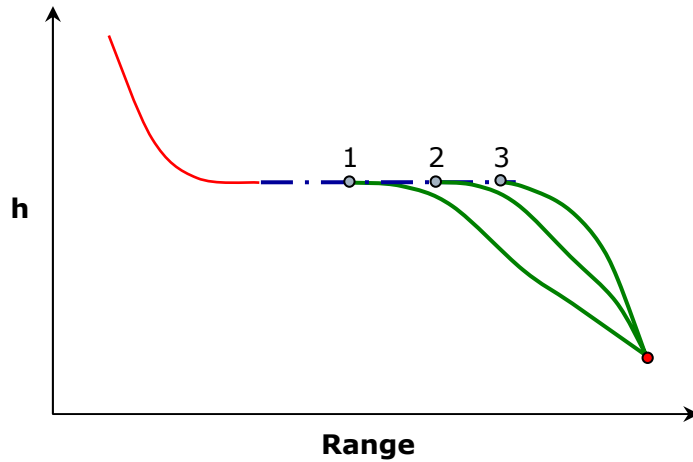


Figure 4-12: Multiple terminal points for desired range

A solution proposed and implemented is to find a control profile (bank angle commands) for third phase of flight for desired range by predicting the trajectory of third phase at different intervals along constant altitude phase. We can say that we can have a maximum control authority if the standard deviation of the bank angles is lowest. The standard deviation of the generated bank angle commands is computed as.

$$\sigma = \sqrt{\frac{\sum_{i=1}^N (\psi' - \psi_i)^2}{N}} \quad 4-10$$

Where ψ' is, -135° , -45° , 45° or 135°

The bank angle commands for desired target point for a test case were generated by predicting the trajectories of third phase. The first point along constant altitude phase is selected where the inertial velocity is nearly equal to orbital velocity i.e. 7800 m/s and repeated at an interval of 100 m/s. Figure 4-13 shows that the standard deviation decreases as the termination point of constant altitude flight is delayed till it reaches minima, after which it start increasing again. So a point where the inertial velocity is about 7500 m/s is found to be suitable to terminate this flight phase.

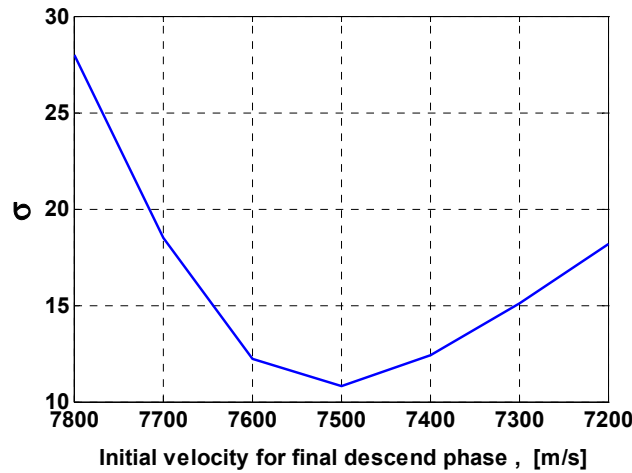


Figure 4-13: Standard deviation of bank angles at different terminal points on constant altitude phase

Control Law:

As mentioned in the previous section that a constant altitude flight is possible only if vehicle generates enough lift to overcome the gravitational and centrifugal forces.

Rewriting the Equation 4-3 which is in accordance with the forces shown in Figure 4-2, the equilibrium flight is possible only if,

$$\frac{1}{m}L + g_r = \frac{V^2}{r} \quad 4-11$$

Or

$$\frac{C_L \cdot Q \cdot S_{ref}}{m} + g_r = \frac{V^2}{r} \quad 4-12$$

Form this equation we get the required lift coefficient in order to hold the altitude, i.e.

$$C_{L,required} = \left[\frac{V^2}{r} - g_r \right] \frac{m}{Q \cdot S_{ref}} \quad 4-13$$

Lift coefficient is a function of angle of attack so the angle of attack required to generate corresponding required lift coefficient can be found.

$$C_{L,required} \Rightarrow \alpha_{required} \quad 4-14$$

The command angle of attack is generated according to the relation given below.

$$\alpha_{command} = \alpha_{required} + K_h \cdot (h(t) - h_{ref}) + K_{\dot{h}} \cdot \dot{h} \quad 4-15$$

Where,

$$\dot{h} = V \cdot \sin \gamma \quad 4-16$$

The second term in Equation 4-15 is added to control the vehicle at a constant reference altitude h_{ref} and the third term represents the rate of change of altitude, which damps the oscillation of vehicle due to second term about reference altitude. The equation is also depicted in the form of a closed loop block diagram in Figure 4-14. The value of reference altitude h_{ref} is the altitude at the end of hyperbolic approach phase. The constants K_h and $K_{\dot{h}}$ are feed back gains selected on hit and trial basis in such a way that the vehicle successfully travels at specified reference altitude.

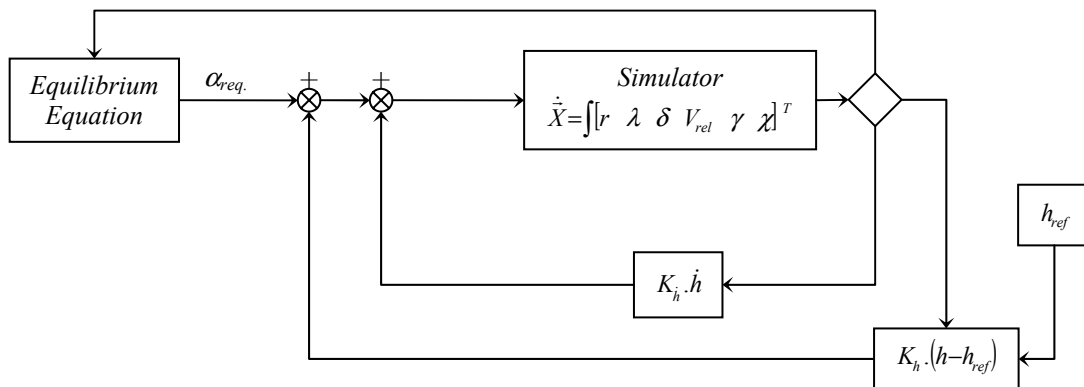


Figure 4-14: Closed loop block diagram of altitude hold controller

4.3.3 Descend Phase with Predicted Guidance

The vehicle is guided to the target point in this phase with the help of bank angle commands. The end restrictions are latitude and longitude of the target point. Flight path restriction of g-load is taken care as well. The stop criterion is an altitude of 8 km, where the vehicle is flying at subsonic speed and it is easy to deploy parachute for final touch down. Control model for this flight phase will be discussed in this section.

Control Model:

The trajectory during this phase is controlled only with the help of bank angle commands. The control model is defined as six parameters of bank angles $p_1, p_2, p_3, p_4, p_5,$ and p_6 as function of flight velocity (inertial) at six different points $v_1, v_2, v_3, v_4, v_5,$ and v_6 (Figure 4-15). Bank angle command at any instant during the flight is computed by linear interpolation between any two points. Point v_1 is equal to the velocity at the end of constant altitude flight phase and point v_6 is a velocity where this flight phase mostly ends. Any command outside the limits of these velocities is extrapolated.

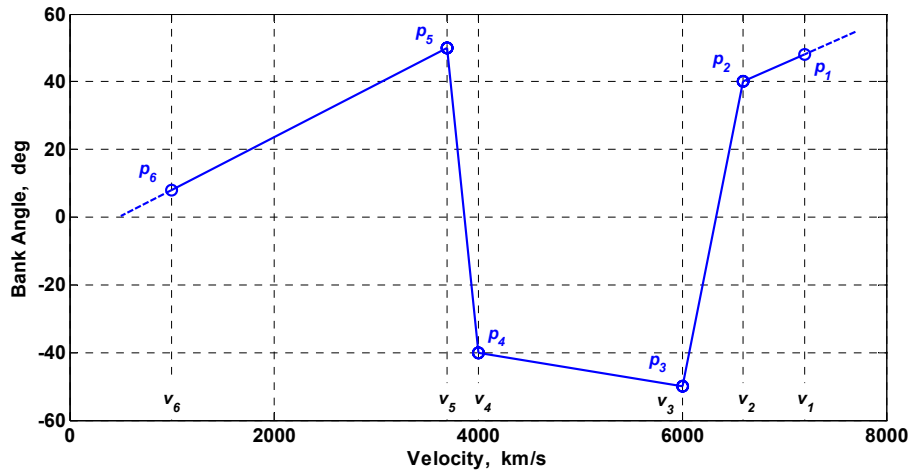


Figure 4-15: Parameterized control model for final descent phase

In order to reduce the computation load onboard by limiting the number of controllable parameter in control model during this guidance phase, a strategy similar to the one proposed by *Graesslin* [47] will be used. The method is to fix the control parameters which lie far from the current state of the vehicle and allow the guidance scheme to adjust less number of parameters to find a suitable flight path for desired end conditions.

In the beginning of the atmospheric guidance phase three parameters p_4 , p_5 , and p_6 will be fixed to the values determined during the pre-atmospheric optimization phase let say μ_4 , μ_5 , μ_6 . Remaining three parameters p_1 , p_2 , and p_3 are left free for guidance scheme to adjust according to the requirements (Figure 4-16 a). The slopes of line segments between points p_1 - p_2 , p_2 - p_3 and p_3 - μ_4 (shown with dashed lines) change with control model updates, whereas the slopes of line segments between points μ_4 - μ_5 and μ_5 - μ_6 (shown with continuous lines) do not change.

As the vehicle passes through the atmosphere its velocity is reduced, with which the influence of the variation of parameter p_1 on the trajectory is reduced. As soon as the velocity reduces to v_2 , parameter p_1 loses its influence on the trajectory. After this point parameter p_1 is fixed to the last adjusted value and parameter p_4 is allowed to be adjustable by the guidance scheme (Figure 4-16 b). From this stage onward the slopes of line segments between points μ_1 - p_2 , p_2 - p_3 , p_3 - p_4 and p_4 - μ_5 (shown with dashed lines) change with control model updates, whereas the slopes line segments between points μ_5 - μ_6 (shown with continuous lines) do not change.

The same action is repeated when the velocity of the vehicle reduces to v_3 , parameter p_2 is fixed and parameter p_5 is freed (Figure 4-16 c) and the velocity of the vehicle reduces to v_4 , parameter p_3 is fixed and parameter p_6 is freed (Figure 4-16 d). No action is taken when the velocity is further reduced to v_5 and the trajectory is controlled by only two parameters p_5 and p_6 (Figure 4-16 e). Similarly when the velocity of the vehicle is less than v_6 and the trajectory is controlled with only one parameter p_6 (Figure 4-16 f).

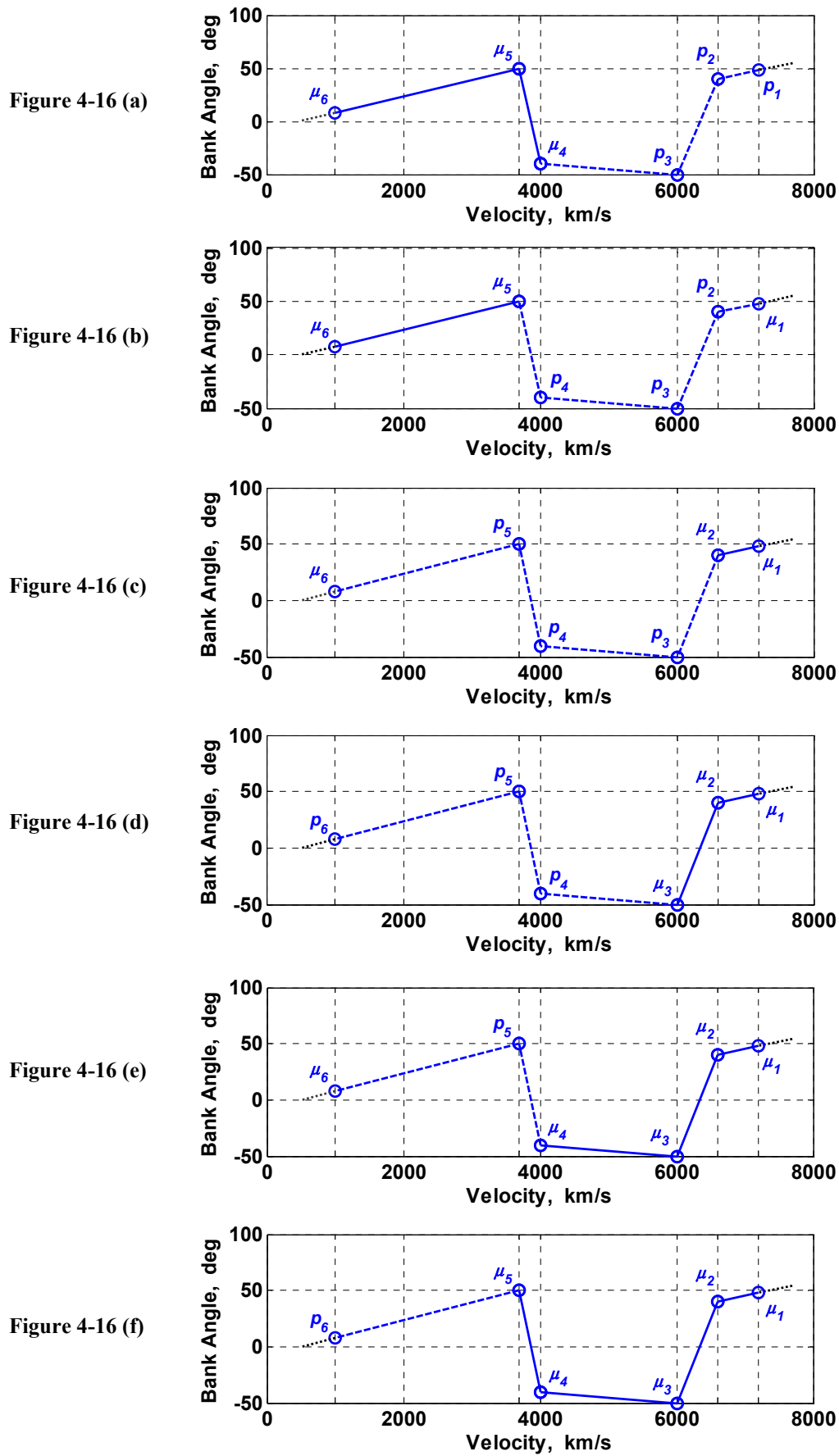


Figure 4-16 (a-f): Stepwise update of control model for final descent phase

5 Evaluation of Guidance Scheme

In actual flight of a re-entry vehicle, there will exist a number of uncertainties because of deviation of atmospheric conditions, deviation of vehicle mass and aerodynamic properties, and variations of entry conditions etc. one way to overcome these uncertainties is to develop a robust GNC system. It is therefore important that already during the design process, as many uncertainties as possible are studied to see how the GNC system deal with them. Once the GNC system has been developed for the nominal mission, common practice is to simulate a number of test cases with different error sources included. Moreover, it is obvious that more the error sources included, higher the confidence level will be. However, more error sources in principle also mean more possible combinations for simulations. If the simulation is done for each possible combination, then the total number of simulations will greatly increase. For this reason, different sensitivity analysis methods have been developed

The execution of these simulations and the analysis of the results, usually combined under the term *sensitivity analysis*, can be done in a number of ways, of which Monte Carlo [12] analysis is the most familiar one. With this simulation technique the parameters that can be subjected to errors are defined with a mean value and a standard deviation and sufficiently large number of simulations is executed while using a random number generator using normal distribution to define the errors for each simulation. An alternative method of McKay [44] is to use *Latin Hypercube Sampling*, in which one must first decide how many sample points to use and for each sample point remember in which row and column the sample point was taken. Another method of Taguchi [17,57] is to use orthogonal distribution to generate a population of parameters, such that the population is distributed uniformly in each sigma level of randomly generated parameters.

In Monte Carlo simulations, sufficiently large the number of simulations is executed and this number is usually based on experiences from previous analysis. A deterministic approach can be used to increase the number of simulations until the mean μ and standard deviation σ of the output do not change significantly.

The guidance scheme described in previous chapter is evaluated in three steps. First the guided trajectories of each flight phase are evaluated separately to see the

behaviour of various trajectory parameters for off-nominal conditions. To identify the sensitive parameter and to find the maximum allowable errors, a sensitivity analysis is conducted. A robust analysis of guidance scheme of entire re-entry flight is done in the third step with the help of Monte-Carlo simulations. Finally a comparison with other guidance schemes is present in the end.

5.1 Guidance Evaluation of Each Flight Phase

5.1.1 Hyperbolic Approach Phase

A solution of parameterized angle of attack commands found by the optimization program before the vehicle actually enters the Earth atmosphere (step 1 of Figure 4-1) is given in Table 5-1 and shown in Figure 5-1. The stop condition and the end restriction of this flight phase are:

$$\text{Stop criteria: } \gamma_{end} = 0 \pm 0.1^\circ$$

$$\text{End restriction: } \frac{1}{m} L_{\max} - \frac{V^2}{r} - g_r > 0.5 \text{ m/s}^2 \text{ (see Equation 4-6)}$$

Table 5-1: Parameterized control model for hyperbolic approach phase

v_1	11300 m/s	p_1	8.544°
v_2	10900 m/s	p_2	7.706°
v_3	10500 m/s	p_3	8.251°

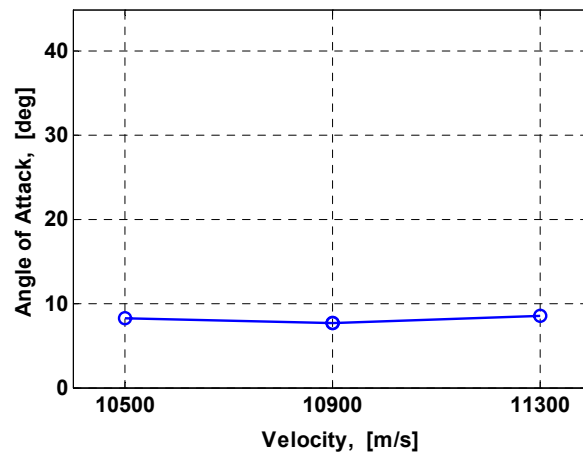


Figure 5-1: Required angle of attack during hyperbolic approach phase

It seems to be a very good solution at this stage, since low angle of attack is required throughout. This means we have a plenty of margin during the guidance phase to steer the vehicle on both sides i.e. lift up trajectory with zero bank angle or lift down trajectory with bank angle equal to 180°.

A guided simulation without any disturbance and with same simulation models used for optimization, implements $+10^\circ$ of angle of attack command in this case with modulation of bank angle according to Equation 4-9 (Figure 5-2).

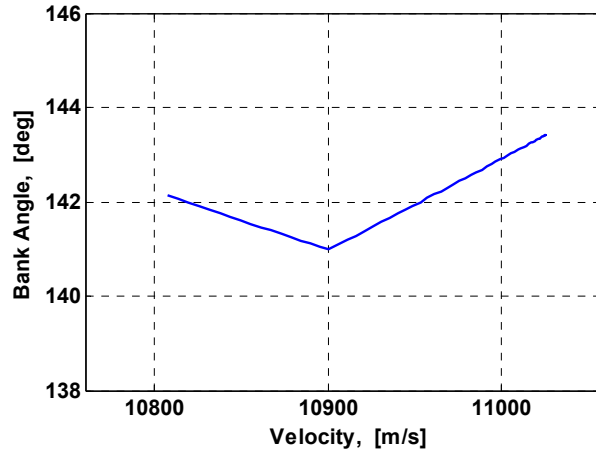


Figure 5-2: Bank angle adjustment for angle of attack less than 10° during hyperbolic approach phase

Figure 5-3 shows how the control parameters p_1 , p_2 and p_3 are updated by the guidance algorithm for deviations in initial velocity of ± 50 m/s and initial flight path angle of $\pm 0.1^\circ$. Since these deviations are the errors in initial conditions only, therefore the guidance algorithm successfully updates the control model just in the beginning of the flight to restore the trajectories to desired end conditions.

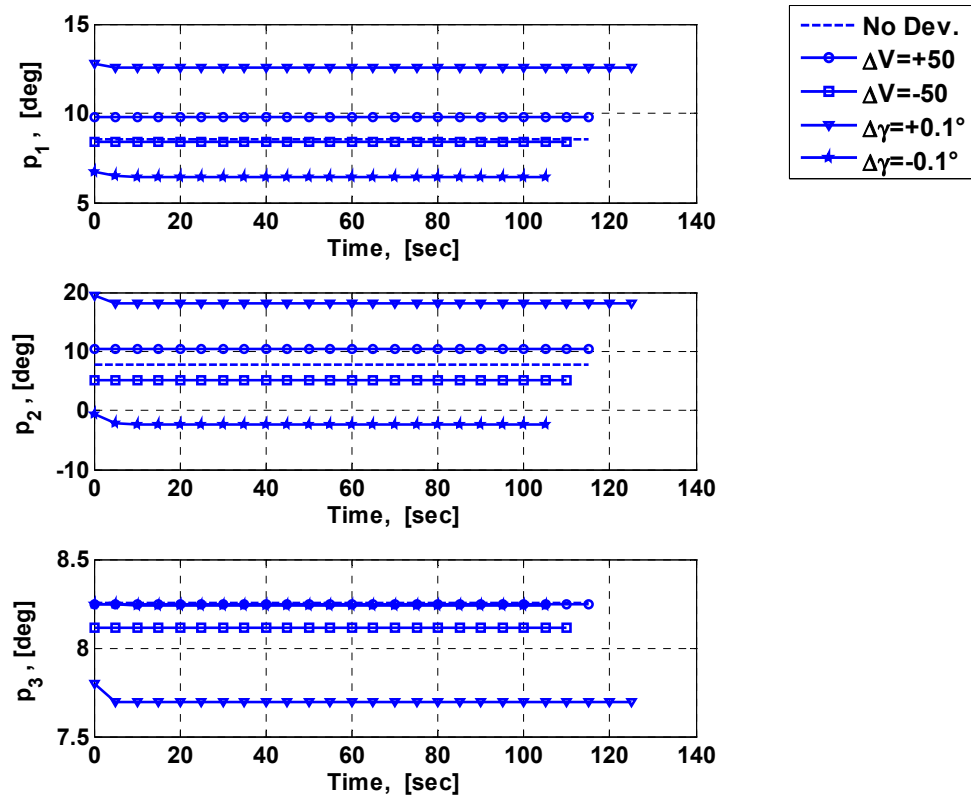


Figure 5-3: Updates of control parameters for velocity and flight path angle variations during hyperbolic approach phase

In general, parameter control model is updated throughout the flight at each guidance cycle, when there are deviations in simulation models e.g. deviation of atmospheric properties, aerodynamic and vehicle properties. As an example a guided trajectory was simulated with simulator using comparatively more precise model of MSIS-93 atmosphere, whereas the predictor using a simple model of exponential atmosphere. In Figure 5-4 it is clear that the guidance algorithm updates the control parameters at each guidance loop because of different atmosphere. In comparison it is also shown in figure that the guidance does not need any update if the atmosphere model remains same in simulator and predictor.

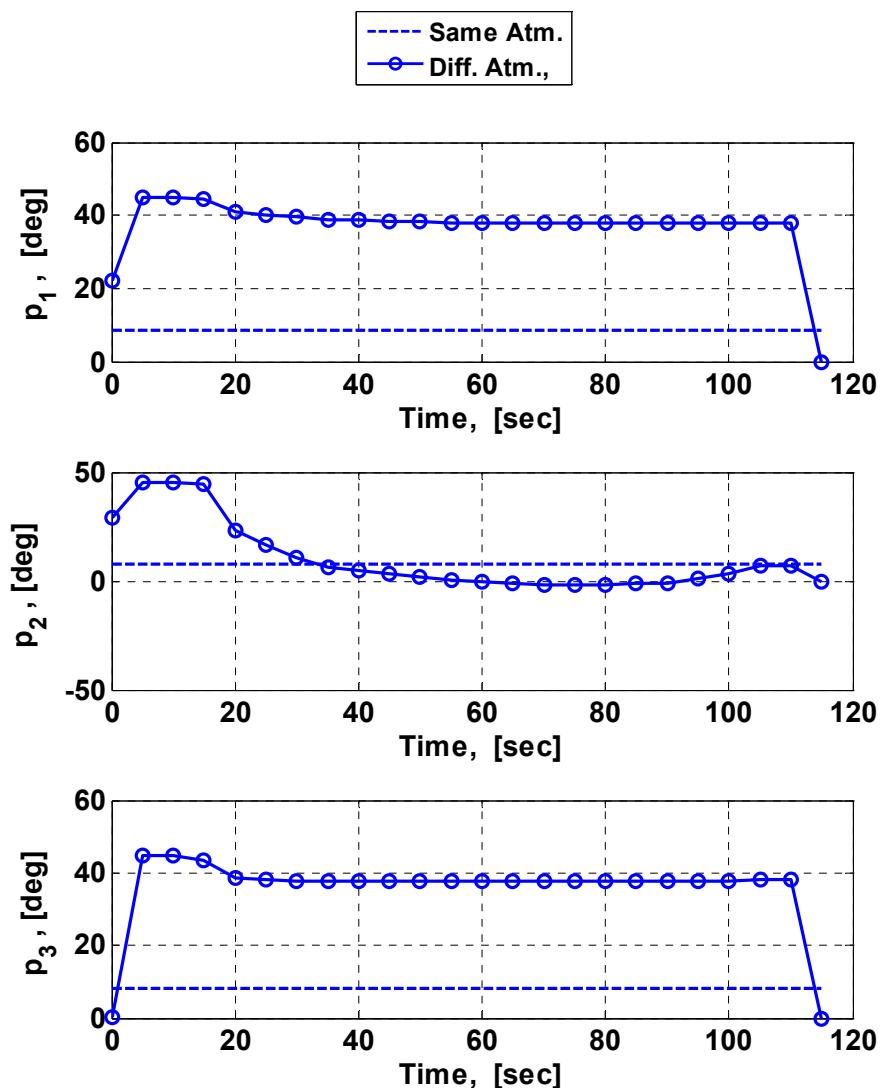


Figure 5-4: Updates of control parameters for atmospheric variations during hyperbolic approach phase

5.1.2 Constant Altitude Flight Phase

Guided simulations of the previous flight phase are continued with deviations in initial velocity of ± 50 m/s and initial flight path angle of $\pm 0.1^\circ$ to see how the height controller expressed by Equation 4-15 controls the vehicle altitude. An oscillation of vehicle about the required constant altitude can be seen in Figure 5-5. This oscillation is successfully damped and the altitude is successfully maintained within a few meters of accuracy. Deviations in initial conditions bring the vehicle to a state where the reference constant altitude varies in a small range of about ± 100 m with respect to a trajectory with no deviations at all.

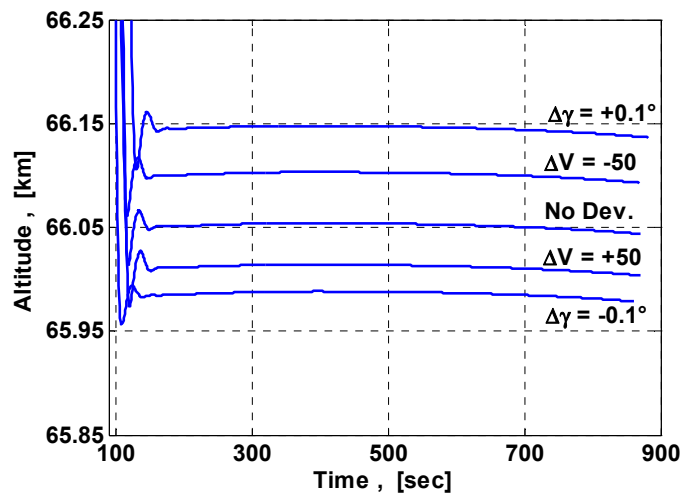


Figure 5-5: Effect of velocity and flight path angle variations on reference constant altitude during constant altitude flight phase

Variation of reference constant altitude was expected to be large as compared to above results in case of variation in atmospheric density. This was confirmed with the help of guided simulation with deviations in atmospheric density of $\pm 20\%$. As shown in Figure 5-6 the reference constant altitude varies in a range of about ± 1500 m with respect to a trajectory with no deviations at all.

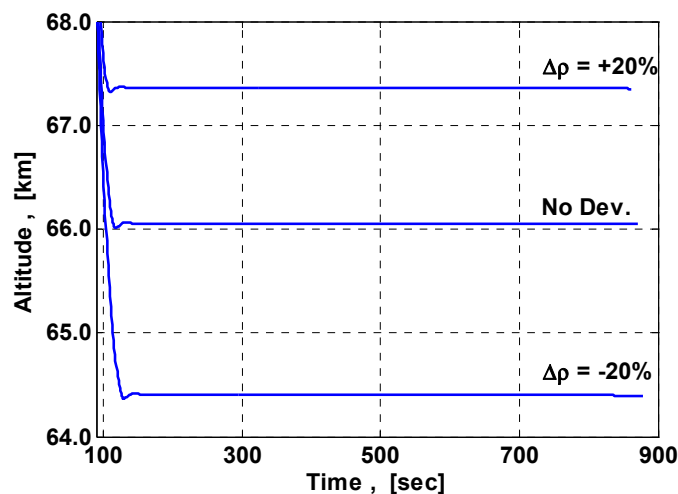


Figure 5-6: Effect of atmospheric variations on reference constant altitude during constant altitude flight phase

Duration of flight during this flight phase is very long and deviation in vehicle's drag coefficient greatly influences vehicle's energy during the flight. Velocity of the vehicle decreases rapidly in case if the drag coefficient is too high, thus having insufficient energy at the end of this flight phase or at any instant during this flight phase to fly a required downrange up to target point. Similarly the energy will be too high in case of lower drag coefficients that the vehicle will descend in the final descend phase with higher g-loads.

Figure 5-7 below depicts this situation and shows a feasible flight corridor along this flight phase on velocity versus range-to-go axes. Range-to-go is the remaining downrange to target at any instant during the flight. Corridor boundary is shown in this figure with two thick dashed lines. All the trajectories falling between these two lines are feasible and meet the target successfully while at the same time not exceed the upper limit of g-load. If the vehicle is flying a trajectory, which lies below the lower boundary of feasible corridor, than the constant altitude flight phase will end up at a point from where the vehicle is too far from the desired target point. And it does not have sufficient energy to cover the remaining downrange. Similarly if the vehicle is flying a trajectory, which lies above the upper boundary of feasible corridor, than the constant altitude flight phase will end up at a point from where the vehicle is too short from the desired target point. Since a full lift down is required in this case to reach the target, which means the vehicle will experience high g-loads, exceeding 4 g limit. Examples of infeasible trajectory with range-to-go value too large and a trajectory with g-load too high were simulated with deviations in drag coefficient of $\pm 15\%$. Figure 5-7 shows that these trajectories fall outside the boundaries of feasible corridor.

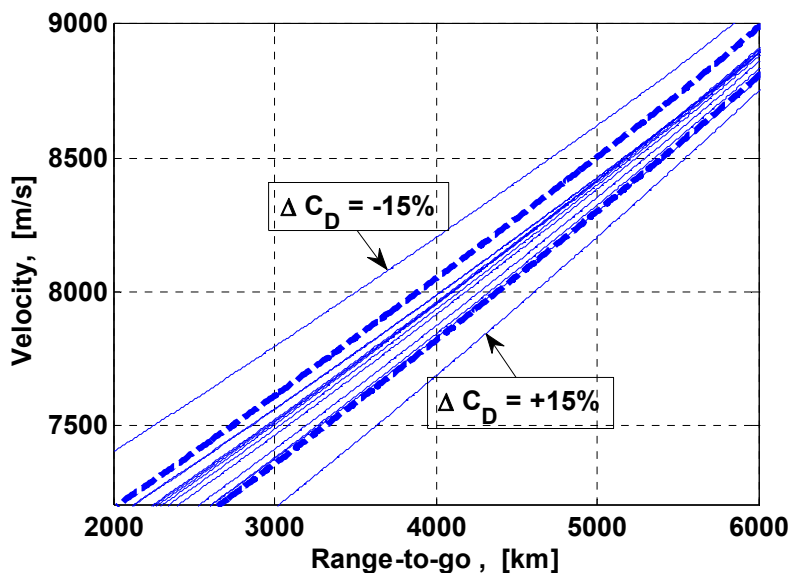


Figure 5-7: Feasible flight corridor along constant altitude phase

A solution to this problem is implemented in the form of an angle of attack switch. The simulator computes the values of instantaneous range-to-go during the constant altitude flight phase and compares it with instantaneous velocity of the

vehicle and if the velocity is found to be outside the lower or upper boundary of the feasible corridor respectively, angle of attack switch is activated. A step command is generated to decrease or increase the angle of attack by 5° . A decrease or increase in angle of attack will decrease or increase the deceleration respectively, thus bringing the vehicle inside the feasible corridor. The bank angle in this situation is then adjusted accordingly to generate required amount of lift in vertical plane. Results of simulations without activation as well as with activation of this switch are shown in figures below (Figure 5-8).

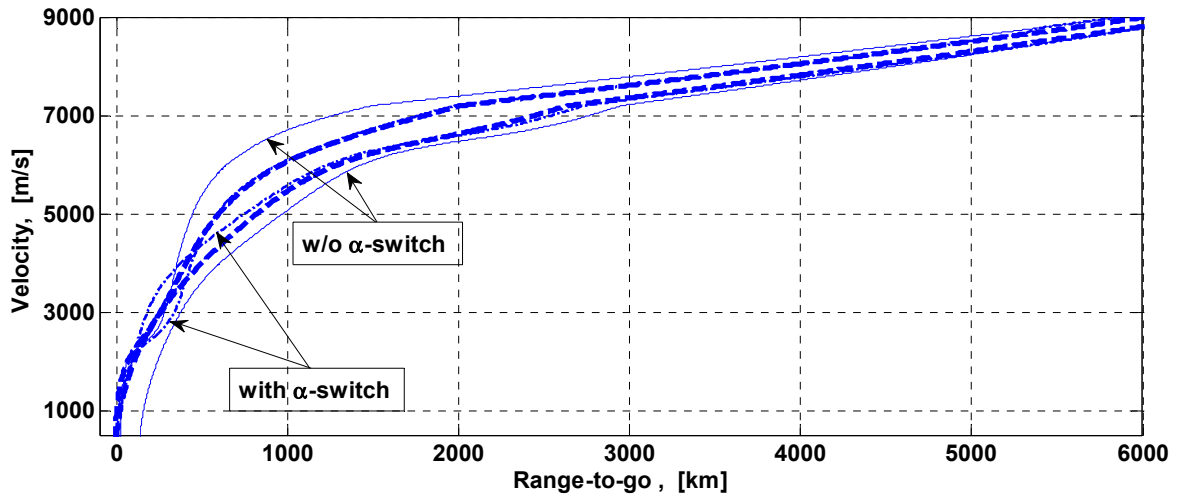


Figure 5-8: Adjustment of infeasible trajectories by increasing or decreasing the command angle of attack

The effect of decreasing angle of attack in case of trajectory with +15% deviation of drag coefficient on range to go is clear in Figure 5-8. Similarly the effect of increasing angle of attack in case of trajectory with -15% deviation of drag coefficient on deceleration load can be seen in Figure 5-9.

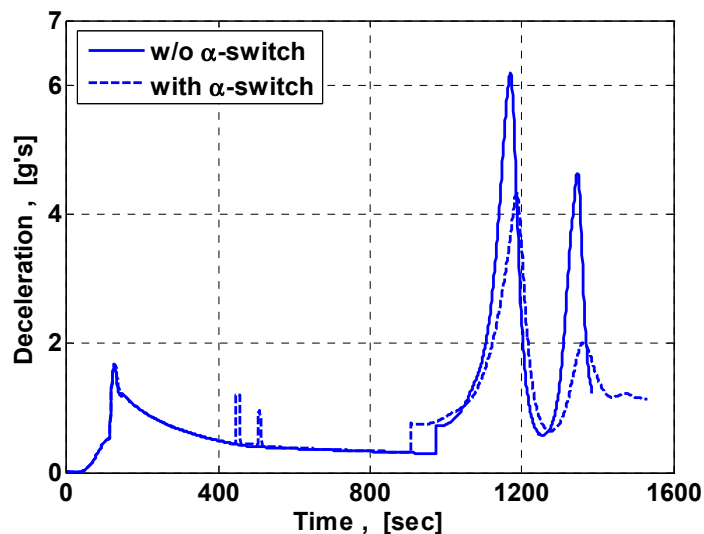


Figure 5-9: Effect of angle of attack command adjustment to an infeasible trajectory along constant altitude phase on deceleration load

5.1.3 Descend Phase with Predicted Guidance

A solution of parameterized angle of attack commands found by the optimization program before the vehicle actually enters the Earth atmosphere (step 1 of Figure 4-1) is given in Table 5-2 and shown in Figure 5-10. The stop condition, end restriction and in-flight constraint of this flight phase are:

Stop criteria: $h_{end} = 8 \pm 0.1$ km

End restriction: $\Delta R \leq 2.0$ km

In-flight constraint: $\max(\bar{a}) \leq 4.0$ g

Where ΔR is the radial dispersion of vehicle at the end of flight from the desired target point, and \bar{a} is the absolute value of acceleration experienced by the vehicle.

Table 5-2: Parameterized control model for final descend phase

v_1	7209 m/s	p_1	+60.122°
v_2	6500 m/s	p_2	+50.109°
v_3	6400 m/s	p_3	-50.095°
v_4	4000 m/s	p_4	-50.070°
v_5	3900 m/s	p_5	+50.068°
v_6	1000 m/s	p_6	+09.991°

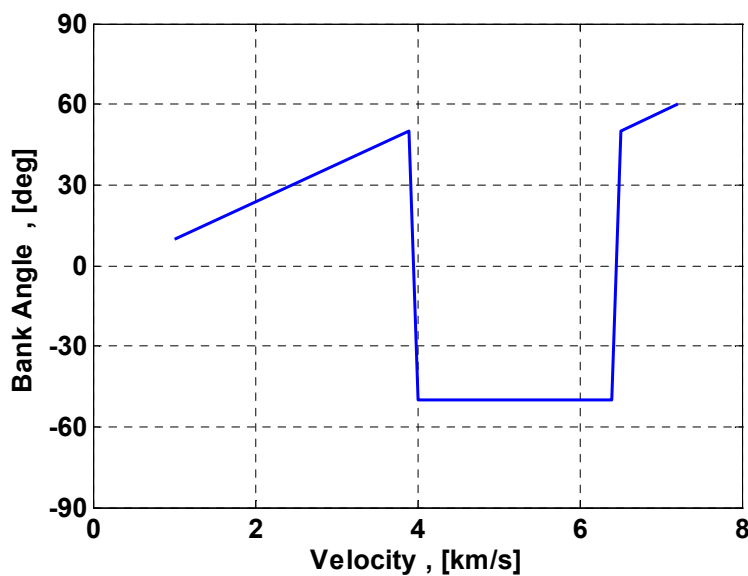


Figure 5-10: Parameterized control model for final descend phase

Guided trajectories of this flight phase were also simulated to evaluate for nominal and different off-nominal conditions. Guidance algorithm successfully guides the vehicle to the desired target point while taking care of the in-flight constraint of g-load. A plot of predicted radial dispersion with respect to desired target point at any instant of time during the third phase of guidance simulation is shown in figure below (Figure 5-11). It can be seen in the figure that whenever the vehicle tries to deviate beyond a specified limit of 2km (shown with a horizontal dotted line) from the target point the restoration step in the guidance loop bring it back to the desired target. This plot shown below is an example of a single guided simulation with +10% variation of atmospheric density.

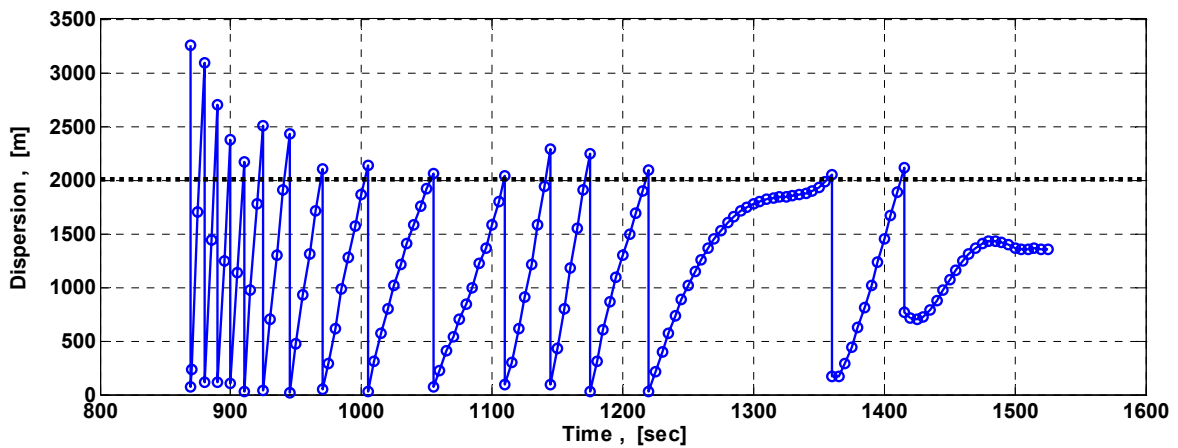


Figure 5-11: Radial dispersion from target point and 2km of dispersion limit

5.2 Sensitivity Analysis

To identify the sensitive parameter and to find the maximum allowable errors, a sensitivity analysis is conducted. The influence of variations of entry velocity, entry flight path angle and entry azimuth, entry positions, atmospheric density variation, variation of vehicle mass and variation of drag and lift coefficient on heat flux and deceleration load is studied. Uncertainty range of these parameters is shown in Table 5-3 and Table 5-4.

Table 5-3: Uncertainty ranges of entry conditions

	Parameter		Uncertainty Range	Unit
1	Entry Velocity	ΔV	[-50 +50]	m/s
2	Entry Angle	$\Delta \gamma$	[-0.1 +0.1]	deg
3	Entry Azimuth	$\Delta \chi$	[-1 +1]	deg
4	Latitude	$\Delta \delta$	[-0.1 +0.1]	deg
5	Longitude	$\Delta \lambda$	[-0.1 +0.1]	deg

Table 5-4: Uncertainty ranges of vehicle and atmospheric properties

	Parameter		Uncertainty Range	Unit
6	Vehicle Mass	ΔM	[-50 +50]	kg
7	Drag Coefficient	ΔC_D	[-10% +10%]	---
8	Lift Coefficient	ΔC_L	[-10% +10%]	---
9	Atmospheric Density	$\Delta \rho$	[-20% +20%]	kg/m ³

5.2.1 Influence of variations on Heat Flux

Influence of variations of parameters on heat flux is presented below Figure 5-12. All the lines in Figure 5-12 (left) are the variation of heat flux due to variation of parameters (increasing from left to right) with in prescribed range of errors. The behaviour of influences are in accordance to the aero-thermodynamics, since the heat flux increases with increase in entry velocity, atmospheric density and mass of the vehicle, where as it decreases with increase in drag coefficient and entry angle. Figure 5-12 (right), shows that the sensitivity of heat flux for lift coefficient is the highest. Heat flux variation for entry angle, entry velocity and atmospheric density is also high, whereas its variation for drag coefficient and vehicle mass is comparatively low. Variations of entry azimuth, entry latitude and longitude have no significant influence on heat flux.

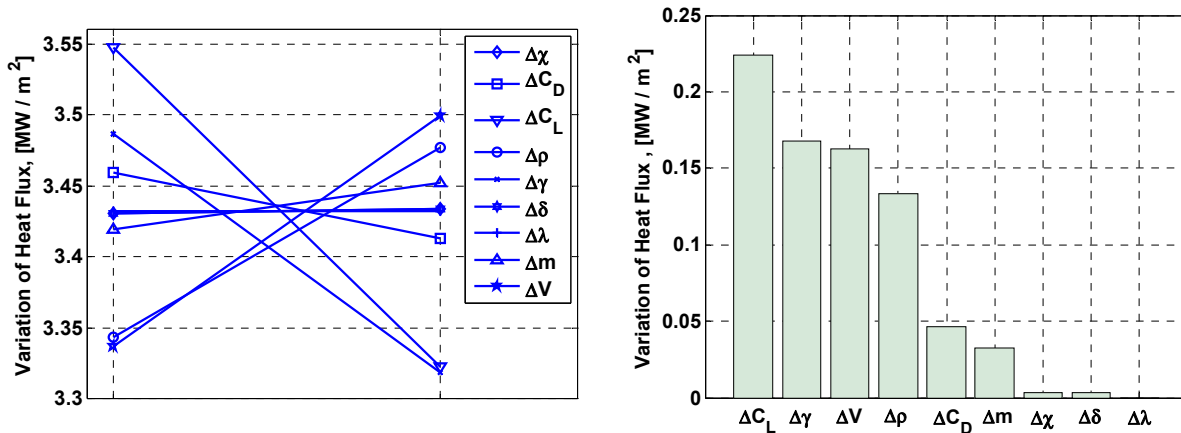


Figure 5-12: Influence of parameter variations on heat flux

5.2.2 Influence of variations on Deceleration Load

Influence of variations of parameters on deceleration load is presented below Figure 5-13. All the lines in Figure 5-13 (left) are the variation of heat flux due to variation of parameters (increasing from left to right) with in prescribed range of errors. Figure 5-13 (right), shows that the sensitivity of deceleration load for atmospheric density is the highest. Variation of deceleration load for drag

coefficient and lift coefficient atmospheric density is also high, whereas its variation for entry angle, entry velocity and entry azimuth is comparatively low. Variations of vehicle mass, entry latitude and longitude have no significant influence on deceleration load.

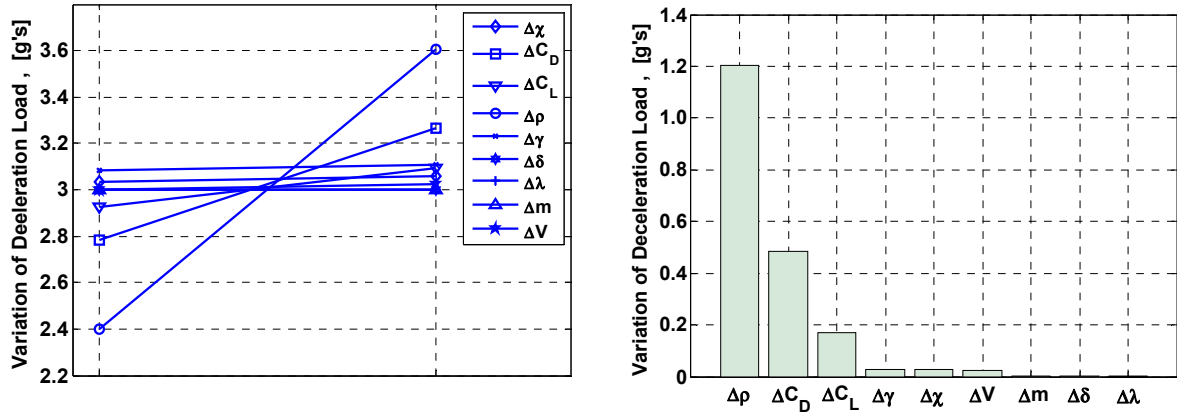


Figure 5-13: Influence of parameter variations on deceleration load

5.3 Robust Analysis of Entire Re-entry Flight

Robust analysis of the proposed guidance scheme for entire re-entry flight is done with the help of Monte Carlo simulations. A population of each parameter, for 2000 simulations, is randomly generated satisfying a normal distribution with $\pm 3\sigma$. Guided simulation are done for variations of entry velocity, entry flight path angle and entry azimuth, atmospheric density variation, variation of vehicle mass and variation of drag and lift coefficient. Uncertainty range of these parameters was given in and Table 5-3 and Table 5-4.

5.3.1 Altitude vs. Range

Contours of all trajectories generated by Monte Carlo runs are presented below in Figure 5-14, which shows the plots of downrange covered by the vehicle with respect to altitude. For a number of runs the vehicle starts with a little skip at the beginning of third phase before its final descent to the Earth surface. This happens in cases when the range to go is more and the vehicle's energy is less due to extra drag or denser atmosphere. So, a solution with little skips before final descend is found by the guidance loop for such cases to reach the desired target point.

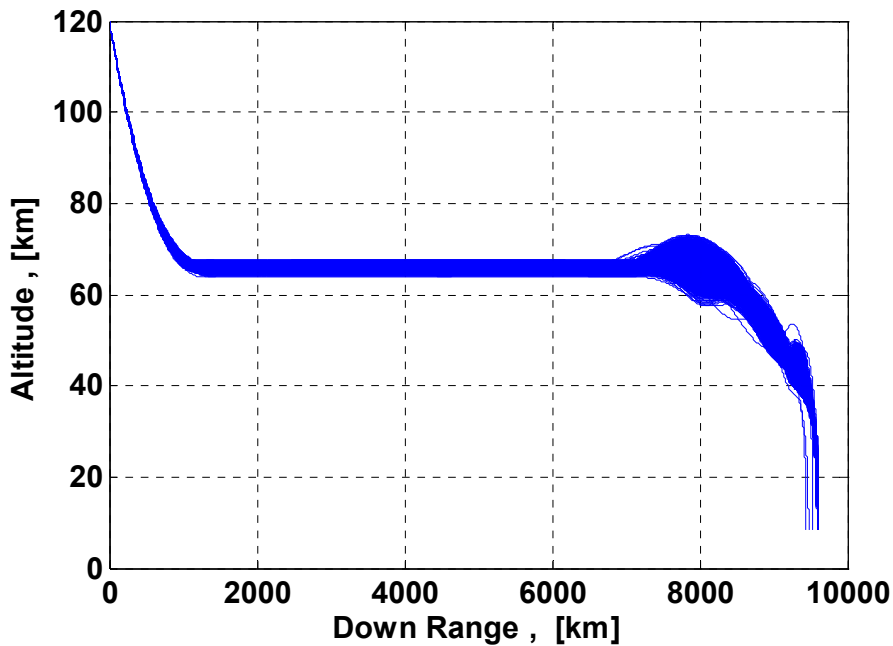


Figure 5-14: Monte Carlo Simulations - Downrange Vs Altitude

5.3.2 Dispersion of Landing Point

Landing points on Earth of all guided simulations, over a 200 km range of radial dispersion, are shown in Figure 5-15. Only two trajectories fall near to a circle of 100 km of radial dispersion and on trajectory fall near to a circle of 200 km of radial dispersion. All other trajectories, except these three, fall within a circle of 2 km of radial dispersion which is shown in Figure 5-16. The circle of 2 km of radial dispersion express the tolerance on the end restriction of final descend phase.

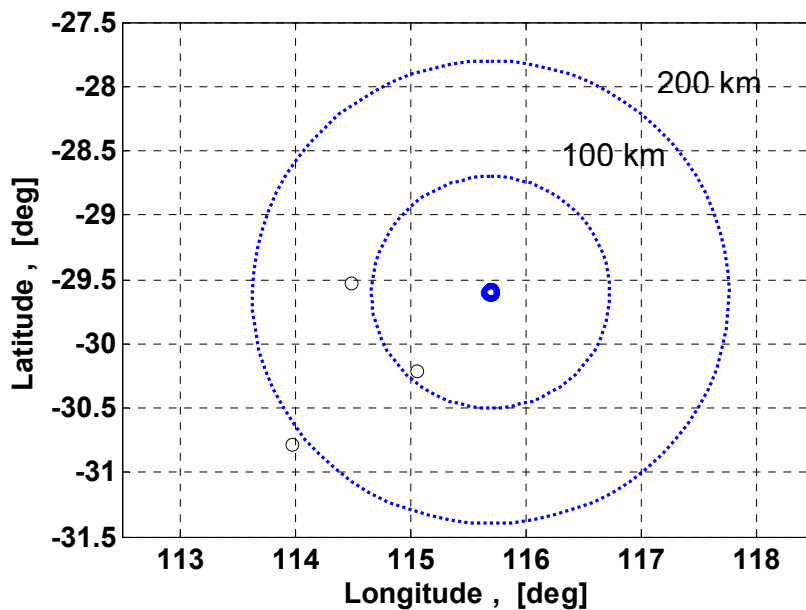


Figure 5-15: Monte Carlo Simulations – Landing points in 200 km range on surface of Earth

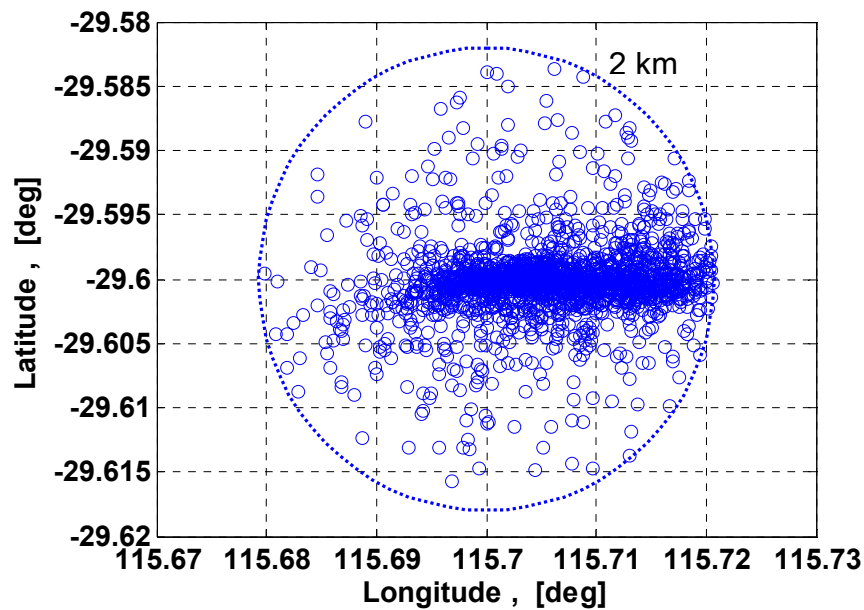


Figure 5-16: Monte Carlo Simulations – Landing points in 2 km range on surface of Earth

5.3.3 Heat Flux

Variation of stagnation point heat flux as a function of time is shown in Figure 5-17. A peak in stagnation point heat flux occurs during the first phase of re-entry and it occurs nearly at 100 seconds after entry interface. A variation 0.3 MW/m^2 is noted among the peaks of all simulation runs.

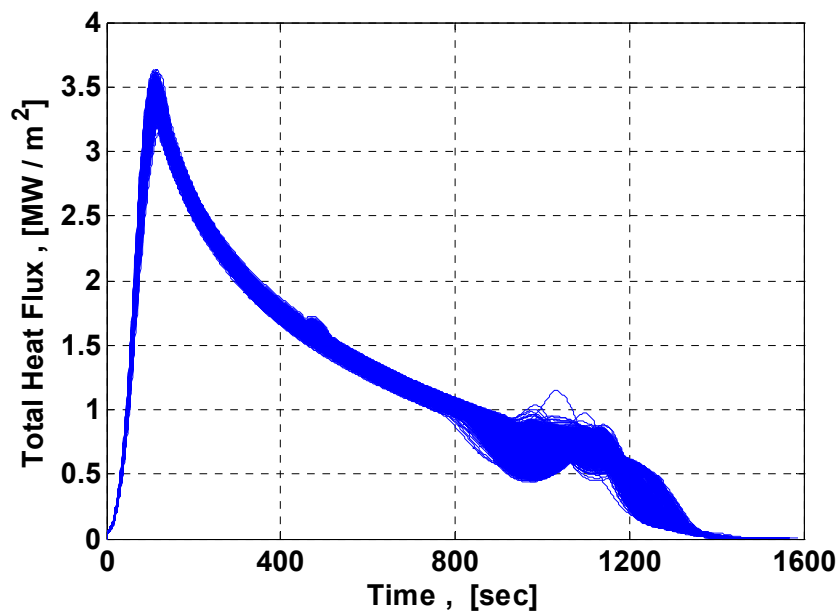


Figure 5-17: Monte Carlo Simulations – Variation of stagnation point heat load vs. time

5.3.4 Deceleration Load

Variation of deceleration load due to aerodynamic force is likewise shown in Figure 5-18. It is seen that of the trajectories remain within the limit of 4 g's, which proves the functionality of guidance algorithm for in-flight constraint. Peak deceleration load is observed mostly during the third phase; when the vehicle starts its final descent to the surface of Earth.

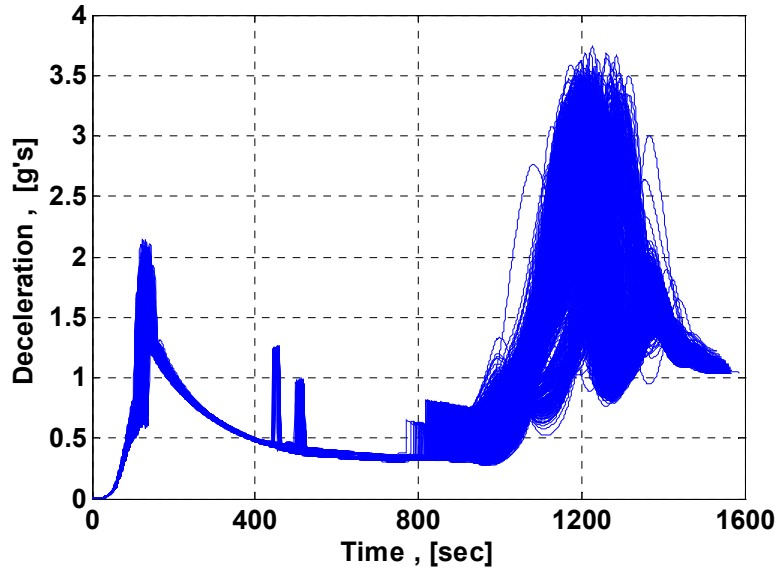


Figure 5-18: Monte Carlo Simulations – Variation of deceleration load vs. time

5.3.5 End Velocity and Mach number

Important trajectory parameters at the end of flight like velocity and Mach number are also considered (Figure 5-19 and Figure 5-20) in order to make sure that a safe deployment of parachute at the end of flight is possible. Mach number at the end of flight for all runs remain in the range of 0.4 and 0.5, which is well below transonic limit and also the speed is not too slow for safe deployment of parachute. It is to be noted that the trajectory is terminated in all cases when the vehicle is at about 8 km of altitude above earth surface.

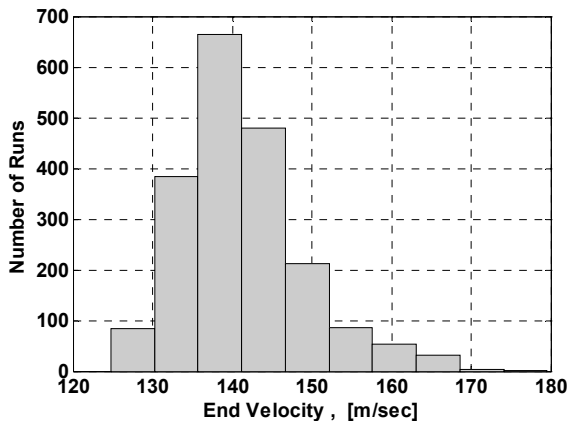


Figure 5-19: Monte Carlo Simulations – Velocity at the end of re-entry flight

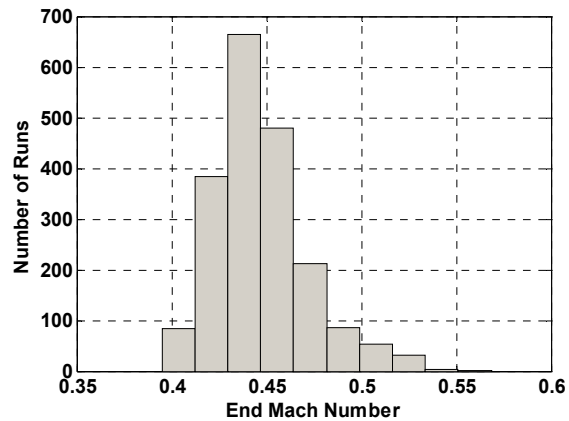


Figure 5-20: Monte Carlo Simulations – Mach number at the end of re-entry flight

5.4 Stability of Guidance Algorithm

From the results of Monte Carlo simulation for uncertainty ranges as given in Table 5-3 and Table 5-4, it is seen during the initial entry phase that the vehicle never skipped out of atmosphere as well as it does not fall deep into the atmosphere (Figure 5-14). Thus the stop criterion and the end restriction for this flight phase are efficiently selected and implemented, and the guidance algorithm always comes to a solution to bring the vehicle to the desired end conditions. The use of predictor update model in guidance scheme (section 4.3.1) made it possible to accurately predict the future trajectories based on feedbacks from accelerometer to the guidance system at predefined intervals of time.

Landing points of all the trajectories from Monte Carlo simulations in Figure 5-15 and Figure 5-16 also show that the guidance algorithm always find a solution to bring the vehicle inside the prescribed tolerance of the desired target point, except for three out of 2000 simulation runs, where it did not converge to a solution and the vehicle falls from 100 to 200 km away from the desired target point. Here again the use of predictor update model in guidance scheme (section 4.3.1) made it possible to accurately predict the future trajectories based on feedbacks from accelerometer to the guidance system at predefined intervals of time. Thus whenever the guidance scheme converges to a solution, it always brings the vehicle within the tolerance of the radial dispersion.

It was also observed, in few cases of Monte Carlo simulations, that the guidance algorithm does not converge to a solution on a number of consecutive guidance cycles. As a result the dispersion continues to increase, which can be seen in Figure 5-21 between time intervals of about 1150 seconds and 1310 seconds, which is one example from the complete set of Monte Carlo simulations. But a guidance cycle at time of about 1310 seconds converges to a solution in order to the guide the vehicle to desired target point. The horizontal dotted line in this figure is the specified tolerance of 2km from the target point.

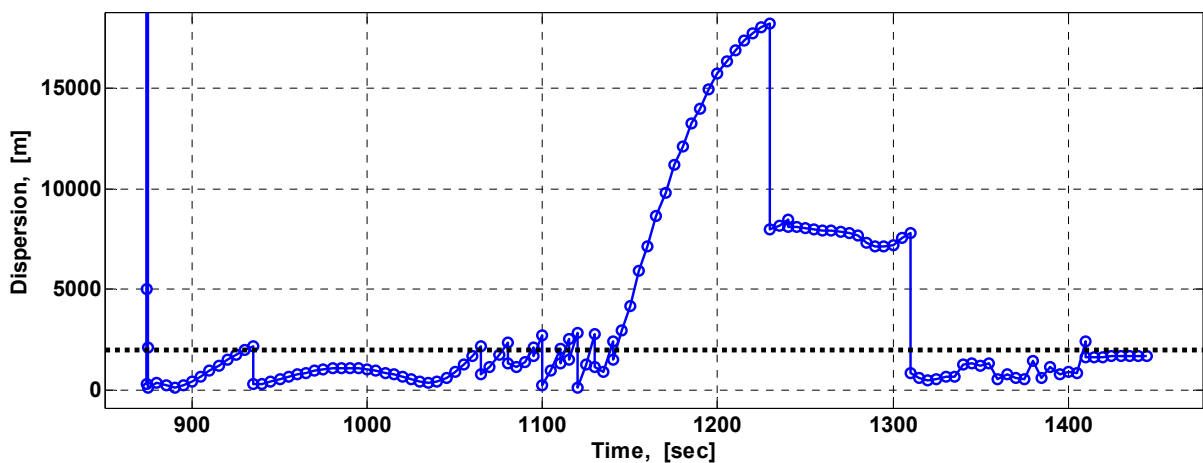


Figure 5-21: Non-convergence and then converged solutions by guidance algorithm

This phase of non-convergence during guided simulations was seen in a few cases of simulations, but every time guidance algorithm finds solutions with the passage of time, except in 3 cases, as mentioned the above. These three cases, in which the guidance algorithm never converged to a solution, are shown in Figure 5-22.

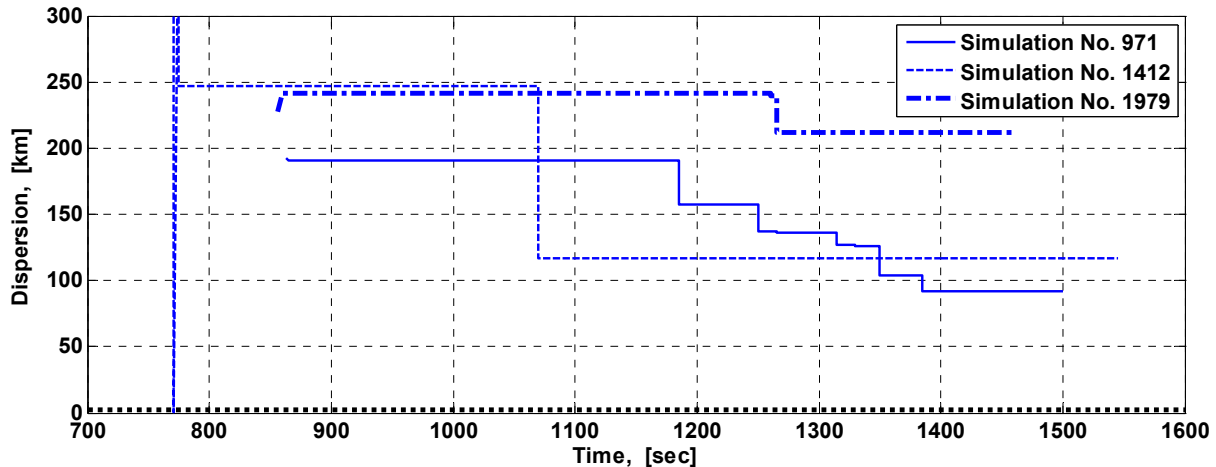


Figure 5-22: Three cases of non-convergence from set of 2000 Monte Carlo simulation

5.5 Comparison with other Guidance Schemes

A direct comparison of many of the flight parameters from other guidance concepts is generally not possible, because of different number of flight segments, different in-flight and terminal constraints, as well as unavailability of complete re-entry trajectory data of other missions. It is however tried in this section to compare different flight segments of different re-entry missions with each other and to compare some trajectory parameters which are commonly available for other re-entry missions. Original guidance concept for the re-entry of NASA's Apollo missions [26,63] and an improved Apollo guidance algorithm for crew entry vehicle (CEV) suggested by Sarah H. Bairstow [63] are considered here for comparison. CEV has a shape similar to Apollo re-entry vehicle, with larger dimensions and more weight. It will be used by NASA for future space exploration missions.

The predictive guidance scheme proposed in this thesis includes three flight phases, which have been already described and evaluated in the preceding sections. Re-entry guidance for Apollo re-entry and similarly the improved Apollo guidance for CEV [63] include a number of flight segments (see section A.6 for details). These flight segments are grouped here into three main flight phase in order to make a comparison with the predictive guidance scheme proposed in this thesis. These three phases are; initial re-entry flight phase, intermediate flight phases and final descend phase. A comparison of these flight phases for all three schemes is presented with the help of Table 5-5. Figure 5-23 also presents various flight phases of these three missions in consideration.

Table 5-5: A comparison of various guidance schemes

		Predictive Guidance Scheme (This Thesis)	Original Apollo Guidance Scheme [26,63]	Improved Apollo Guidance Scheme for CEV [63]
Initial Re-entry Phase	Description:	Starting from $h=120\text{km}$ till a safe capture is ensured.	Starting from $h\approx 120\text{km}$ till a safe capture is ensured.	Starting from $h\approx 120\text{km}$ till a safe capture is ensured.
	Capture:	Restricted by a skip function and an end condition (Sec. 4.3.1)	Pre- defined entry corridor by upper and lower limits of g-load.	Pre- defined entry corridor by upper and lower limits of g-load.
	End Condition:	Vehicle has enough lifting capability to fly horizontally.	Deceleration load is greater than a prescribed limit.	Deceleration load is greater than a prescribed limit.
	Guidance Method:	Predicted Guidance with guidance cycle at every 2 seconds interval.	Predicted Guidance with guidance cycle at every 2 seconds interval.	Predicted Guidance with guidance cycle at every 2 seconds interval.
Intermediate Phases	Description:	Constant altitude flight till safe to descend.	Constant drag phase Hunttest, down-control, up-control and ballistic phase (Kepler) phases are grouped here.	Constant drag phase Hunttest, down-control, up-control and ballistic phase (Kepler) phases are grouped here.
	End Condition:	Maximum control margin (Sec. 4.3.1)	Centre of the final phase energy bucket is targeted [26,63].	Centre of the final phase energy bucket is targeted [26,63].
	Guidance Method:	No guidance: Vehicle is controlled only to maintain a constant altitude with the help of a control law.	Constant drag policy till up-control. Reference following controller in up-control phase. Uncontrolled flight in ballistic phase.	Constant drag policy till up-control. Predicted guidance in up-control phase to target centre of final phase energy bucket. Predicted guidance in ballistic phase.
Final Descend Phase	Description:	Starting from the end of constant altitude phase.	Starting from the end of ballistic phase when g-load is more than 0.2g.	Starting from the end of ballistic phase when g-load is more than 0.2g.
	End Condition:	Pre-stored altitude.	Pre-stored velocity.	Pre-stored velocity.
	End Restriction	Tolerance on radial dispersion.	Tolerances on downrange and cross range errors.	Tolerances on downrange and cross range errors.
	Guidance Method:	Predicted Guidance with guidance cycle at every 2 seconds interval.	Reference following controller guides the vehicle to self-generated reference trajectory generated during Hunttest.	Reference following controller guides the vehicle to self-generated reference trajectory generated during Hunttest.

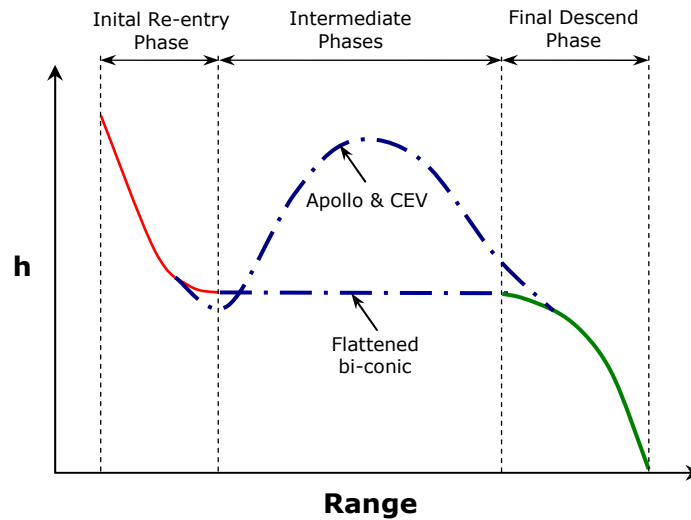


Figure 5-23: A comparison of various guidance schemes

A number of flight segments of Apollo and CEV are grouped together in intermediate flight phase. These flight segments are constant drag flight and Hunttest, down-control, up-control and ballistic flight segments. These flight segments can be seen separately in Figure A-5, and a description of each segment is also given in section A.6.

Original Apollo algorithm uses reference following controller in the up-control segment and there is no control available during the ballistic segment of flight. A Monte Carlo analysis of original Apollo guidance algorithm was done for CEV by Sarah H. Bairstow [63]. The algorithm was tested as-is for the CEV vehicle configuration. Figure 5-24 shows the landing error scatter plots for all target ranges from the results of Monte Carlo analyses, which were performed by Sarah for various target ranges: 2400 km, 3500 km, 4600 km, 7300 km, and 10000 km.

For short target ranges (i.e. 2400 km) and medium target ranges (i.e. 3500 km and 4600 km) the Apollo re-entry guidance performed with acceptable precision landing. However, long target ranges (7,300 km and 10,000 km, requiring a substantial skip and extended periods of time in the Ballistic phase) did not achieve acceptable precision landing. This large error in landing is mainly due to the non availability of a control system during a long duration of ballistic flight. Although the concept of final phase energy bucket is used in this algorithm to fly the final descend phase with sufficient control margin, but the terminal errors at the end of up-control phase are integrated over a long duration of time during ballistic flight. As a result the deviation of states at the start of final descend phase are sufficiently large. The reference following controller in such cases fails to guide the vehicle to a predefined reference trajectory.

In the proposed guidance scheme of this research work for flattened bi-conic vehicle, the flight of the vehicle is controlled during the constant altitude flight phase with the help of a control law and terminates at a point from where the vehicle can fly final descend phase with sufficient control margin.

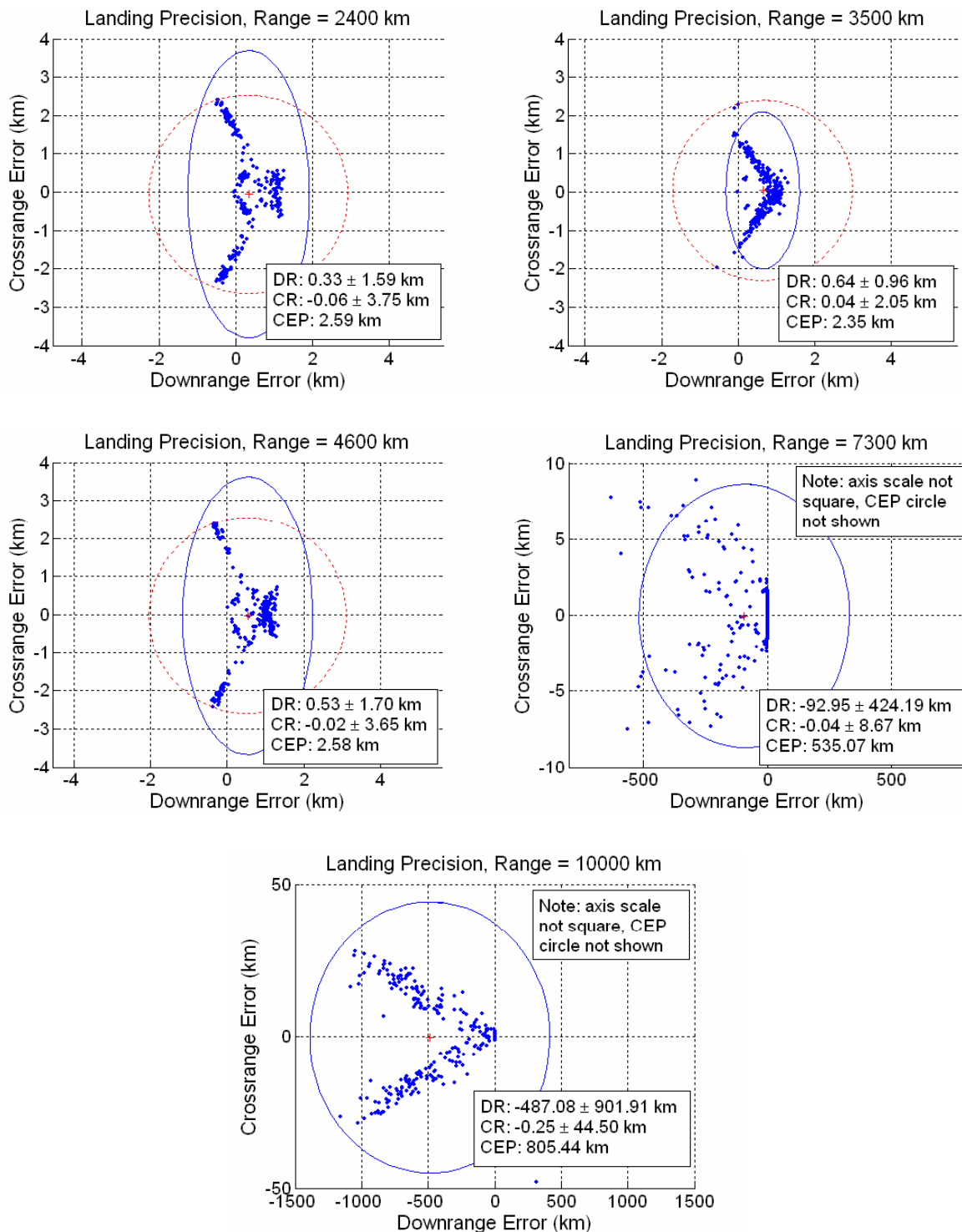


Figure 5-24: Landing error plots from simulations of original Apollo guidance algorithm by S. H. Bairstow [63]

Sarah H. Bairstow [63] analysed the results of original Apollo guidance and proposed to use predicted guidance in up-control as well as in ballistic flight segments. Despite a limited controllability during ballistic flight, because of very thin atmosphere, the results show the improved precision landing performance for the 10,000 km target range (Figure 5-25).

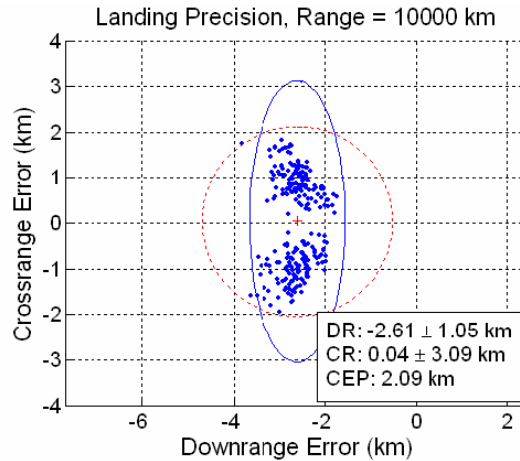


Figure 5-25: Landing error plots from simulations of improved Apollo guidance algorithm by S. H. Bairstow [63]

The proposed guidance scheme for flattened bi-conic vehicle in this thesis does not have any guidance during constant altitude flight phase, or intermediate flight phase (to compare with Apollo and CEV). Conditions to terminate this flight phase are efficiently implemented, which results in a same precision of landing compared to the improved Apollo guidance (using predicted guidance in up-control as well as ballistic flight segments).

5.6 Summary

A guidance algorithm has been developed, which can be implemented onboard, with capabilities of onboard trajectory optimization of entire re-entry flight prior to entry interface and onboard trajectory prediction and correction during re-entry flight. The proposed guidance scheme for flattened bi-conic vehicle is successfully implemented and guided simulations a done for different conditions. A number of guided simulations were also done to check the functionality of the guidance scheme as well as to see the effects of deviations of different parameters on important trajectory parameters e.g. maximum heat flux, maximum g-load, velocity or mach number at the end of flight. From the results of guided simulations it was seen that the proposed guidance scheme is successfully working with most of the trajectory parameters under acceptable range. Sensitivity analysis with the help of Monte Carlo simulations has further proved the functionality and robustness of the scheme. The prominent features of the algorithm are as follows:

Complete guidance scheme is divided into three phases and each phase has its own objective and end conditions. The first phase of flight for example is completely independent of the next phases. In the guidance loop of this phase future trajectories of are predicted only till the end of this phase and the only objective of this phase is to bring the vehicle to such a state that the vehicle achieve enough aerodynamic controllability to maintain a constant altitude in the next phase.

In the proposed guidance scheme for flattened bi-conic vehicle, the flight of the vehicle is controlled during the constant altitude flight phase with the help of a control law and terminates at a point from where the vehicle can fly final descend

phase with sufficient control margin. Whereas original Apollo algorithm ends up with large deviations from landing point in case of large target ranges due to the non availability of a control system during a long duration of ballistic flight. The proposed guidance scheme for flattened bi-conic vehicle in this thesis does not have any guidance during constant altitude flight phase, or intermediate flight phase (to compare with Apollo and CEV). The improved Apollo guidance by Sarah H. Bairstow [63] used predicted guidance in two flight segments of intermediate flight phase (up-control and ballistic flight segments) to achieve the required landing precision for larger target ranges.

6 Conclusion

6.1 Summary of the Research

In this thesis mission and vehicle analysis of various vehicle concepts for a human rated lunar return mission has been investigated. The vehicles for this analysis are either taken from the proposed vehicle concepts from literature or taken from real re-entry missions like Apollo. The reference mission for this investigation is the Earth capture and re-entry phase of lunar return mission with crew inside. The research consists of three areas of interest of a re-entry mission.

1. Mission and vehicle analysis of different types of vehicles suitable for such mission.
2. The development and implementation of guidance logics during different flight segments of the re-entry flight till parachute deployment.
3. The evaluation of re-entry flight and a guidance scheme with the help of sensitivity analysis to determine the influence of off-nominal conditions.

An existing three degree of freedom trajectory simulation tool TDS is used to simulate re-entry trajectories in a three dimensional space while treating the vehicle as a point mass. The software was already used at IRS for the analysis of a number of sub-orbital, orbital, and super-orbital re-entry missions. Mission and system analysis of different vehicles for re-entry from interplanetary return missions was already carried out at IRS using this simulation tool before the beginning of this research. The results of uncontrolled Stardust re-entry vehicle from the already performed analysis were regenerated for this research work, before using it for the mission and vehicle analysis of vehicle with control capabilities as well as for the development of guidance environment. A direct comparison showed that the simulated trajectory results were in agreement with actual flight data of Stardust re-entry vehicle. Analysis of variations of various trajectory parameters were found to be in agreement with dynamics and aero-thermodynamics, i.e. the variations of aerodynamic and aero-thermal loads and deviation of trajectories from standard conditions are found to be in accordance with the variation in input conditions.

Mission and vehicle analysis was further extended for different types of re-entry vehicles and then the performance of 3 different configurations of re-entry vehicles

were assessed with the help of TDS simulation tool. Three vehicles in consideration were; an Apollo like capsule, a flattened bi-conic and a winged vehicle. The L/D ratio of these vehicles about 0.3, 0.7, and 2.2 respectively places them in the categories of low, medium and high lifting vehicles respectively. A comparative analysis from the results of mission and system analysis these vehicles were performed using five performance parameters; 1- *volumetric efficiency*, 2- *controllability*, 3- *peak deceleration during re-entry*, 4- *stagnation point heating rates*, and 5- *total heat load during re-entry*. The result of the comparison is concluded in the following paragraphs:

Apollo like capsule has the advantages of lower integral heat load, simplest adaptability in the launcher system and maximum volumetric efficiency.

High-lift vehicle keeps a constant altitude where the atmospheric density is much less and therefore flying at much lower deceleration loads. Requirement of large wing span make it difficult to integrate with the launcher system. Total heat input to the vehicle is almost 22 times the integral heat load of Apollo capsule. Already having low volumetric efficiency, a large amount of thermal protection would be required to protect the vehicle itself, and astronauts and instruments inside it.

Flattened bi-conic has the advantages of better controllability, launcher system adaptability, better volumetric efficiency and lesser integral heat load as compared to high lifting vehicle. It re-enters at lower deceleration load of around 2 g's but with higher stagnation point and higher total heat load, about 8 times the integral heat load of Apollo capsule.

Flattened bi-conic vehicle found to be most suitable among three vehicles which gained highest score in the assessment of performance parameters since; its design is simple, it does not experience very high integral load when compared with high-lift vehicle, it does not experience very high deceleration load like Apollo capsule, and it has better controllability.

After definition of a reference mission for flattened bi-conic vehicle, the development of a guidance algorithm was started. The proposed guidance method is an evolution of IRS guidance algorithm, which is based on predictive guidance method (explicit guidance). The guidance methods, till the start of this research work, were developed for various *sub-orbital* and *orbital* missions, and applied to complete flight scenarios (including launch, coasting and re-entry phases) as well as to individual flight phases e.g. only re-entry, TAEM, etc. The guidance method in this research work was extended to missions re-entering at *super-orbital* speed.

The proposed guidance scheme was successfully implemented for flattened bi-conic vehicle and guided simulations were done for different conditions. Use of lift forces during interplanetary re-entry is considered and a re-entry approach with a constant altitude flight phase is studied. Since re-entry from space to ground includes three phases, i.e. hyperbolic approach phase, constant altitude phase, and final descend phase. So the guidance algorithm is also implemented in three phases, i.e. hyperbolic approach phase with predicted guidance, constant altitude phase with a control law, and final descend phase with predicted guidance. In

addition there is also a Pre-entry phase, which begins as soon as the guidance algorithm gains control of the vehicle. In this phase time is used for the costly flight path optimization of the upcoming flight phase. The attitude (upside down) of the vehicle is achieved and maintained during this phase until a sensible atmosphere has been detected.

Since, complete guidance scheme is divided into three phases, so each phase has its own objective and end conditions. The first phase of flight for example is completely independent of the succeeding phases. In the guidance loop of each phase future trajectories are predicted only till the end of this phase and the only objective of this phase is to bring the vehicle to such a state that the vehicle achieve enough aerodynamic controllability to maintain a constant altitude in the succeeding phase.

A number of guided simulations were also done to check the functionality of the guidance scheme as well as to see the effects of deviations of different parameters on important trajectory parameters e.g. maximum heat flux, maximum g-load, velocity or mach number at the end of flight. From the results of guided simulations it is seen that the proposed guidance scheme is successfully working with most of the trajectory parameters under acceptable range.

Sensitivity analysis with the help of Monte Carlo simulations has further proved the functionality and reliability of the scheme. This guidance scheme offers a high degree of autonomy and self solving capability due to its onboard trajectory optimization which is necessary to obtain cost saving as well as safety and flexibility options in future applications.

Results of Monte Carlo simulations showed that the guidance algorithm did not converge to a solution only for 3 out of 2000 simulation runs and the vehicle falls from 100 to 200 km away from the desired target point. It was also observed, in few cases of Monte Carlo simulations, that the guidance algorithm does not converge to a solution on a number of consecutive guidance cycles during a single guided simulation. As a result the dispersion continues to increase, but a guidance cycle at later stages converges to a solution and brings the vehicle to desired target point.

The proposed guidance scheme was also compared with original Apollo guidance algorithm and an improved Apollo guidance algorithm. In the proposed guidance scheme for flattened bi-conic vehicle, the flight of the vehicle is always controlled during the constant altitude flight phase with the help of a control law and terminates at a point from where the vehicle can fly final descend phase with sufficient control margin. Whereas original Apollo algorithm ends up with large deviations from landing point in case of large target ranges due to the non availability of a control system during a long duration of ballistic flight. The proposed guidance scheme for flattened bi-conic vehicle in this thesis does not have any guidance during constant altitude flight phase, or intermediate flight phase (to compare with Apollo and CEV). The improved Apollo guidance used predicted guidance in two flight segments of intermediate flight phase (up-control

and ballistic flight segments) to achieve the required landing precision for larger target ranges.

6.2 Future Improvements

A computer program was developed in this research for the implementation of the proposed guidance algorithm. A number of sub-programs work together in the main program to simulate the guided flights. The sub-programs include the existing TDS simulation tool as well as the subroutines which were developed in this research work where required. The program can be said to be in an un-optimised state, since various subroutines or portions of subroutines from TDS tool remained unused and are redundant. Optimisation of the code would allow for faster operating speeds.

A possible inclusion of the concept of final phase energy bucket as used in original Apollo algorithm can be studied in future, to see if it helps to achieve same precision of landing point for a wider range of uncertainties.

A better comparison to the other guidance methods could be achieved by performing simulations in a common analysis tool consisting of the same vehicle and environmental models, mission profile and off-nominal conditions.

Random sampling with Gaussian distribution was used in Monte Carlo simulations to carry out sensitivity analysis of the guidance algorithm. Other sampling methods, as mentioned in this thesis, e.g. *latin hypercube sampling* or *orthogonal sampling* can be used in future to see if they produce better distribution of parameters with smaller sampling size in the specified range of uncertainties.

References

1. Aerocapture Technology; NASA, FS-2004-09-127-MSFC, July 2004.
2. *Anderson, J. D.*; Hypersonic and High Temperature Gas Dynamics; AIAA, 2006, Chapter 3, pp 59.
3. *Anderson, J. D.*; Hypersonic and High Temperature Gas Dynamics; AIAA, 2006, Chapter 6, pp 349.
4. *Anderson, J. D.*; An Engineering Survey of Radiating Shock Layers; AIAA Journal, Vol. 7, No. 3, September 1969.
5. Apollo-8 Mission Report; NASA, MSC-PA-R-69-1, Manned Spacecraft Centre, Houston, Texas, February 1969.
6. Apollo-8 Mission Report - Trajectory Reconstruction and Post-flight Analysis; NASA, MSC-PA-R-69- 1 Supplement 1, Manned Spacecraft Centre, Houston, Texas, November 1969.
7. Apollo-8 Mission Report – Guidance, Navigation and Control System Performance Analysis; NASA, MSC-PA-R-69-1 Supplement 2, Manned Spacecraft Centre, Houston, Texas, November 1969.
8. *Arden L. Albee, Raymond E. Arvidson, Frank Palluconi and Thomas Thorpe*; Overview of the Mars Global Surveyor mission; Journal of Geophysical Research, Vol. 106, No. E10, Pages 23,291–23,316, October 25, 2001.
9. *Betts J. T.*; Survey of numerical methods for trajectory optimization; Journal of Guidance, Control and Dynamics, 21(2):193–207.
10. *Bonnet, M. R., Swings, J. P.*; The Aurora Programme; ESA Publication Division, Noordwijk, the Netherlands – 2004.
11. *Brian Hoelscher*; Orion Entry, Descent, and Landing Performance and Mission Design; AIAA-2007-6428, AIAA Guidance, Navigation and Control Conference and Exhibit, Hilton Head, South Carolina, Aug. 20-23, 2007.
12. *Daan Frenkel*; Introduction to Monte Carlo Methods; Computational Soft Matter: From Synthetic Polymers to Proteins, Lecture Notes, NIC Series, Vol. 23, ISBN 3-00-012641-4, pp. 29-60, 2004.

13. *David S. F. Portree*; Mir Hardware Heritage; *NASA RP 1357, March 1995.*
14. *Daniela Bolz*; Eintrittsflugbahnen für interplanetarer Rückkehrmissionen; *Studienarbeit, Institut für Raumfahrtsysteme, Universität Stuttgart, IRS-06-S-45, November 2006.*
15. *E. Wallner, J. Burkhardt, F. Zimmermann, U. M. Schoettle, K. H. Well*; A Guidance and Control Concept for the X-38 Re-entry Vehicle; *IAF-99 A.1.04, 50th International Astronautical Congress, Amsterdam – 1999*
16. *E. Wallner, M. Graesslin, S. Mueller, K. Well, U. Schoettle, O. Wagner, G. Sachs*; Development of Guidance and Control Algorithms Applied to the X-38 Return Vehicle; *DGLR-JT2002-100, Deutscher Luft- und Raumfahrtkongress, Stuttgart – 2002*
17. *F. Mistree, U. Lautenschlager, S. O. Erikstad, and J. K. Allen*; Simulation Reduction Using the Taguchi Method; *NASA Contractor Report 4542, October 1993.*
18. *Florian Hindenlang*; Evaluating a Local Approximate Method on Surface Heating for Hypersonic Vehicle Design; *IRS-06-S39.*
19. *Frank J.A.*; Re-Entry Vehicle Dynamics; *AIAA Education Series; 1984.*
20. *Frank J.A., Satya M.A.*; Dynamics of Atmospheric Re-entry; *AIAA Education Series; 1993.*
21. *Graves, C. and Harpold, J.*; Re-Entry Targeting Philosophy and Flight Results from Apollo 10 and 11; *AIAA Paper 70-28, 1970.*
22. Guidance and Navigation of Entry Vehicles; *NASA SP-8015, November 1968.*
23. *Hedin. A.E.*; Extension of MSIS Thermosphere Model into the Middle and Lower Atmosphere; *Journal of Geophysical Research, 96, A2, pp1159-1172, 1991.*
24. *Henry C. Leasing, Robert E. Coate*; A Simple Atmospheric Re-entry Guidance Scheme for Return From the Manned Mars Mission; *NASA TN D-3422.*
25. Human Space Flight Mission Programme; *Indian Space Research Organisation, <http://www.isro.org/scripts/futureprogramme.aspx#Human>, retrieved 11.03.2010.*
26. *I. Bogner*; Description of Apollo Entry Guidance; *NASA TM-66-2012, August 1966.*
27. *James Chartres, Michael Graesslin, Gerald Schneider*; A New Method of Terminal Area Guidance for Future Reusable Launch Vehicles; *IAC-05 C1.8.05, 56th International Astronautical Congress, Fukuoka – 2005.*
28. *James Chartres, Michael Graesslin, Gerald Schneider*; Optimization of Terminal Flight Phase for a Future Reusable Launch Vehicle; *AIAA-2005-6060, AIAA Guidance Navigation and Control Conference, San Francisco – 2005.*

29. James T. A. Chartres; Trajectory Design, Optimization and Guidance for Reusable Launch Vehicles during the Terminal Area Flight Phase; *PhD Thesis, The University of Adelaide, Feb.-2007.*
30. Joel M. Broome, Dr. Wyatt Johnson; Orion Entry, Descent, and Landing Performance and Mission Design; *AIAA-2007-6430, AIAA Guidance, Navigation and Control Conference and Exhibit, Hilton Head, South Carolina, Aug. 20-23, 2007.*
31. J. L. Speyer, H. J. Kelley, N. Levine, W. F. Denham; Accelerated Gradient Projection Technique with Application to Rocket Trajectory Optimization; *Automatica, Vol 7, pp. 37-43, 1971.*
32. Johannes Burkhardt, Michael Graesslin, Ulrich M. Schoettle; Impact of Mission Constraints on Optimal Flight Trajectories for the Lifting Body X-38; *AIAA-99-4167, AIAA Atmospheric Flight Conference, Portland – 1999.*
33. John F. Connolly, Constellation Program Overview, *October 2006, http://www.nasa.gov/pdf/163092main_constellation_program_overview.pdf, retrieved 12.03.2009.*
34. Jon C. Harpold, Claude A. Graves; Shuttle Program: Shuttle Entry Guidance; *NASA-TM-79949, February 1979.*
35. Jose F. Padilla, Iain D. Boyd; Assessment of Rarefied Hypersonic Aerodynamics Modelling and Wind Tunnel Data; *AIAA 2006-3390.*
36. J. Telaar, U. M. Schoettle; Leistungsvergleich NLP-Basierter Lenkkonzept für Trägeraufstiegsmissionen mit Optimalsteuerungen; *DGLR-JT2003-190, Deutscher Luft- und Raumfahrtkongress, Munich – 2003.*
37. Jürgen Telaar; Entwicklung eines prädiktiven Lenkverfahrens für wiederverwendbare Raumtransportsysteme, *Dissertation der Universität Stuttgart, 2005.*
38. L. Schwartz; Optimization Techniques – A Comparison; *FDL-TDR-64-21; 1964.*
39. Lunar Exploration Program; *<http://www.jspec.jaxa.jp/e/enterprise/moon.html>, retrieved 11.03.2010.*
40. Man-Systems Integration Standards - NASA Technical Standards Program; *NASA-STD-3000.*
41. Maria S. Smith; China's Space Program: An Overview; *October 18, 2005 <http://fas.org/sgp/crs/space/RS21641.pdf>, retrieved 11.03.2010.*
42. Mario De Stefano Fumo; A Study of a High Lift Wing-Body Configuration for Low Earth Orbit Re-Entry; *PhD Thesis, Chapter 6, Faculty of Engineering, Universita' Degli Studi Di Napoli, Italy.*
43. Mark S. Gockenbach; An Introduction to Sequential Quadratic Programming; *<http://www.math.mtu.edu/~msgocken/ma5630spring2003/lectures/sqp1/sqp1.pdf>; cited 22.12.2009.*

44. M. D. McKay, R. J. Beckman, W. J. Conover; A Comparison of Three Methods for Selecting Values of Input Variables in the Analysis of Output from a Computer Code; *Technometrics*, Vol. 21, No. 2 (May, 1979), pp. 239-245.
45. M. E. Tauber, K. Sutton; Stagnation-Point Heating Relations for Earth and Mars Entries; *Journal of Spacecraft*, Vol. 28, No. 1, Jan-Feb 1991.
46. M. Graesslin, U. Schoettle; A NLP Based Re-entry Flight Guidance Algorithm; *International Symposium on Space Flight Dynamics (2004) Munich / Germany.*
47. M. H. Graesslin; Entwurf und Analyse eines prädiktiven Lenkkonzepts für Rückkehrmissionen auftriebsgestützter Raumfahrzeuge; *Dissertation der Universität Stuttgart, D93, 2004.*
48. M. H. Graesslin, J. Telaar, U. M. Schoettle; Ascent and Re-entry Guidance Concept Based on NLP Methods; *Acta Astronautica*, 55 (2004) 461–471.
49. M. H. Graesslin, U. M. Schoettle, E. M. Wallner, K. H. Well, J. Burkhardt; Adaptive Guidance and Control Algorithms Applied to the X-38 Reentry Mission; *IAC-02 A.1.08, 53rd International Astronautical Congress, Houston – 2002*
50. M. H. Graesslin, U. M. Schoettle, E. M. Wallner, K. H. Well, J. Burkhardt; Ascent and Re-entry Guidance Concept Based on NLP Methods; *IAC-03 A.2.07, 54th International Astronautical Congress, Bremen – 2003.*
51. M. I. Afzal M. H. Graesslin, H. -P Roeser; Study of Various Re-entry Vehicle Configurations for Future Interplanetary Missions; *Deutscher Luft- und Raumfahrtkongress 2008, Darmstadt / Germany.*
52. M. I. Afzal M. H. Graesslin, H. -P Roeser; An Explicit Guidance Method for a Lifting Interplanetary Re-entry Vehicle; *AIAA- 2009-6108, AIAA Guidance Navigation and Control Conference 2009, Chicago II / USA.*
53. Nelder J. A.; Mead, R. A; Simplex Method for Function Minimization; *Computer Journal* 7(1965) 308-313.
54. Pasquale M. Sforza; EAS4710 Aerospace Design 2 – Space Access Vehicle Design, *Department of Mechanical and Aerospace Engineering, University of Florida, <http://aemes.mae.ufl.edu/~sforza/EAS4710>.*
55. Planetary Mission Entry Vehicles, Quick Reference Guide, Version 2.1; *NASA Ames Research Centre.*
56. Prasun N. Desai, Dan T. Lyons, Jeff Tooley, Julie Kangas; Entry, Descent and Landing Operations Analysis for the Stardust Re-entry Capsule; *AIAA-2006-6410*
57. Resit Unal, Edwin B. Dean; Taguchi Approach to Design Optimization for Quality and Cost: An Overview; *Annual Conference of the International Society of Parametric Analysts 1991.*

58. R. Monti, R. Janovsky, M. De Stefano Fumo; Exploiting Lift Force in Re-entries from Exploration Missions; *DGLR International Symposium 'To Moon and Beyond', Bremen – 2007.*
59. Roach John; NASA Aims for Moon by 2018, Unveils New Ship; *National Geographic (September 19, 2005) http://news.nationalgeographic.com/news/2005/09/0919_050919_moon_space.html Retrieved July 14, 2009.*
60. Roberto Armellin, Michèle Lavagna; Multidisciplinary Optimization of Aerocapture Maneuvers; *Journal of Artificial Evolution and Applications Volume 2008 (2008), Article ID 248798, 13 pages.*
61. Rodney C. Wingrove; A Study of Guidance to Reference Trajectories for Lifting Re-entry at Super-circular Velocity; *NASA TR R-151 Dec-1963.*
62. R. Wernitz, M. Fertig, G. Herdrich, S. Löhle, M. Winter, H.-P. Röser; Assessment of PWT Conditions for the Stardust Post Flight Evaluation; *6th International Planetary Probe Workshop, Atlanta – 2008.*
63. Sarah Hendrickson Bairstow; Reentry Guidance with Extended Range Capability for Low L/D Spacecraft; *MS Thesis, Massachusetts Institute of Technology, Feb.-2006.*
64. Schittkowski K.; NLPQLP: A FORTRAN Subroutine Solving Constrained Nonlinear Programming Problems; *Annals of Operations Research 5(1985/6) 485-500.*
65. Schoettle U., Bregman E., Hillesheimer M., Inatani Y.; Conceptual study of a small semiballistic re-entry experiment vehicle; *Zeitschrift für Flugwissenschaften und Weltraum-forschung, Nr. 15, Seiten 362-372, Springer-Verlag 1991.*
66. Spies J., Grallert H.; Configuration Finding and Characterisation of ASTRA Reference Concepts; *Proceedings of 2nd International Syniposiuni on Atmospheric Re-entry Vehicles and Systems, Arcachon, Frankreich, 26.-29. Marz 2001.*
67. S. S. Rao; Optimization – Theory and Applications (Second Edition); *Wiley Eastern Ltd. 1984.*
68. Stephan A. Whitmore, Daniel W. Banks, Benjamin M. Andersen, Patrick R. Jolley; Direct-Entry, Aero-braking, and Lifting Aero-capture for Human-Rated Lunar Return Vehicles; *AIAA-2006-1033, 44th AIAA Aerospace Sciences Meeting and Exhibit, Reno – 2006.*
69. Sygulla D., Sabath D., Pittmann N., Schmid V., Caporicci M., Anderson B.; The US-European Cooperation in the X-38 and CRV Programs; *53rd International Astronautical Congress, IAC-02-V.3.0 1, Houston, Texas, October, 2002.*
70. Tauber M. E., Lyne J. E., Anagnost A.; A parametric study of manned aerocapture at Mars; *A91-47151 20-08, AIAA Atmospheric Flight Mechanics Conference, New Orleans, LA, Aug. 12-14, 1991.*

71. The Vision for Space Exploration; *NASA February 2004* http://www.nasa.gov/pdf/55583main_vision_space_exploration2.pdf. Retrieved December 5, 2009.
72. Will Knight; Russia proposes manned Mars mission by 2015 – 08; *New Scientist July 2002* <http://www.newscientist.com/article/dn2511-russia-proposes-manned-mars-mission-by-2015.html>, 11.03.2010.
73. Wingrove, R.C.; Survey of Atmospheric Re-entry Guidance and Control Methods; *AIAA Journal, Vol. 1, No. 9, September 1963*.

Appendix

A.1 Reference Coordinate Systems and Transformations

Various coordinate systems are required, to express the equations of motion of a spacecraft and to describe position and orientation of the spacecraft. The choice of some of these coordinate systems depends on the mission of the spacecraft. Since this work deals with the re-entry into the Earth atmosphere which implies that the spacecraft flies only in the neighbourhood of the Earth, therefore, the coordinate systems which are Earth-bound in some way, has been used throughout this report.

Three basic right-handed rotations occur frequently throughout this report, to transform from one coordinate system to another one. The transformations for these rotations are,

$$R_x(\theta_x) = \begin{bmatrix} 1 & 0 & 0 \\ 0 & \cos\theta_x & \sin\theta_x \\ 0 & -\sin\theta_x & \cos\theta_x \end{bmatrix} \quad \text{A-1}$$

$$R_y(\theta_y) = \begin{bmatrix} \cos\theta_y & 0 & -\sin\theta_y \\ 0 & 1 & 0 \\ \sin\theta_y & 0 & \cos\theta_y \end{bmatrix} \quad \text{A-2}$$

$$R_z(\theta_z) = \begin{bmatrix} \cos\theta_z & \sin\theta_z & 0 \\ -\sin\theta_z & \cos\theta_z & 0 \\ 0 & 0 & 1 \end{bmatrix} \quad \text{A-3}$$

Here, $R_x(\theta_x)$ is the transformation for a right-handed rotation about the X -axis through an angle θ_x and so on.

Geocentric Inertial Coordinate System, $C_i (O_i-x_i-y_i-z_i)$

- Origin O_i is at Earth centre.
- Axis z_i is perpendicular to equatorial plane and points to North Pole.
- Axis x_i points to the point of *Vernal Equinox* and in equatorial plane.
- Axis y_e is defined by right-hand rule

Geocentric Earth-fixed Coordinate System, $C_e (O_e-x_e-y_e-z_e)$

- Origin O_e is at Earth centre.
- Axis x_e points to the point of intersection of Greenwich meridian and equatorial plane.
- Axis z_e is perpendicular to equatorial plane and points to North Pole.
- Axis y_e is defined by right-hand rule

This frame is fixed to the Earth, hence has an angular velocity of Earth rotation

$$\omega_E = 7.292114 \times 10^{-5} \text{ rad/s}$$

The Cartesian coordinates x_e, y_e, z_e and spherical coordinates r, λ, δ are related by,

$$r^2 = x_e^2 + y_e^2 + z_e^2 \quad \text{A-4}$$

$$\sin \delta = \frac{z_e}{r} \quad \text{A-5}$$

$$\tan \lambda = \frac{y_e}{x_e} \quad \text{A-6}$$

Transformation from inertial coordinate system C_i to Geocentric Earth-fixed coordinate system C_e is done as (see Figure A-1),

$$C_i \xrightarrow{R_z(\alpha_G)} C_e$$

The angle α_G between x_e and x_i varies with time t ,

$$\alpha_G = \alpha_{G0} + \omega_E(t - t_0) \quad \text{A-7}$$

Where, α_{G0} is the value of α_G at initial time t_0

The matrix of transformation is formed by,

$$T_i^e = R_z(\alpha_G) \quad \text{A-8}$$

i.e.

$$T_i^e = R_z(\alpha_G) = \begin{bmatrix} \cos \alpha_G & \sin \alpha_G & 0 \\ -\sin \alpha_G & \cos \alpha_G & 0 \\ 0 & 0 & 1 \end{bmatrix} \quad \text{A-9}$$

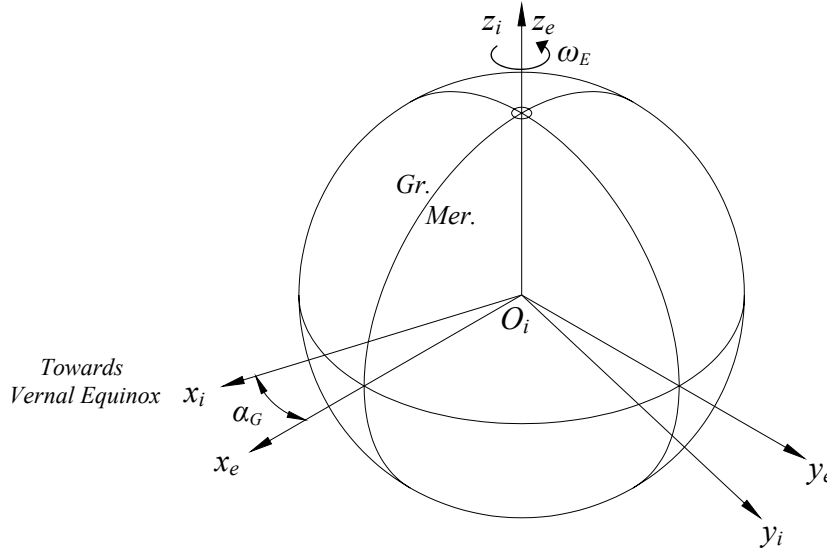


Figure A-1: Geocentric Inertial- and Geocentric Earth-fixed Coordinate Systems

Local Horizontal Coordinate System, $C_h (O_h-x_h-y_h-z_h)$

- Origin O_h is at centre of mass of spacecraft.
- Axis y_h is locally vertical, upward.
- Axis x_h locally horizontal and northward.
- Axis z_h is locally horizontal and eastward.

Transformation from geocentric Earth-fixed coordinate system C_e to local horizontal coordinate system C_h is done as (see Figure A-2),

$$C_e \xrightarrow{R_z(\lambda)} \cdot \xrightarrow{R_y(-\phi-\pi/2)} \cdot \xrightarrow{R_x(-\pi/2)} C_h$$

Where, λ and ϕ are longitude and geodetic latitude of spacecraft at current time.

The matrix of transformation is formed by the following sequence of matrix multiplications,

$$T_e^h = R_x(-\pi/2) \cdot R_y(-\phi-\pi/2) \cdot R_z(\lambda) \quad \text{A-10}$$

i.e.

$$T_e^h = \begin{bmatrix} -\sin \phi \cos \lambda & -\sin \phi \sin \lambda & \cos \phi \\ \cos \phi \cos \lambda & \cos \phi \sin \lambda & \sin \phi \\ -\sin \lambda & \cos \lambda & 0 \end{bmatrix} \quad \text{A-11}$$

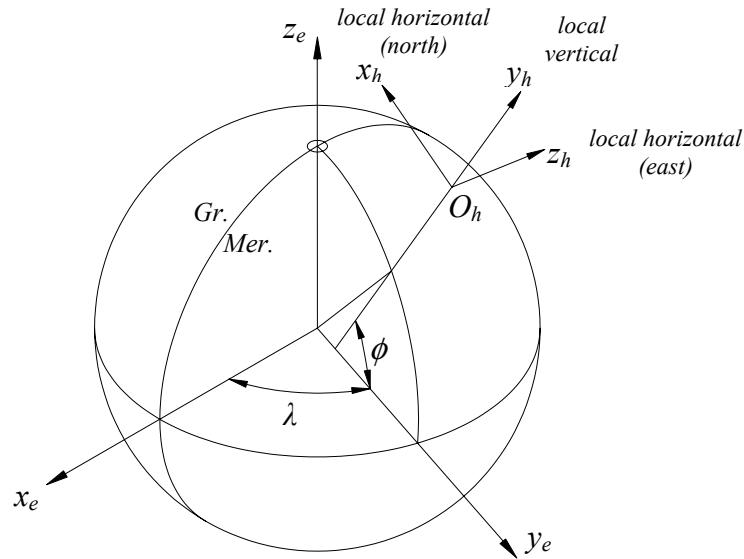


Figure A-2: Local horizontal coordinate system

The orientation of instantaneous velocity vector w.r.t local horizontal coordinate system C_h is described by flight path angle γ and azimuth angle χ as shown in Figure A-3.

Flight path angle γ : angle between the velocity vector V_{rel} and y_h .

Azimuth angle χ : angle between axis x_h and projection of velocity vector V_{rel} on local horizontal plane x_h - z_h .

The two angles are determined by the components of spacecraft velocity in launch frame as follows,

$$\sin \gamma = \frac{V_{yh (rel)}}{V_{rel}} \quad \text{A-12}$$

$$\tan \chi = \frac{V_{zh (rel)}}{V_{xh (rel)}} \quad \text{A-13}$$

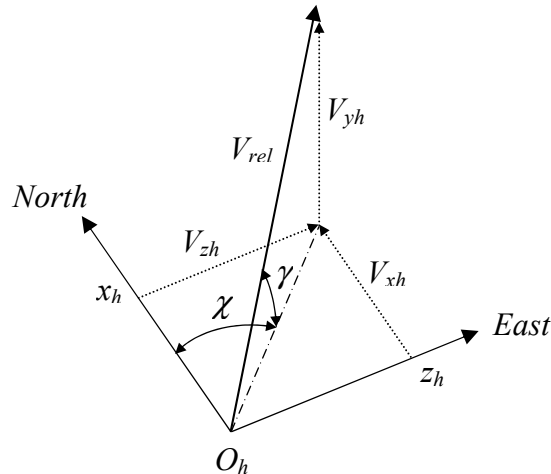


Figure A-3 Orientation of velocity vector with local horizontal coordinate system

Body Frame, C_b (O_b - x_b - y_b - z_b)

- Origin O_b is at centre of mass of spacecraft.
- Axis x_b along spacecraft longitudinal axis.
- Axis z_b is along right wing.
- Axis y_b complements right-hand system.

Aerodynamic Coordinate System, C_a (O_a - x_a - y_a - z_a)

- Origin O_a is at centre of mass of spacecraft.
- Axis x_a along air-stream velocity V .
- Axis y_a perpendicular to V , and in plane of symmetry.
- Axis z_a complements right-hand system.

The relation between aerodynamic coordinate system C_a and body coordinate system C_b is (see Figure A-4),

$$C_a \xrightarrow{Ry(\beta)} \cdot \xrightarrow{Rz(\alpha)} C_b$$

Where,

Angle of Attack, α : is angle between longitudinal axis and projection of air stream velocity V_a on plane of symmetry x_b y_b . It is positive when V has a downward component.

Angle of Side Slip, β : is angle between plane of symmetry and air-stream velocity V . It is positive when V has a rightward component.

And relation between aerodynamic coordinate system C_a and local horizontal system C_h is,

$$C_h \xrightarrow{R_y(-\chi)} \cdot \xrightarrow{R_z(\gamma)} \cdot \xrightarrow{R_x(\psi)} C_a$$

Where,

Bank Angle, ψ : is angle between plane of symmetry and local vertical plane.

The matrix of transformation is formed by the following sequence of matrix multiplications,

$$T_h^a = R_x(-\psi) \cdot R_z(\gamma) \cdot R_y(-\chi) \quad \text{A-14}$$

i.e.

$$T_h^a = \begin{bmatrix} \cos \gamma \cos \chi & \sin \gamma & \cos \gamma \sin \chi \\ -\cos \psi \sin \gamma \cos \chi - \cos \psi \cos \chi & \cos \psi \cos \gamma & -\cos \psi \sin \gamma \sin \chi + \sin \psi \cos \chi \\ \sin \psi \sin \gamma \cos \chi - \cos \psi \sin \chi & -\sin \psi \cos \gamma & \sin \psi \sin \gamma \sin \chi - \cos \psi \cos \chi \end{bmatrix}$$

A-15

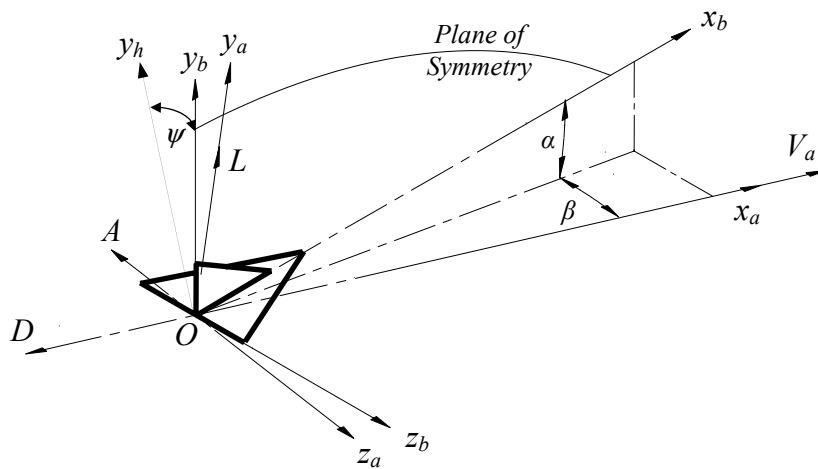


Figure A-4: Aerodynamic and body coordinate systems

A.2 Forces Acting on Re-entry Vehicle

Aerodynamic Forces

Components of aerodynamic force in aerodynamic coordinate system as shown in Figure A-4 are,

- Drag, D , opposite to velocity V i.e. opposite to x_a .
- Lift L , along axis y_a .
- Side Force A , along axis z_a .

With corresponding coefficients C_D, C_L, C_A

Magnitude of aerodynamic forces in aerodynamic coordinate system,

$$D = \frac{1}{2} \rho V^2 C_D S_{ref} \quad \text{A-16}$$

$$L = \frac{1}{2} \rho V^2 C_L S_{ref} \quad \text{A-17}$$

$$A = \frac{1}{2} \rho V^2 C_A S_{ref} \quad \text{A-18}$$

The acceleration vector due to aerodynamic forces can be calculated as:

$$\vec{a}_{aero} = \frac{1}{m} \cdot [T_h^a]' \cdot \begin{bmatrix} -D \\ L \\ -A \end{bmatrix} \quad \text{A-19}$$

Gravitational Forces

The acceleration vector due to gravitational force is:

$$\vec{a}_{grav} = \begin{bmatrix} g_\delta \\ g_r \\ g_\lambda \end{bmatrix} \quad \text{A-20}$$

Where g_r , g_λ and g_δ are presented by Equation 2-9 to Equation 2-11 respectively

Relative Forces

The acceleration vector due to the rotation and angular rate of horizontal coordinate system is given by,

$$\vec{a}_{rel} = \begin{bmatrix} \sin \delta \sin \chi & \sin \delta & \sin \gamma \cos \chi + \cos \gamma \sin^2 \chi \tan \delta \\ -\sin \delta \cos \chi + \tan \gamma \cos \delta & 0 & \sin \chi (\sin \gamma - \cos \gamma \cos \chi \tan \delta) \\ \cos \delta \sin \chi & \cos \delta & \cos \gamma \end{bmatrix} \begin{bmatrix} -2\omega_E V_{rel} \cos \gamma \\ -r\omega_E^2 \cos \delta \\ -\frac{V_{rel}^2}{r} \cos \chi \end{bmatrix}$$

A-21

A.3 Properties of Earth form, Gravity and Atmosphere

Table A-1: Reference ellipsoid

Symbol	Definition	Value	Units
R_e	Equatorial Radius	6378.137	km.
R_p	Polar Radius	6356.752	km.
f	Flatness = $\frac{R_e - R_p}{R_e}$	$\frac{1}{298.257}$	---

Table A-2: Earth's gravity model

Symbol	Definition	Value	Units
μ	Earth Gravitation Parameter =	3.986005×10^{14}	m^3/s^2
g_e	Gravitational Acceleration at	9.780326771	m/s^2
J_2	2nd Order Jeffery Constant	1.08623×10^{-3}	---
J_3	3rd Order Jeffery Constant	2.532153×10^{-7}	---
J_4	4th Order Jeffery Constant	1.6109876×10^{-7}	---

Table A-3: Atmospheric constants [20]

Symbol	Definition	Value	Units
P_o	Sea-level pressure	1.01325×10^5	N/m^2
T_o	Sea-level Temperature	288.15	K
ρ_o	Sea-level Density	1.225	kg/m^3
R^*	Universal gas constant	8.31432×10^3	J/kg-mole-
R	Gas constant (air)	287	J/kg-K
γ	Adiabatic polytropic constant	1.405	---
g_o	Sea-level gravity acceleration	9.806	m/s^2

A.4 Range and Azimuth between Two Points on Surface of Spherical Earth

Problem 1:

Given: Latitude and Longitude of two points on the surface of Earth

Find: Range and Azimuth

$$\Psi_{1 \rightarrow 2} = \cos^{-1}[\sin \delta_1 \cdot \sin \delta_2 + \cos \delta_1 \cdot \cos \delta_2 \cdot (\cos \lambda_2 - \cos \lambda_1)] \quad \text{A-22}$$

$$\chi_{1 \rightarrow 2} = \tan^{-1} \left[\frac{\cos \delta_1 \cdot \cos \delta_2 \cdot \sin(\lambda_2 - \lambda_1)}{\sin \delta_2 - \sin \delta_1 \cdot \cos \Psi_{1 \rightarrow 2}} \right] \quad \text{A-23}$$

$$\text{Range} = R \cdot \Psi_{1 \rightarrow 2} \quad \text{A-24}$$

Where $\Psi_{1 \rightarrow 2}$ is the range angle between point 1 and point 2, $\chi_{1 \rightarrow 2}$ is the azimuth angle measured from point 1 towards point 2 and R is the mean radius of Earth.

Problem 2:

Given: Latitude and Longitude of starting point and Range and Azimuth

Find: Latitude and Longitude of end point

$$\Psi_{1 \rightarrow 2} = \frac{\text{Range}}{R} \quad \text{A-25}$$

$$\delta_2 = \sin^{-1}[\cos \Psi_{1 \rightarrow 2} \cdot \sin \delta_1 + \sin \Psi_{1 \rightarrow 2} \cdot \cos \delta_1 \cdot \cos \chi_{1 \rightarrow 2}] \quad \text{A-26}$$

$$\lambda_2 = \lambda_1 + \sin^{-1} \left[\frac{\sin \Psi_{1 \rightarrow 2} \cdot \sin \chi_{1 \rightarrow 2}}{\cos \delta_2} \right] \quad \text{A-27}$$

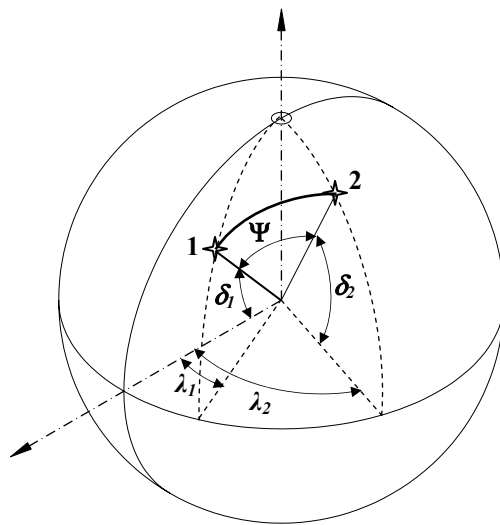


Figure A-5: Range and Azimuth between two points on surface of Earth

A.5 Radiative Heating Velocity Function

Table A-4: Radiative heating velocity function (Tauber and Sutton [45])

$V,$	$f(V)$
9000	1.5
9250	4.3
9500	9.7
9750	19.5
10000	35
10250	55
10500	81
10750	115
11000	151
11500	238
12000	359
12500	495
13000	660
13500	850
14000	1065
14500	1313
15000	1550
15500	1780
16000	2040

A.6 Original Apollo Re-entry Guidance Strategy

The primary function of Apollo re-entry guidance algorithm is to manage energy as the spacecraft descends until it is feasible to deploy the parachute. There are two channels in the guidance strategy: vertical and lateral. However, there is only one control: bank angle modulation. The guidance algorithm updates the bank angle command once every guidance cycle. For the original Apollo algorithm, which is described in this chapter, a guidance cycle occurs once every two seconds.

Energy, and thus downrange to the target, is managed in the vertical channel by orienting the lift vector. Full lift-up provides maximum range while full lift-down provides the steepest descent. Lift-down may be constrained by the maximum allowed g-loads that can be experienced by the crew and vehicle. Any bank orientation other than full lift-up or full lift-down will place a component of lift in the lateral channel. Guidance's primary goal is to manage lift in the vertical channel so that the vehicle enters into the wind corrected parachute deploy box (defined by values of dynamic pressure and Mach number) at the appropriate downrange position. Cross range position is maintained by the lateral channel by reversing the lift command into the mirror quadrant (e.g. $+30^\circ$ from vertical to -30°) once the lateral range errors to the target cross a threshold. The vehicle continues this bank command reversal strategy as it descends to the target. As the energy (velocity) decreases, the lateral threshold shrinks so that the vehicle maintains control authority to minimize the lateral errors prior to parachute deploy. The guidance phases and phase-transition logic are discussed fully in Reference [26,63].

Downrange management is achieved by commanding the amount of lift in the vertical channel. The baseline Apollo algorithm consists of seven phases designed to control the downrange position of the vehicle, as shown in Figure 4-2.

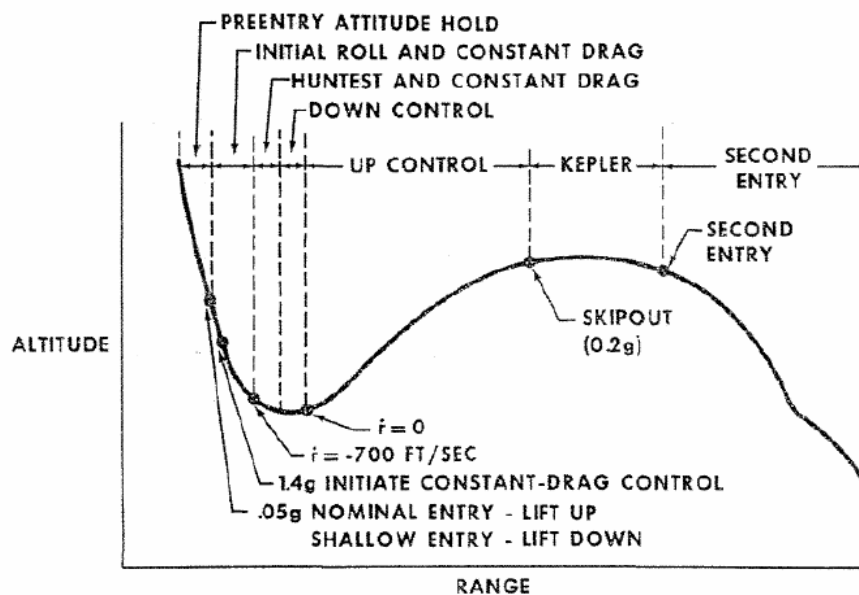


Figure A-5: Apollo Guidance Strategy [63]

The first phase is the Pre-entry Attitude Hold phase, which begins as soon as the guidance algorithm gains control of the vehicle. This phase maintains current attitude until a sensible atmosphere has been detected, at which point the algorithm begins to control the lift vector of the vehicle as part of the Initial Roll phase. This phase seeks to guide the vehicle toward the centre of the re-entry corridor. It does so by commanding the lift vector upward to make a steep re-entry path shallower, or commanding the lift vector downward to steepen a shallow re-entry.

Once atmospheric capture is assured, the Hunttest and Constant Drag phase begins. This phase maintains constant drag while “hunting” for an “estimate” of the appropriate trajectory to reach the target. Here, the algorithm determines whether the vehicle will need to perform an upward “skip” in order to extend the vehicle’s range, decides which of the possible phases to use, and calculates the conditions which will trigger those phases. For short target ranges, the Hunttest phase will determine that no skip is necessary, and the algorithm will transition directly into the Final (“Second Entry”) phase. Otherwise, if a skip is necessary, guidance will transition into the Down control phase.

Down control guides the vehicle to the trigger conditions, using a constant drag policy, until a velocity and drag trigger previously determined by Hunttest activates the Up control phase. Up control guides the vehicle along a self-generated reference trajectory, previously generated by the Hunttest phase, using a reference-following controller. It is important to note that this trajectory is not updated during the Up control phase. The reference trajectory is indicated in terms of velocity and altitude rate reference variables, which are functions of the independent variable, aerodynamic drag. If the vehicle does not exit the atmosphere, the algorithm will enter the Final phase at the peak of the skip. Otherwise, the Ballistic (“Kepler”) phase will take over. For the purposes of the Apollo algorithm, atmospheric exit is defined to take place when aerodynamic acceleration drops below 0.2 g’s.

The Ballistic phase is assumed to be simply a ballistic trajectory, and since atmospheric density is very low, it is assumed that there is not enough dynamic pressure for the vehicle to have enough control authority to make steering effective. Thus, bank angle commands are no longer updated and remain at the previously commanded value until aerodynamic acceleration rises above 0.2 g’s again, at which point the Final phase begins. Like the Up control phase, the Final phase is based on a reference-following controller. Unlike the Up control phase, however, the reference is based on a stored nominal trajectory which was calculated pre-flight, and is indicated in terms of drag and altitude rate as functions of velocity. Once the velocity drops below a threshold value, the algorithm stops updating bank commands until parachute deploy, when the guidance algorithm would be disabled.

The component of lift in the vertical channel, and thus the component of lift in the lateral channel, is dictated by the downrange management phases. Lateral control can still be achieved, however, by periodically rotating to the mirror quadrant. Such a ‘bank angle reversal’ allows the same amount of lift to remain in the vertical

channel while reversing the direction of the lift in the lateral channel. In this manner, the vehicle can 'zigzag' its way to the target.

In order to limit the number of reversals required during the entire trajectory, the amount of cross range error allowed before a reversal is commanded is large at first and then decreases as the vehicle's remaining cross range capability diminishes.

The allowable cross range error does not go to zero as the target approaches; otherwise, the vehicle would be making constant bank reversals toward the end of the trajectory. Instead, there is a bias term which allows about 2 km of cross range error.

Curriculum Vitae

Name: Muhammad Imran Afzal
Date of Birth: 13th September 1975
Place of Birth: Karachi / Pakistan
Nationality: Pakistani
Family status: Married
1980-1987: Kindergarten and Primary School
Taimuria Children Nursery School
Karachi / Pakistan
1987-1992: Middle- and Secondary School
Placid High School
Karachi / Pakistan
1992-1994: Higher Secondary Education
Government College for Men - Nazimabad
Karachi / Pakistan
1994-1999: Bachelor of Engineering, (Mechanical Engineering)
NED University of Engineering and Technology,
Karachi / Pakistan
2001-2004: Master of Science, (Flight Vehicle Design)
Beijing University of Aeronautics and Astronautics
Beijing / China
2006-2010: Research Fellow (PhD Candidate)
Institute of Space Systems, Universität of Stuttgart
Stuttgart / Germany

Publications

- 1) *M. I. Afzal M. H. Graesslin, H. -P Roeser; Study of Various Re-entry Vehicle Configurations for Future Interplanetary Missions; Deutscher Luft- und Raumfahrtkongress 2008, Darmstadt / Germany.*
- 2) *M. I. Afzal M. H. Graesslin, H. -P Roeser; An Explicit Guidance Method for a Lifting Interplanetary Re-entry Vehicle; AIAA- 2009-6108, AIAA Guidance Navigation and Control Conference 2009, Chicago II / USA.*